A THEORETICAL AND EXPERIMENTAL INVESTIGATION OF PROTON TRANSPORT BETWEEN THE ELECTROLYTE IN A REVERSIBLE FUEL CELL AND A CARBON-BASED HYDROGEN STORAGE

A thesis submitted in fulfilment of the requirements for the degree of Doctor of Philosophy

By

Shahin Heidari

College of Science, Engineering and Health
RMIT University

Melbourne, Victoria, Australia

March 2017

DECLARATION

I, Shahin Heidari, hereby submit the thesis entitled “a theoretical and experimental investigation of proton transport between the electrolyte in a reversible fuel cell and a carbon-based hydrogen storage” for the degree of Doctor of Philosophy, and certify that except where due acknowledgement has been made, the work is that of the author alone; the work has not been submitted previously, in whole or in part, to qualify for any other academic award, and that the content of the thesis is the result of work that has been carried out since the official commencement date of the approved research program.

Shahin Heidari

March 2017

ACKNOWLEDGMENTS

I would like to acknowledge my senior supervisor, Professor John Andrews, for sharing his ideas and knowledge and supporting me in every step of my PhD journey.

I would like to thank Professor Aliakbar Akbarzadeh and Doctor Abhijit date for giving me the opportunity of teaching and tutoring.

I would like to thank all my friends and colleagues at RMIT University SAMME School and specifically Energy CARE group for their support.

Many thanks also go to our hydrogen group at RMIT, specifically Dr. Amandeep Oberoi and Mr. Saeed Seif Mohammadi for sharing with me their knowledge in this field of study.

I would like to thank my family and friends in Melbourne for supporting me during my study.

I dedicate this thesis to my parent Behrouz Heydari and Akram homafar, for their never-ending love, support, and encouragement.

Contents

List of figures

List of tables

EXECUTIVE SUMMARY

Hydrogen is considered to be an important fuel for the future because of its high energy content per unit mass and the possibility of production from renewable energy and used in a fuel cell to provide a sustainable zero-emission energy system.
Storing hydrogen is often considered a barrier to its widespread introduction in a sustainable energy economy. Hydrogen can be stored as pressurised gas, cryogenic liquid, and as chemical or physical combination with materials, such as metal hydrides or carbon particles. The main limitations of metal hydride storage are that the weight percent of stored hydrogen is still low, usually less than 2 wt%, and they are very expensive since most hydrogen storage alloys employ costly rare earth elements

Recent work at RMIT University has proposed and investigated experimentally the innovative concept of integrating a metal hydride (MH) storage into a unitised regenerative fuel cell (URFC). This integration was achieved by constructing one electrode of the cell from MH material so that H^+ ions emerging from the membrane enter the solid storage directly and then react with electrons and the metal atoms to form metal hydride. The novel system was called a "proton flow battery" (or more simply a "proton battery"), because in charging mode just an inflow of water is needed, and in discharge mode just air is fed into the cell.

The research at RMIT University has focussed on investigating electrochemical storage of hydrogen in porous carbon-based electrodes. Promising results were obtained using various forms of activated carbon with a dilute acid as the liquid electrolyte and proton conductor. However, prior to the present project it had not been shown convincingly that a proton battery with such a hydrogen-storage electrode was technically feasible.

The present project has therefore continued the investigation of carbon-based hydrogen storage electrodes for a proton battery.

The **aim** of this project is therefore to investigate theoretically and experimentally proton transport between a membrane in a reversible fuel cell and a carbon-based hydrogen storage material.

The **objectives** of the project are:

- To review the literature on proton conduction in electrolytes that penetrate into porous carbon-based materials, and the electric charge distributions and electrochemical reactions that take place on the inner and outer surfaces of the carbon particles
- To obtain theoretical estimates of the electron conductivity through the carbon particles, and proton conductivity through the proton conducting electrolyte within the hydrogen storage material using classical electrical conductivity and potential theory, and classical theories of diffusion through tortuous porous media, and MATLAB simulations
- To gain an improved understanding at the nanoscale of the movement of protons, other ions, and electrons, and the associated electrochemical reactions, at or near the surfaces of carbon electrode materials using galvanostatic charging and discharging approach.
- To compare estimates of the double-layer capacitance and hydrogen storage potential of a selection of composite electrodes made from various carbon materials and interspersed proton-conducting media, with experimental measurements
- To identify the structures and compositions of composite electrodes that promise to have the best performance as supercapacitors and/or hydrogen storage media.

The **main research questions** addressed are:

- To what extent can the theoretical model developed represent the hydrogen storage process in the selected carbon-based material?
- What are the key structural and electrochemical characteristics and properties of carbon-based hydrogen storage material that are dual proton and electron conductors and suitable for use in a proton battery?
- To what extent the best-performing material can be used in a proton battery device?

This thesis has contributed to a better understanding of the process of hydrogen movement and storage in carbon-based material by developing a theoretical analysis and introducing the

effect of input variables into the shape of the theoretical V-I curve obtained for different structural carbon-based electrodes.

A one-dimensional theoretical analysis normal to the active surface of the electrodes in a reversible electrochemical cell has been developed. A Butler-Volmer type equation related the rate of adsorption of hydrogen to the potential difference between the activated carbon surface and the electrolyte in the porous hydrogen storage electrode. A second-order differential equation has been derived that relates the potential between the proton conducting medium and the hydrogen-storage medium.

A MATLAB program has been developed to solve the equation numerically. It was shown that changing the charge transfer coefficient on both sides changed the slope of both overpotential and V-I curves, while changing the exchange current density shifted these V-I curves up and down. Increasing the exchange current density decreased the overpotential in charging mode to obtain a given current. The reversible potential affected the cut-in value of voltage at which current starts to increase on the V-I curve.

The VI curves generated using the theoretical model and Matlab solution in electrolyser mode for a reversible electrochemical cell were found to be able to fit the corresponding experimental curves accurately.

The first experimental component of the thesis involved measuring the hydrogen storage capacities of carbon-based electrodes with a liquid acidic electrolyte. Four different forms of carbon were used to make sample electrodes: a commercial activated charcoal (Norit); an activated carbon made by treating phenolic resin with KOH at high temperature; spherical graphite, as used in lithium ion batteries; and ‘graphene platelets’ comprising around 20 stacked layers of graphene. Solid electrodes from these carbons were fabricated using a PTFE binder.

Their bulk electron and proton conductivities, double layer capacitance, and reversible electrochemical hydrogen storage capacity when soaked in a dilute sulphuric acid electrolyte (as ‘internal’ proton conductor) were then measured. The electron conductivity of the samples was found to be in the range 4 to 12 S/cm, which compares to 16 S/cm for pure graphite. Their proton conductivities, due to the acid filling the pores, was found in the range 0.001 – 0.016 S/cm, compared, for example, to that of 1 M dilute sulphuric acid and fully hydrated nafion of ~0.1 S/cm. The double-layer capacitance of the carbon electrodes was

found to be in the range of 6–15 F/g, which compares to 200 F/g for supercapacitor materials. The total reversible electrochemical hydrogen storage capacities of the carbon electrodes immersed in 1 M dilute sulphuric acid were in the range of 0.01– 0.6 mass%.

The porous activated carbons investigated in this project showed better performance in storing hydrogen than the graphitic carbon-base materials. Specifically, porous activated carbon made from phenolic resin activated by KOH 1:7 with high BET surface area at around 3800 m^2/g revealed highest amount of hydrogen storage by 0.6 wt% compared to spherical graphite at 0.2 wt%.

A possible explanation for storing more hydrogen in porous activated carbon than the graphite is as the liquid electrolyte (1 Mol sulphuric acid) can penetrate into the meso and microporos channels of the activated carbon, the protons are transported to the active storage site and hence the storage wt% is higher than the graphite samples which the proton could not penetrate between the gaps of the graphite layers.

The second experimental component of the thesis involved measuring the reversible hydrogen storage performance of the best performing carbon material identified from the earlier experiments in a proton battery. The aC KOH 1:7 sample was selected since it yielded the highest wt% hydrogen stored based upon the electrochemical hydrogen storage capacity experiment. This activated carbon had substantial micropore and mesopore volumes, a combination suitable for storing hydrogen.

It was therefore shown successfully that hydrogen can be stored electrochemically in the activated carbon electrode soaked in dilute sulphuric acid in a proton battery. Two samples from phenolic resin with 10 wt% and 30 wt% PTFE as binder were tested and the results showed that the more PTFE used, the less the hydrogen storage wt% obtained. The results for the non-optimised proton battery and carbon-based electrode showed the maximum amount of hydrogen storage was very nearly 1 wt%, while in discharge mode 0.83 wt% was released.

Overall this thesis has shown for the first time that a proton battery with an integrated solid carbon-based hydrogen storage electrode is technically feasible.

It is recommended that further detailed study be conducted to evaluate and investigate the performance in a proton battery of other forms of carbon-based materials such as carbon hydrogels and carbon nanotubes, which can be designed and fabricated with the desired

properties to improve and optimise the performance of this promising new battery technology.

1. INTRODUCTION

1.1 Background

Hydrogen is considered to be an important fuel for the future because of its high energy content per unit mass and the possibility of using hydrogen produced from renewable energy in a fuel cell. Nowadays hydrogen plays a very limited role in the energy industry, but is used for a variety of purposes in a range of other industries (Andrews and Shabani 2013). Considering that fossil fuel resources are limited in supply, hydrogen produced from renewable energy can be a good substitute, since it is a sustainable and zero-greenhouse gas emission option. Jacobson and Delucchi (2011), for example, made extensive use of hydrogen produced by electrolysis of water using renewable energy sources of electricity in their global energy scenario to achieve radical greenhouse gas reduction targets. The role of hydrogen in their scenario was concentrated in the medium and heavy road transport, rail, sea, and air transport sectors. Unlike fossil fuels, hydrogen is environmentally friendly and non-polluting simply because its combustion product is water. Provided it is produced by renewable energy source, it is a zero greenhouse gas emission fuel (Pozzo and Alfe, 2009).
Storing hydrogen is often considered a barrier to its widespread introduction in a sustainable energy economy (Züttel, 2008). Hydrogen can be stored as pressurised gas, cryogenic liquid, and as chemical or physical combination with materials, such as metal hydrides (Sakintuna et al. 2007) or carbon particles (Jurewicz et al. 2001). The main limitations of metal hydride storage are that the weight percent of stored hydrogen is still low, usually less than 2 wt%, and they are very expensive since most hydrogen storage alloys employ costly rare earth elements (Zhou, 2004).

At RMIT University, Andrews and Seif Mohammadi (2014) have recently proposed and investigated experimentally the innovative concept of integrating a metal hydride (MH) storage into a unitised regenerative fuel cell (URFC) that is undertaking the water splitting (Andrews and Seif Mohammadi, 2014). This integration was achieved by constructing one electrode of the cell from MH material so that H^+ ions emerging from the membrane enter the solid storage directly and then react with electrons and the metal atoms to form metal hydride. For discharge mode or fuel cell usage, hydrogen atoms are released from a very weak bond with metal atoms in low temperature (less than 100 C). These released hydrogen

atoms then give up an electron to the metal atoms and move toward the nafion membrane due to an electrical field. They called their system a “proton flow battery” because in charging mode just an inflow of water is needed, and in discharge mode just air is fed into the cell.

Jazaeri (2014), in his M Eng (by research) thesis at RMIT University investigated the feasibility of a unitised regenerative fuel cell with a reversible carbon-based hydrogen storage electrode.

Amandeep Oberoi (2015) continued Jazaeri (2014) work by using activated carbon for the electrochemical hydrogen storage. The results in his work proved that porous activated carbon is a suitable material for hydrogen storage (Oberoi *et al*. 2015), but the experiments conducted on a proton battery with a carbon-based electrode had a number of anomalous results that could not be explained within the scope of that study.

The present project continues the investigation of hydrogen storage electrodes for a proton battery from the stages where Andrews and Seif Mohammadi (2014), Jazaeri (2014), Oberoi *et al*. (2015) have reached. Here in this thesis the name ‘proton flow battery’ has been shortened to ‘proton battery’ for economy of expression, but these names are used synonymously.

In particular, this project seeks to develop an improved theoretical understanding of the processes of hydrogen diffusion into carbon-based electrodes, and subsequent bonding to surface carbon atoms within these porous media. Experiments have then been conducted to test the theoretical predictions, and prove the technical feasibility of a proton battery with a carbon-based storage electrode.

1.2 Aim and, objectives

The **aim** of this project is therefore to investigate theoretically and experimentally proton transport between a membrane in a reversible fuel cell and a carbon-based hydrogen storage material.

The **objectives** of the project are as follows:

- To review the literature on proton conduction in electrolytes that penetrate into porous carbon-based materials, and the electric charge distributions and electrochemical reactions that take place on the inner and outer surfaces of the carbon particles
- To obtain theoretical estimates of the electron conductivity through the carbon particles, and proton conductivity through the proton conducting electrolyte within the hydrogen storage material using classical electrical conductivity and potential theory, and classical theories of diffusion through tortuous porous media, and MATLAB simulations
- To gain an improved understanding at the nanoscale of the movement of protons, other ions, and electrons, and the associated electrochemical reactions, at or near the surfaces of carbon electrode materials using galvanostatic charging and discharging approach.
- To compare estimates of the double-layer capacitance and hydrogen storage potential of a selection of composite electrodes made from various carbon materials and interspersed proton-conducting media, with experimental measurements
- To identify the structures and compositions of composite electrodes that promise to have the best performance as supercapacitors and/or hydrogen storage media.

1.3 Research questions

The **main research questions** addressed are:

- To what extent can the theoretical model developed represent the hydrogen storage process in the selected carbon-based material?
- What are the key structural and electrochemical characteristics and properties of carbon-based hydrogen storage material that are dual proton and electron conductors and suitable for use in a proton battery?
- To what extent the best-performing material can be used in a proton battery device?

1.4 Scope

The scope of this project is limited to:

- Theoretical analysis on the proton transport into carbon-based electrodes made from a relatively small selection of carbon samples
- Hydrogen storage material suitable for use with reversible PEM fuel cells in a proton battery set-up.

The research has sought to improve theoretical understanding of the processes of proton diffusion and bonding in composite carbon electrodes. This improved understanding is critical for the further development of the novel proton battery concept.

More generally, developing systems based on the proton battery can facilitate the usage of renewable energy hydrogen systems in society and industry in order to reduce greenhouse gas emissions and also development of more cost effective and reliable RAPS systems. Australian industry can also benefit from this project because of its potential industrial development opportunities.

Potential advantages of the carbon-based storage electrodes studied in the present project, compared to metal hydrides are the following:

- Higher mass and volumetric energy densities of the hydrogen stored in carbon materials
- Lower roundtrip energy losses since the weak bonds between the C atoms and hydrogen can be easily formed and broken when hydrogen is released to be used.

Potential areas of application of the proton battery, incorporating the carbon electrodes studied in the present project, are the following:

- Electrical energy storage in central electricity grids with major energy inputs from inherently variable renewable
- As a hydrogen energy store for solar and wind systems for remote, other standalone and back-up power supplies
- For energy storage in consumer electronics
- An integrated hydrogen storage and fuel cell for hydrogen fuel cell vehicles.

The research in the present project remains quite fundamental, so that it will take some time before these ultimate benefits in terms of practical applications of the proton battery concept can be realised.

1.5 Planned outcomes

The planned outcomes of the project were the following:

- A better theoretical understanding of:
    - The process of proton / hydronium diffusion in the nafion or other proton conducting medium between the carbon particles.
    - The extent of proton conduction medium penetration into the pores of varying sizes within the carbon particles.
    - Whether we need an additional proton conduction medium, e.g. liquid acids or protic ionic liquids (see Tremblay *et al.* (2013), to enable protons to reach potential storage sites within the ultra-micro pores of carbon based electrode.
    - The pore structure and surface chemistry within carbon based material that is best suited for reversible hydrogen storage.
    - The form(s) of bonding, and the associated binding energy, between hydronium/ protons and the inner carbon surfaces of the pores within carbon particles that is most suitable for reversible hydrogen storage in this application.

These theoretical studies are complemented by some experimental work on measuring the hydrogen storage capacity and double-layer capacitance of electrodes made from activated carbon soaked in a number of different proton conducting liquids; and, most importantly, investigating the performance of the most promising of these electrodes in a proton battery.

1.6 Guide to thesis

In chapter 2, the overall method used for the present project is discussed and the activities done through this research from beginning to the end is shown.

In chapter 3, a comprehensive study on the previous works on electrochemical storage of hydrogen is discussed in details. The earlier works and findings conducted at RMIT University are presented.

In chapter 4, a theoretical analysis on the concept of hydrogen movement and storage in electrolyser mode is presented.

In chapter 5, a set of MATLAB codes has been developed based on the theoretical approaches explained in chapter 4 and solving these equations numerically. A comprehensive parametric study on the effect of changing variable inputs on the voltage-current curves generated has been conducted.

In Chapter 6, the double-layer capacitance and hydrogen storage capacity measurements of selected carbon-based electrodes are reported. The experimental procedures employed are described in detail along with the data obtained.

In Chapter 7, the concept of proton battery is covered. Design modification and construction of the proton battery with a solid state carbon-based electrode is described. Design of a test-rig is presented and the testing procedure is discussed in details. The performance of the best-performing activated carbon electrode in charge and discharge mode is reported.

Chapter 8 draws on all the theoretical analysis and experimental results to provide answers to the research questions set for this thesis. Additional conclusions from the research are presented and recommendations for the future research direction in this area made.

Finally the list of publication is presented at the end of the thesis.

2. METHOD

2.1 Overall methodological approach

This research has involved theoretical investigations on proton movement in carbon-based electrodes based on classical electromagnetic theory, and simplified one-dimensional models. The equations for the electric potentials and current density derived from theory were solved numerically using MATLAB. These modelling results were employed in a complementary way to the basic theory, to develop a better understanding of the processes occurring. Key outputs from the modelling were voltage – current curves for the electrochemical cells studied, and these were compared with the experimental measurements. The combined findings from the experimental and theoretical/computer modelling programs are used to draw conclusions about preferred designs for suitable carbon-based electrode used in hydrogen fuel cell and proton battery.

2.2 Theoretical investigations

In this part of the study, the process of hydrogen generation, hydrogen movement and hydrogen bonding with carbon particles has been investigated. A theoretical model is presented of the process of H^+ ion (proton) conduction through an acid electrolyte into a highly porous activated carbon electrode where it is neutralised and absorbed on the inner surfaces of pores. It is important to mention here that the hydrogen storage process can be in the form of adsorption of hydronium to the charged surfaces of carbon-based material, or a chemical reaction between protons and carbon particles. A Butler-Volmer type equation is employed to relate the rate of adsorption of protons which are mainly in the form of hydronium to the potential difference between the activated carbon surface and the electrolyte.

This model for the hydrogen storage electrode was then incorporated into a more general computer model based on MATLAB software of the entire electrochemical cell including the oxygen electrode. Hence a theoretical voltage-current curve was generated for given input parameters for a particular carbon-based electrode. The effect of changing variable input parameters such as exchange current density and charge transfer coefficient has been

investigated. The values for the input parameters on the hydrogen-side electrode that generated a VI curve that best fitted the corresponding experimental VI curve are found by minimising the voltage differences between the curves for each value of current. The values of exchange current density for each selected carbon electrode on the hydrogen side indicate the attractiveness of the storage process of the carbon hydrogen reaction. The presented charge transfer coefficient values show the reversibility of the hydrogen storage process.

2.3 Experimental procedures

2.3.1 Carbon-base materials as the hydrogen storage medium

As the literature indicates a range of carbon-based materials offer potential advantages in the field of energy storage (A. Zuttel *et al.* 2010). In this research different types of carbon-based material such as activated carbon, graphene platelets and spherical graphite have been chosen to investigate their electrochemical hydrogen storage capacity. The previous works at RMIT (S. Mohammadi 2013 and J. Jazaeri 2013 respectively) showed some promising results in case of using activated carbon in a proton battery but the outcomes of their research was much lower than the desired values. This research then has been conducted to overcome the limitations of the previous works and also to present a better understanding of the process of hydrogen storage in the carbon-based materials.

2.3.2 Fabrication of solid-state electrode

The activated carbon powders made from phenolic resin KOH 1:7 were supplied by Dr Mamun Mollah from Monash University. The previous work at RMIT (Oberoi, 2015) showed that this sample performs well in terms of hydrogen storage in an electrochemical hydrogen storage cell. Two graphitic types of carbon-base material has also been candidate to investigate the hydrogen storage capacity.

The method used to fabricate the carbon-based electrodes for testing was to mix the primary carbon powders with PTFE solution followed by heating so that the PTFE served as the binder. The details of this procedure are given in chapter 6.

Proton conductivity of all selected carbon-based material has been measured within an electrode soaked in dilute acid. The electron conductivity of the carbon composite samples was measured simply by using a multimeter.

2.3.3 Double layer capacitance measurement

Double-layer capacitance of all carbon-base electrodes was measured by cyclic voltammetry in a constant potential range, monitored in terms of scan rate. A typical split flat coin cell was employed with a non-conducting separator between the two fabricated working electrodes made from selected carbon materials and PTFE binder, as explained in detail in chapter 6.

2.3.4 Hydrogen storage capacity measurement

An experimental set up of combining electrochemical cell and Hofmann apparatus was designed and improved to measure the hydrogen storage capacity of each samples. Hydrogen storage capacity of all carbon sample electrodes was measured by galvanostatic charging and discharging approach at constant currents. The electrolytic cell in the designed set up was filled with 1 mol sulphuric acid to act as an electrolyte, and connected to a VERSASAT 3 electrochemical workstation. This procedure is fully described in chapter 6.

2.3.5 Testing the best performing electrode in proton battery

The activated carbon sample from phenolic resin KOH 1:7 was tested in the proton battery to prove its feasibility working concept and performance (chapter 7). Dilute sulphuric acid of 1 mol concentration was used to act as the proton and hydronium conductor from the membrane into the electrode while operating the PB in E-mode. The PB was charge at the constant current until the rate of hydrogen gas production was double as oxygen gas collected. After charging the cell in E-mode the cell rested for 30 minutes and then was tested in discharge cycles.

2.3.6 Activities

The main activities conducted to achieve the objectives set for this research were as follow:

- **Literature review**
    - Electrochemical storage of hydrogen in carbons: a state of the art review

- **Theoretical analysis**
    - Theoretical analysis of proton transport with an integrated hydrogen storage electrode
    - A general proposed model for cell potential and cell current
    - MATLAB simulation for the electrochemical cell
    - Parametric analysis, effect of varying key input parameters

- **Experimental design and measurements**
    - Fabrication of hydrogen storage electrodes with selected carbon-based materials
    - Proton and electron conductivity measurement of the carbon electrodes
    - Double layer capacitance of carbon electrodes
    - Electrochemical hydrogen storage in carbon composite electrodes
    - Experimental investigation of a proton battery with selected best-performing carbon-based electrodes

- **Thesis write up and publications**

3 ELECTROCHEMICAL STORAGE OF HYDROGEN IN CARBONS: A STATE OF THE ART REVIEW

3.1 Concept of reversible hydrogen fuel cell

A reversible hydrogen fuel cell is an electrochemical device that operates in two modes. In charging mode water is split into hydrogen and oxygen by an electrolyser, and in discharge or fuel cell mode, stored hydrogen and oxygen recombine together to produce electricity and water (Ioroi *et al.* 2001):

$$H_2O + electricity + heat \rightarrow H_2 + \frac{1}{2}O_2 \quad \text{(a)} \quad \text{: Charging mode}$$

$$H_2 + \frac{1}{2}O_2 \rightarrow H_2O + electricitypower + heat \quad \text{(b)} \quad \text{: Fuel cell mode}$$

The concept of a PEM Unitized regenerative fuel cell (URFC) was introduced in 1961, mainly focused on space applications (Bone *et al.* 1961). One of the disadvantages of their system was low electrochemical performance due to problems with membrane and electrocatalyst materials. Actually the system was suffering from chemical instability due to the very oxidising conditions found at anodes of water electrolysers. Later on, in 1972, General Electric Co. obtained promising results on the feasibility of using a PEM fuel cell in reversible mode (Mitlitsky *et al.* 1999).

A URFC stack was first used and tested as a primary fuel cell (FC) by LLNL supported by US Department of Energy (DOE) in Mid 1990s. These systems included high altitude long endurance (HALE) solar rechargeable aircraft (SRA), Zero emission vehicle, and hybrid energy storage for spacecraft (Mitlitsky *et al.* 1999).

In 1992 The Lawrence Livermore National Laboratory (LLNL) proposed URFCs as an ideal energy storage system to be used in unmanned long endurance aircraft (Mitlitsky *et al.* 1999). During the day power is supplied from solar energy. In electrolysis mode, surplus electricity over the direct load requirement is supplied from solar panels located on the aircraft wings, and generates hydrogen and oxygen. The hydrogen generated is then stored in a tank and can be used in fuel cell mode to generate power during the night to run the electrically-driven propellers. Figure 1 shows the proposed model built in the US in mid 1990s.

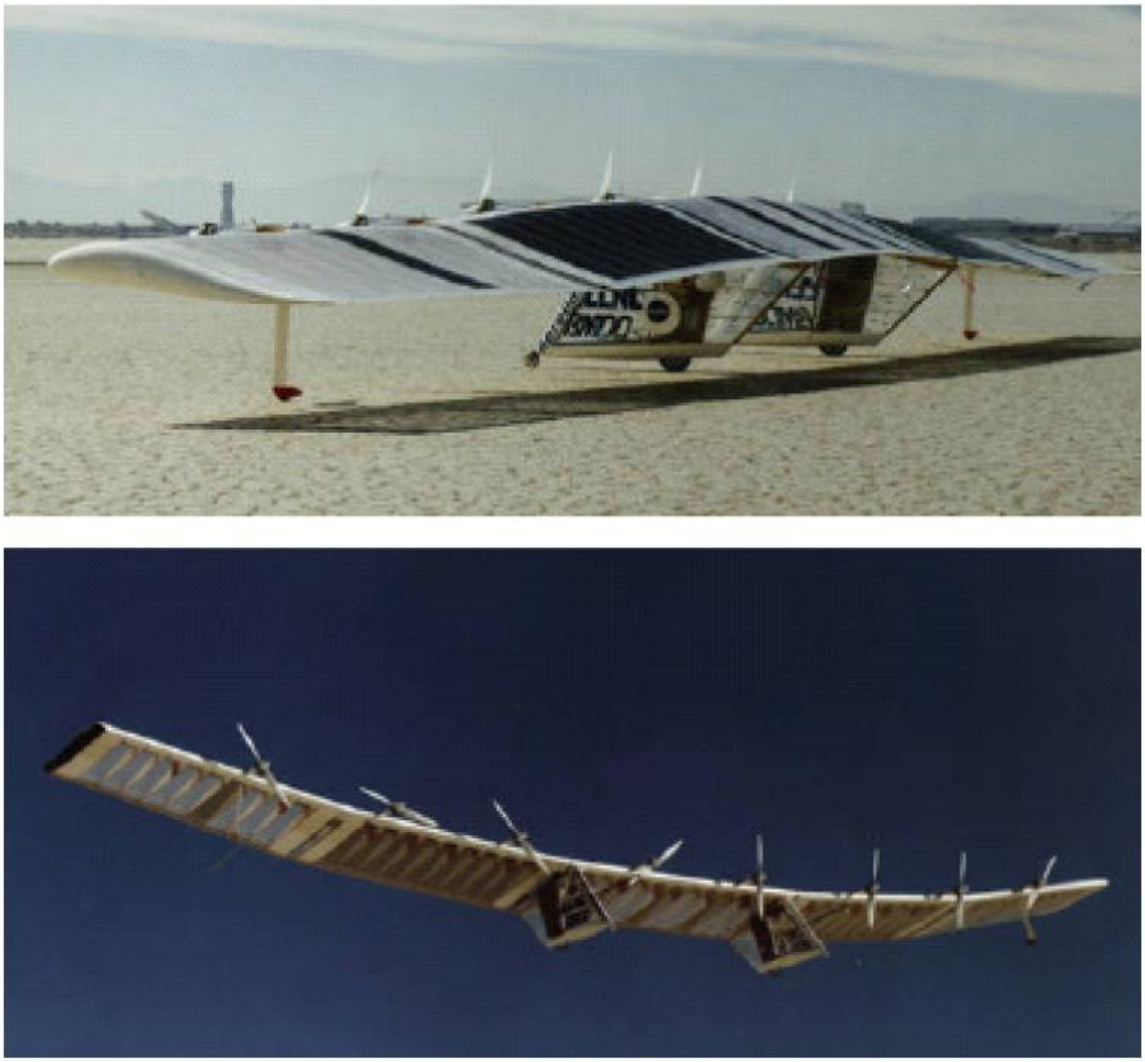

Figure 1: The solar-powered aircraft with a URFC-based energy storage system built in USA in mid 1990s (Mitlitsky *et al.*1999)

A portable power supply based on a reversible fuel cell was proposed and developed by LLNL in 1993 (Mitlitsky *et al.* 1999). The design was similar to their previous work. Actually pressurised hydrogen and oxygen were generated and stored in the storage tank in electrolysis mode using electricity supplied by solar PV panel. In fuel cell mode the hydrogen and oxygen were fed back to the URFC system to generate power and run the propeller. The maximum power able to be supplied was in the order of 5 W. Figure 2 shows this system. The URFC comprised a stack of nine cells each with active area around 46 cm^2. Several versions of this URFC propeller unit were built to demonstrate that from low pressure water electrolysis can commence (using solar power) to produce pressurised hydrogen and oxygen in separate storage tanks (all embodied in transparent polycarbonate. The results in fuel cell

mode showed that the system can be useful for portable application below 5 Watts (Mitlitsky *et al*. 1999).

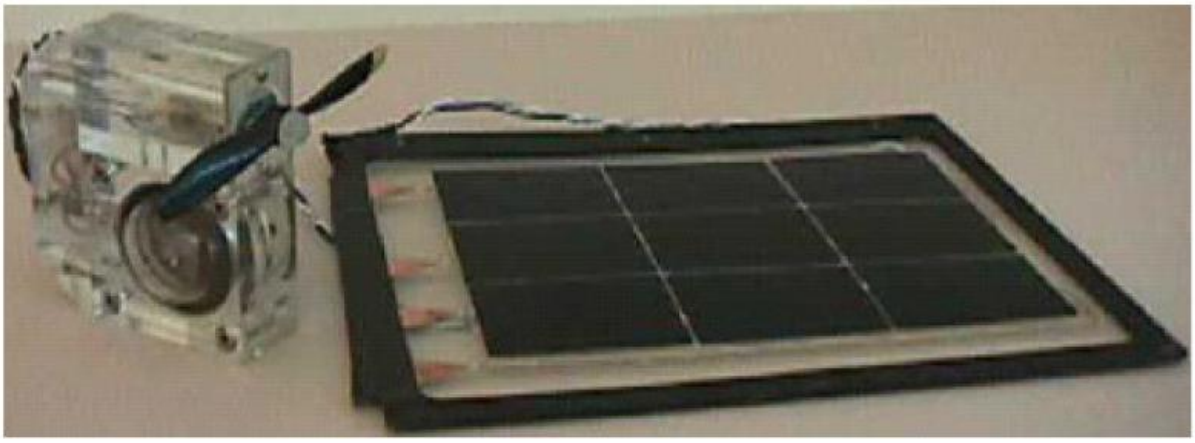

Figure 2: LLNL/ URFC unit (Mitlitsky *et al.*1999)

This early URFC system was developed primarily with autonomous unmanned aircraft vehicle (UAV) aircraft and airspace applications in mind. However, there was no information provided about the gas storing equipment and the amount of stored hydrogen and its rate of usage by the URFC.

LLNL was the first organisation during 1990s to design, construct and test URFCs. Although all their applications mainly were limited to airspace, it was the first attempt to develop such a system to store energy based on solar energy that is renewable and sustainable. The United States was thus the early leader in this field of study due to all the companies and researchers involved, such as United Technology, Hamilton Standard, Giner Inc, Lynntech Inc, with governmental support from the US department of energy) NASA, and the US Missile Defence Agency aerospace application.

In 1998 Proton Energy Systems has developed a commercial product (Unigen reversible module), consuming 15 kW on electrolysis mode and could get up to 5 kW on fuel cell mode (Mitlitsky *et al.* 1999),

The scientists in Netherlands recently improved the R&D projects on URFC to develop energy supply system and power supply such as using solar PV panel to produce hydrogen for long term energy storage. This work has been conducted by Hynergreen Technologies,

Spain, Fraunhofer-Gesellschaft, Germany, NedStack Fuel Cell Technology, and others (Nedstack, 2007).

In Russia, plus working with French group Grigoriev and co-worker in 2010 developed URFC stack made by seven electrochemical cell (each active area around 256 cm^2) and by consuming 1.5 kW in electrolysis mode could get 0.5 kW of electricity in fuel cell mode. A mean cell voltage of 1.74 V has been measured during electrolyser mode at 0.5 A cm^{-2} (85% efficiency) and a mean cell voltage of 0.55 V has been measured during fuel cell mode at the same current density (37% electric efficiency). Figure 3 shows the experimental setup which has been set to evaluate the electrochemical performance of the stack.

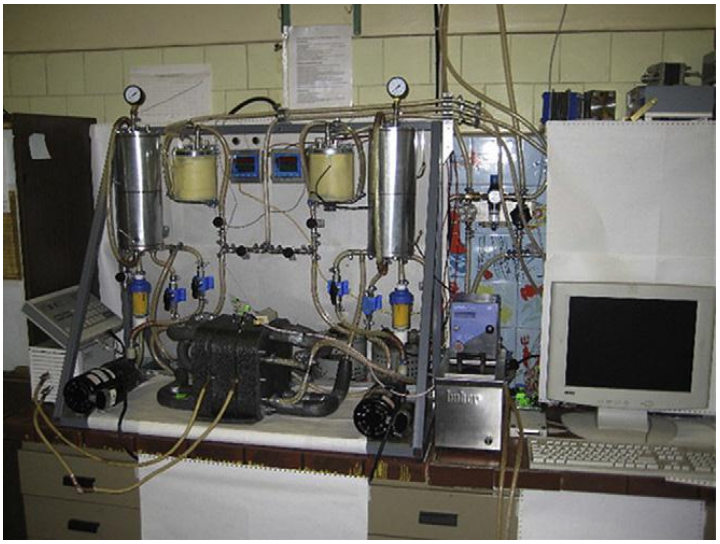

Figure 3: URFC stack with thermal insulation installed in the test bench. (Grigoriev *et al.* 2011)

In China Su *et al.* (2009) designed, fabricated and tested the performance of a novel micro planar fuel cell power supplier, in which a six-cell PEM unitised regenerative fuel cell (URFC) stack was used as the power generator. They fixed each cell by sandwiching a membrane electrode assembly (MEA) between two graphite monopolar plates. When the stack was used in electrolysis mode, the hydrogen was generated by splitting water and stored using a hydrogen storage alloy as a metal hydride. In fuel cell mode, the stored hydrogen was supplied by the hydrogen storage alloy along with the oxygen from air. The results showed that at room temperature and atmospheric pressure, the open circuit voltage of the stack reached at around 4.9 V and the working voltage was around 2.9 V. A maximum power density of 74.8 mW cm^{-2} was obtained at 34 mA cm^{-2} in fuel cell mode. One of the problems

encountered with this stack used was that it was only able to maintain stable performance for 10 charge-discharge cycles.

Over recent years, many research workers have focussed on optimising URFCs by working on improved electrodes, electrolytes and storage mechanisms. For example, Yim *et al.* (2005) prepared several electrocatalysts such as Pt black, and mixed materials such as PtIr, PtIrOx, PtRu, PtRuOx and PtRuIr for the oxygen electrode to fabricate higher efficiency bifunctional electrodes. They found PtIr showed the best URFC performance. On the other hand PtIr catalyst with just 1 wt% Ir had the highest URFC roundtrip energy efficiency.

Another significant work on developing an improved oxygen electrode by introducing membrane electrode assemblies (MEA) has been done by Wittstadt *et al.* (2005). They used different MEAs in fuel cell and water electrolysis mode at different pressure and temperature conditions. The results indicated that better performances in both charging and discharging modes could be achieved with an additional layer of sputtered platinum on the oxygen electrode, leading to an increase by 4% in the roundtrip energy efficiency.

Chen *et al.* (2008) continued the work done by Wittstadt (2005) by introducing a novel membrane electrode assembly to be used in URFC by using the Nafion polarization method. The URFC using the novel MEA showed a higher performance during water electrolysis, and a much higher fuel cell performance, than those of the URFC using the conventional MEA. The efficiency in fuel cell mode, and roundtrip energy efficiency were reported as around 13.5% and 10.8% respectively at 700 mA/cm^2 with the novel MEA. The last three works mainly focused on the enhancement and development of the oxygen electrode. These researches did not show any effort and work to improve the hydrogen electrode as storage medium.

PEM URFCs can be classified into two types (Doddathimmaiah 2008). In the first one, hydrogen is produced on one electrode in electrolysis mode and used on the other electrode in fuel cell mode. The same arrangement applies for oxygen as well. The second type, which is closer to our work, involves an exclusive hydrogen electrode and an exclusive oxygen electrode. Hence hydrogen is produced and consumed on the same electrode, and the same applies for oxygen too. Figure 4 shows the schematic of this type.

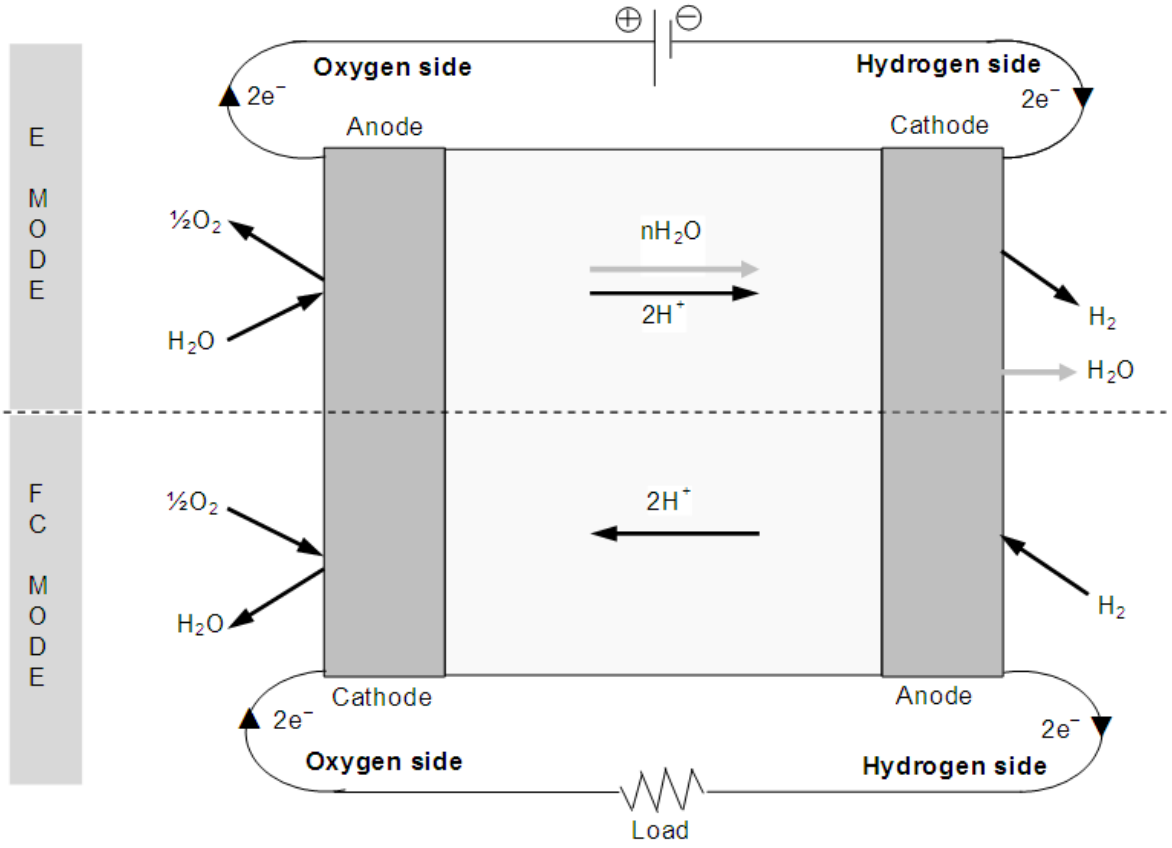

Figure 4: Schematic of constant electrode type PEM URFC (Doddathimmaiah, 2008)

The advantage of this type is that hydrogen and oxygen are completely separated and never mix. Another one is that water enters and is re-formed on the same electrode.

Based on this brief review of the literature, the novel technology of URFCshas been a subject of considerable interest in the field of storing energy. A lot of research has focussed on improving electrolytes and electrocatalysts, and oxygen and hydrogen electrode types, to boost performance in both electrolyser and fuel cell modes, and hence lift roundtrip fuel cell efficiency. The majority of works in the 1990s were concentrated on aerospace and aircraft applications using solar PV panels as the primary electrical energy source. Also the application of using URFCs were just limited to the aerospace and aircraft while there are many other active areas such as battery and vehicle applications which are needed to be improved. Today many researchers and projects are conducted in the field of storing hydrogen and representing a suitable medium that can lead to get the maximum storage capacities. The concept of this new approach will be investigated in next chapter.

3.2 Proton battery

3.2.1 The concept of the proton battery

A conventional hydrogen fuel cell system for electrical energy storage is shown in Figure 5, which includes electrolyser, compressor, storage media and fuel cell (Andrews and Seif Mohammadi 2014).

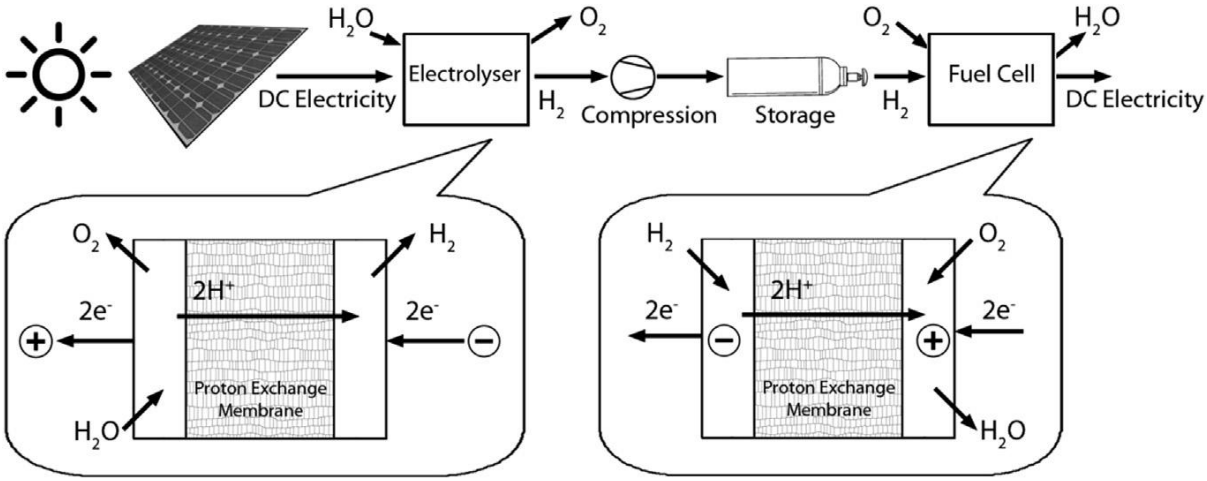

Figure 5: The conventional system for storing electrical energy as hydrogen and then regenerating electricity (Andrews and Seif Mohammadi 2014)

In charging mode, electricity can be supplied from a PV panel to split water molecules into hydrogen and oxygen. Then hydrogen gas is compressed and stored in a storage medium such as a gas cylinder under pressure.

In discharge mode, the stored hydrogen is supplied to the fuel cell where it reacts electrochemically with oxygen (usually from the air) to produce electricity and water.

One of the disadvantages of this system is its complexity in comparison to batteries. The hydrogen system has many more components. It needs a compressor and hence some additional electricity usage to compress the hydrogen gas and send it to the storage medium. The hydrogen produced in the electrolyser is transferred as a gas into a separate compressed gas or solid-state storage. . All these steps involve net energy losses and entropy increases

(Andrews and Seif Mohammadi 2014). Hence the roundtrip electrical energy efficiency (around 40-50 %) is much lower than that of batteries (at 70-80 %)

A novel system proposed by Andrews and Seif Mohammadi (2014) working at RMIT SAMME is shown in Figure 6, which they originally termed a 'proton flow battery'They called their system a "proton flow battery" because in charging mode just an inflow of water is needed, and in discharge mode just air is fed into the cell. More recently, as explained in chapter 1, the name of this concept has been shortened to simply a 'proton battery'.

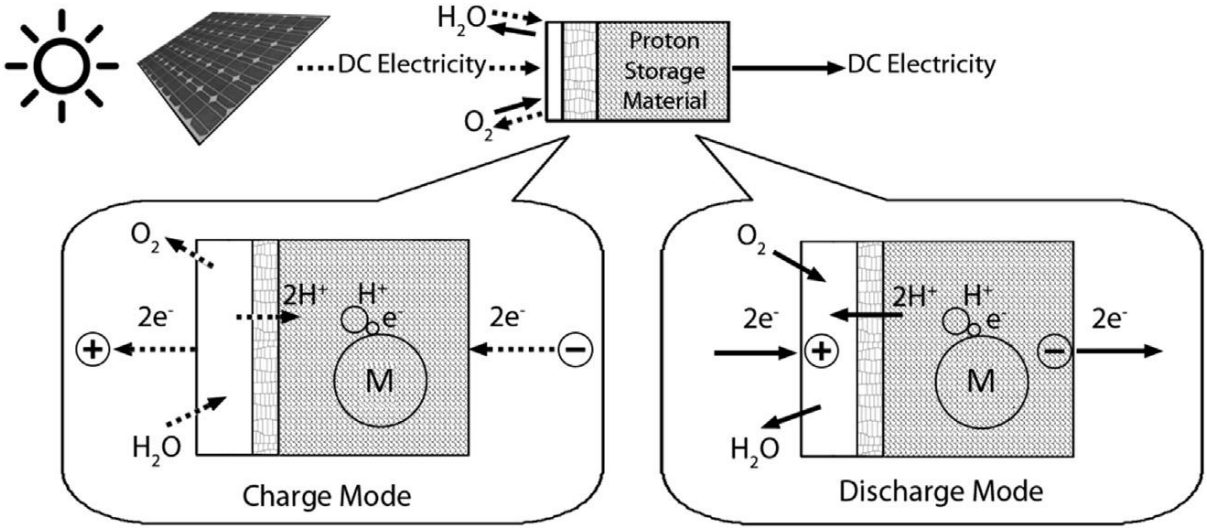

Figure 6: A proposed novel system employing a reversible fuel cell with integrated solid proton storage electrode. M represents a metal atom of the solid storage to which a hydrogen atom is bonded (Andrews and Seif Mohammadi 2014)

In this new system, the protons produced during electrolysis diffuse straight into the solid-state storage to form a bond with the storage material, without combining with electrons to form hydrogen gas molecules and without this gas being compressed for storage.

In fuel cell mode this process is reversed, with hydrogen atoms being released from the storage and giving up an electron to become protons once again. These protons then re-enter the membrane and move back to the oxygen side where they combine with oxygen and electrons from the external circuit to re-form water.

In the proton battery, therefore, many components in the conventional hydrogen-based energy storage system that cause energy losses and irreversible entropy increases are omitted, such as the compressor, compressed gas storages, the associated valves and regulators.

The new system has potentially some advantages over the conventional type such as higher mass and volumetric densities and higher roundtrip energy efficiency.

In the initial design for a proton battery investigated by Andrews and Seif Mohammadi (2014), a solid-state electrode made from a metallic alloy was used for hydrogen storage that is, by formation of a metal hydride from the protons emerging from the membrane and electrons supplied from the external circuit (Figure 7).

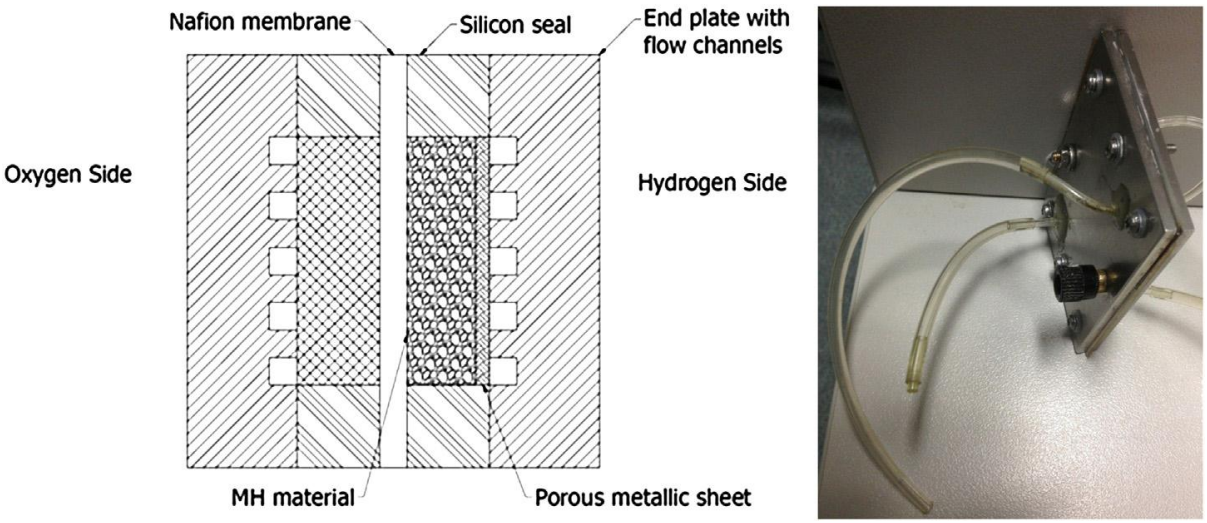

Figure 7: Schematic design (left) and picture (right) of the experimental proton flow battery system, based on a modified URFC cell packed with MH material as the hydrogen storage electrode. (Seif Mohammadi 2013; Andrews and Seif Mohammadi 2014)

The rationale for this design is to fill the gaps between the irregularly-shaped metal particles with nafion, thus providing a continuous medium within the electrode for transport of protons from the cell membrane to the metal particles with which they can react to form MH. In discharge mode, the continuous nafion medium conducts the protons produced from the reverse dehydrating reaction back into the cell membrane.

To make the MH-nafion composite electrode, 0.609 g of MH powder was mixed with 4.5 ml of nafion solution. Then the mixture was left at room temperature for 12 h and stirred every hour to ensure homogenous deposition of nafion over the MH particles.

The electron conductivity of the MH material used to fabricate the hydrogen storage electrodes was measured to be around 124 S/cm. A composite MH-nafion electrode with the same composition but with an area of 0.2×0.2 cm^2 and thickness 0.074 cm was also tested for electron and proton conductivity. The results in different humidity are shown in Figure 8. Interestingly by increasing the relative humidity, and hence degree of hydration of the membrane, proton conductivity will increase, while the electron conductivity decreases (Figure 8).

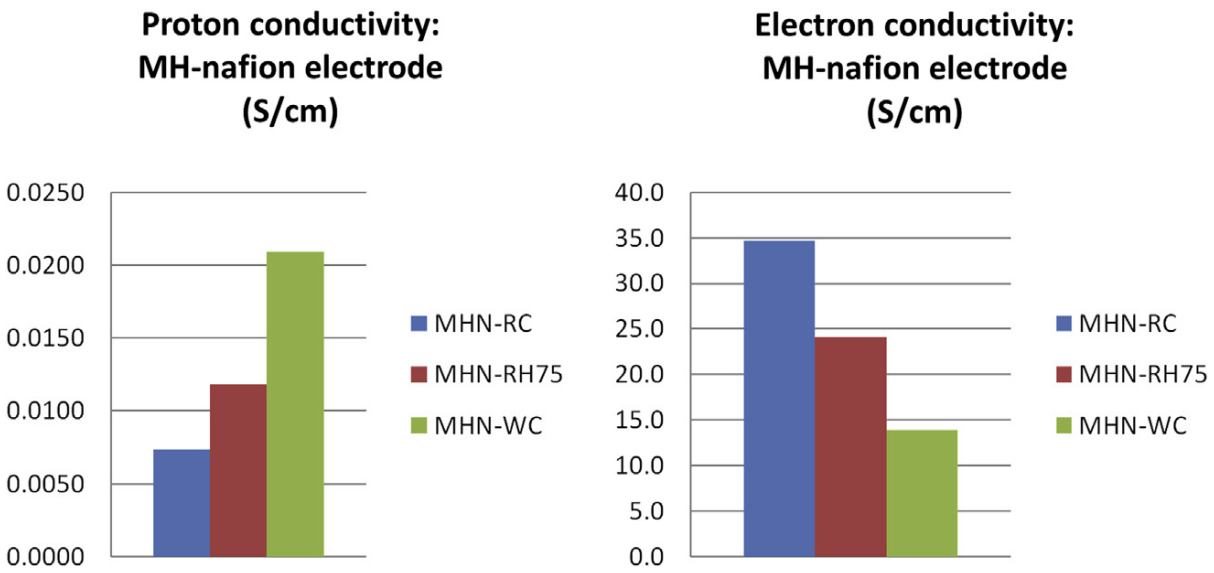

Figure 8: Measured proton and electron conductivities of the MH-nafion (MHN) composite electrode at varying levels of relative humidity and hence hydration of the electrode: RC e room conditions, 25 C, relative humidity 60%; RH75 e relative humidity 75%; WC - fully hydrated electrode, 'wet' condition.

Andrews and Seif Mohammadi found that this early proton battery system had a hydrogen storage capacity of 0.6 wt%; although the amount of hydrogen actually recovered to run the device in fuel cell mode was much lower. This early work did, however, at least indicate that a proton battery system could be technically feasible

3.2.2 Limitations of MH storage electrode

These experiments on a proton battery with a MH electrode revealed a number of limitations and disadvantages in using this material as the hydrogen storage electrode.

Firstly, there was still a significant rate of hydrogen gas production at this electrode alongside the direct bonding of protons with the metal after neutralisation with electrons during charging/electrolyser mode to form a hydride. . One of the likely reasons for this hydrogen gas production was the presence of nickel in the metal alloy powder employed to make the hydrogen storage electrode, which is known to be quite a good catalyst for the hydrogen evolution reaction (S. Mohammadi 2014). Any hydrogen gas production on the negative electrode of a proton battery when charging is not desirable since it results in proportionately less electrochemical hydrogen storage actually within the electrode.

Secondly, the metal alloy powder used in the electrode is very expensive and heavy, since it contains rare earth elements with high atomic mass.

Thirdly, with the particular MH used in this case, the hydrogen storage capacity obtained was only around 0.6 wt%, and in discharge mode very much lower than this again with only a fraction of the stored hydrogen being able to be released. The bonds between the hydrogen and metal particles may this have been stronger than required for this application.

3.3 Electrochemical hydrogen storage in carbon-based materials

3.3.1 Potential advantages of carbon electrodes in a proton battery

An alternative to a metallic hydrogen storage alloy in a proton battery is the use of a porous carbon-based material with electrochemical storage of the hydrogen on its large internal surface area. This option is considered in the following subsections.
Possible advantages of such carbon materials in a proton battery are the following;

- Carbon is cheap compared to metal alloys
- Carbon is lighter in terms of atomic mass

- Carbon is structurally stable to chemical and heat
- Carbon materials can be synthesised that are porous material with a large active area for storing hydrogen.

In the present study, the carbon-based material focussed on is activated carbon, with some consideration also of graphite particles and platelets. Other candidates such as carbon nanotubes, layered graphene materials, and layered carbon nitrides will not be investigated here, although they may in the future be found to be excellent candidates for electrochemical hydrogen storage.

3.3.2 Activated carbons

Activated carbons (ACs) are highly porous and very stable to chemicals and heat (Wang *et al*, 2010). ACs can be synthesized from a variety of inorganic precursors such as black and brown coal (REF); and organic precursors including agricultural wastes, such as coconut shells and fibres, jute fibres, nut shells, soybeans, and oil seeds. There are different types of activated carbon based on the precursor material. Actually activated carbon can be made from coconut shell, wood and peat, corn cob, banana peel, pistachio-nut shell, oil sands coke, wood sawdust, fruit stones and many other materials (Chang *et al.* 2000; Lua and Yang 2004; Mopoung, 2008; Chen and Hashisho 2012). Among aCs made from organic materials, the coconut shell based activated carbon has a predominance of micropores that are suitable for adsorption of small molecular weight species. In contrast, wood and peat-based activated carbons have a predominance of macro and mesopores structure, which are ideal for adsorption of larger molecular species (Vargas *et al.* 2010).

Typical synthetic methods include the generation of highly porous structures via physical or chemical activation. Physical activation involves the gasification of carbonaceous materials in the presence of suitable oxidising agents, CO_2 and steam. In physical activation process, the based material or rich carbon based material is first carbonized in absence of air. Then the activation process is performed with an oxidation specie such as Co2 or steam or a mixture of both of them. The temperature required for the process is in the range of 800-1200C (Vargas *et al.* 2010; Zhao *et al.*, 2013; Sahin and Saka, 2013). Zaini *et al.* (2010) showed that activation with steam may result in more porosity than CO2. The reaction between carbon and oxidation species are as follow are (Marsh and Rodriguez-Reinoso, 2006):

$C + CO_2 \rightarrow 2CO$

$C + H_2O \rightarrow CO + H_2$

In chemical activation, porosity is generated via chemical reactions between agents, usually KOH, and carbonaceous materials, followed by the production of CO_2 generating further porosity, from the decomposition of K_2CO_3 in the case of KOH activation. In this case the activation process is carried out with a chemical component such as zinc chloride, phosphoric acid, sodium hydroxide and potassium hydroxide, in absence of oxygen. Then the activated carbon should be washed with water and dried. (Marsh and Rodriguez-Reinoso 2006; Linares-Solano *et al*. 2012). The chemical activation method has several advantages over the physical activation method, including a lower processing temperature, shorter processing time, and higher porosity. (Yang *et al*. 2012).

Pores in activated carbons are categorised based on their diameter (Marsh and Rodriguez-Reinoso 2006; Achaw 2012):

- macropores, with diameters greater than 50 nm,
- mesopores between 2 and 50 nm,
- micropores between 0.7 and 2 nm, and
- ultra-miropores< 0.7 nm.

So activated carbon may be a suitable medium to be used in the negative electrode of the proton battery to store hydrogen. It has been shown previously that ultramicropores smaller than 0.7 nm are the main sites for electrochemical storage of hydrogen (Vix-Guterl *et al.* 2005).

Gamby *et al.* (2001) tested various activated carbons from the PICA company in order to compare their properties and performances. Figure 9 shows a comparison the resistance and BET surface area for eight different activated carbon name: Norit, PICA A, B, C, D. E and PICACTIF SC.

	Norit	PICA A	PICA B	PICA C	PICA D	PICA E	PICACTIF SC
BET surface (m^2/g)	1200	2315	2100	1500	2100	1500	2315
Resistivity (Ω cm)	3	1.99	0.47	0.72	0.47	0.72	1.99

Figure 9: physical characteristics of the different activated carbon powder tested (Gamby et al. 2001)

These experimental results show that PICACTIF SC type has the best performance to be used as supercapacitor since it has an acceptable BET surface area with a reasonable resistance. The capacitance of an electrode made from of this type of aC was measured to be around 125 F/g.

Sabio and Reinoso (2004) investigated the role of activation method on activated carbon porosity. They chose precursor materials such as olive and peach stones and used phosphoric acid, zinc chloride and potassium hydroxide as activating agents. The results showed that H_3PO_4 leads to a more heterogeneous pore size distribution, while KOH only produce a widening of micropore width.

Yagmur *et al.* (2008) made activated carbon from wasted tea. Activation process has been done by phosphoric acid with and without microwave treatment. The maximum BET surface area was measured around 1157 m^2/g. They showed that the micropore surface area is higher for the sample treated by microwave energy. In other words, microwave heating enhanced both the micropore surface area of the samples as well as the BET surface area.

Harris *et al*. (2008) imaged atomic structure of activated carbon for the first time, using TEM. Figure 10 shows the atomic structure of as-produced carbon and of the carbon following heat treatment at 2000 C.

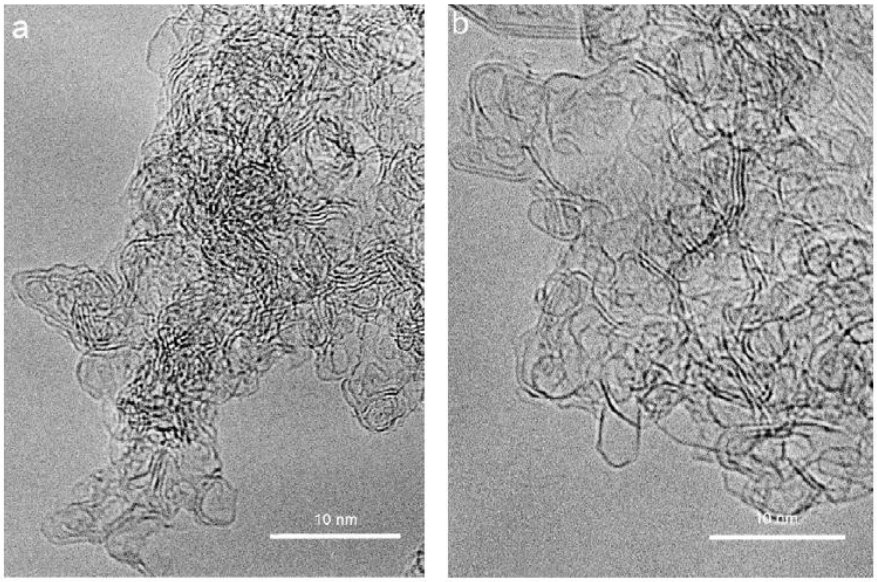

Figure 10: General appearance of (a) fresh activated carbon, (b) activated carbon following heat treatment at 2000 ◦C (Harris et al. 2008).

The results show such a hexagonal ring for fresh activated carbon and non-hexagonal ones. The 200 C heated carbons contain large hexagonal networks. The presence of some pentagonal rings which are naturally porous also has been reported in some cases. One can obtain is that the heating process may lead to larger hexagonal networks as mentioned.

3.3.3 Storage of gaseous hydrogen in activated carbons

Activated carbons (aCs) are highly porous and very stable to chemicals and heat. For these reasons, aCs have been extensively considered for storage of gaseous hydrogen by adsorption of hydrogen molecules onto the inner surfaces of pores (Wang *et al,* 2010).

For example, in Spain Casa-lillo *et al.* (2002) measured the gaseous hydrogen storage capacity of variety of activated carbons over a wide range of pressures (up to 70 MPa) at ambient temperature. For the sample activated carbon from anthracite tested in their experiment they could not find large amount of hydrogen adsorbed. In any case an activated carbon provided around 1 wt% hydrogen storage at 10 bars.

Cazorla Amoros *et al. (*2007) prepared a series of activated carbon using KOH activation method from anthracite and bituminous coal. The activated carbon material had a very high BET surface area at 3000 m^2/g. the gaseous hydrogen storage capacity was measured at

around 1.2 wt% at room temperature (298K) and 200 bar. This work indicated that the micropore and narrow pore size distribution played an important role in hydrogen storage capacity.

Wang *et al.* (2008) prepared activated carbon with high internal surface area of pores by using the KOH chemical activation method. The activation method, using KOH shows remarkable changes in porosity compared to CO_2 activation method. Thus KOH activation may lead to microporosity frameworks in the activated carbon. The results showed a high surface area of up to 3190 m^2 g^{-1}. There was a large gravimetric hydrogen uptake capacity of 7.08 wt % at 77 K and 20 bar pressure, but of course this at a very-low cryogenic temperature

Gao *et al.* (2009) applied two activation methods (physical and chemical) to commercial aC samples and showed that the chemical activation method (KOH) provided a much larger narrow micropores (<1nm) than the physical one. The hydrogen storage capacity was measured at 77 K and 1 bar of around 2.49 wt% and at 77 K and 20 bar of around 7.08 wt%. The results indicated that very low temperature is required for a significant hydrogen storage.

The results of Wang *et al.* and Gao *et al.* showed that a significant quantity of hydrogen can be stored in activated carbon material but only in very low temperature (77) and moderate pressure (20 bars). This very special condition required to achieve low temperature causes a large amount of energy loss during the hydrogen storage which decreases the roundtrip efficiency of the system.

In sum then, activated carbons can be used for storage of gaseous hydrogen by adsorption of hydrogen molecules on pore surfaces. However, cryogenic temperatures and very high pressures are required to achieve usable gravimetric energy densities, with consequent technological complexity and cost, as well as considerable parasitic energy.

3.3.4 Previous work electrochemical storage of hydrogen in activated carbons

An alternative to gaseous storage of hydrogen in aC is electrochemical storage. This has the possible advantages of allowing charging at near ambient pressures and temperatures, and the achievement of high gravimetric and volumetric densities.

The concept of storing hydrogen electrochemically within activated carbon was first proposed by Francois Beguin from CNRS-University, France and Krzysztof Jurewicz and Elizbeta Frackowiak from Poznan University of Technology, Poland. In their first paper Jurewicz *et al.* (2001) investigated the electrochemical hydrogen storage in activated carbon electrode using potassium hydroxide (liquid KOH) of 6 $mol.L^{-1}$ concentration as an electrolyte. The amount of hydrogen released from carbon was reported 1.5%, which was higher than the amount adsorbed under ambient gas atmosphere. The importance of their work is that they stored hydrogen in carbon particles electrochemically for the first time and introduced an alternative way of storing hydrogen for metal hydride and gaseous hydrogen storage.

In their next paper Jurewicz *et al.* (2002) investigated the same concept but in a liquid alkaline electrolyte (KOH) and acidic electrolyte (H_2SO_4). In their experiment the cell was charged at a high current of 500 mA/g for around 12 hours to split water and produce protons, and subsequently discharged at a constant but much lower current. The authors reported the hydrogen capacity to be 1.8 wt% in the alkaline electrolyte, which was four times higher than the hydrogen adsorption capacity under 700 bar pressure for the same activated carbon sample. The hydrogen storage capacity in liquid acidic electrolyte was measured and reported as half that of the alkaline electrolyte. Unlike in the liquid alkaline electrolyte, no distinct discharge plateau was observed in the acidic electrolyte. The results clearly showed that activated carbon in both an alkaline and acidic electrolyte was capable of storing hydrogen electrochemically.

Jurewicz *et al.* (2004) further investigated the mechanism of electrochemical hydrogen storage in porous activated carbon with two types of electrolyte (KOH and H_2SO_4 (aqueous solutions)). The results showed that the total amount of hydrogen adsorbed, and consequently the storage capacity, depended on the kinetics of hydrogen diffusion and incorporation into the nanopores. The low overvoltage value of H_2SO_4 (η=0.32 V) may have led to molecular hydrogen evolution through the chemical (Tafel) or electrochemical (Heyrovsky) reactions and the amount of hydrogen stored decreased. On the other hand KOH showed a higher polarization value (η=0.55 V) and resulted in more hydrogen adsorption. The authors reported a meaningful sorption of hydrogen in an alkaline electrolyte with reversible capacity of 1.3 wt% corresponding to 350 mAh/g. (Based on Faraday law, 1 wt% hydrogen storage is equivalent to a charge flow of 270 mAh/g).

Vix-Guterl *et al.* (2005) used highly-ordered porous carbon materials for supercapacitor applications and electrochemical hydrogen storage. The surface area, pore size distribution and different pore sizes of activated carbon were estimated by CO_2 and N_2 adsorption. The results showed a linear relation between the amount of hydrogen storage and volume of ultramicropores (that those with diameter smaller than 0.7 nm). The stored value of 388 mAh/g, which corresponds to 1.44 wt%, was obtained in their experimental results.

Another significant work in electrochemical storing hydrogen in porous carbon has been done by Fang *et al.* (2006). They worked on physical characteristic and electrochemical hydrogen storage behaviour of the ordered porous carbon with well-tailored pore size. According to their findings, a discharge capacity of around 1.95 wt% hydrogen storage was achieved in 6 M KOH. They also found that ultramicroporous media (pore size smaller than 0.7 nm) played the predominant role in hydrogen storage, while meso and micro porous media served as mass transport pathways for rapid hydrogen.

Another significant paper by this group was published in 2006 (Beguin *et al.* 2006). They investigated specifically the mechanism of bonding between carbon and hydrogen in a reversible hydrogen storage system. They reported that hydrogen formed a weak bond with carbon in the electrolyte mixture of water and KOH, with activation energy of around 110 KJ/mol.

Babel and Jurewicz (2008) investigated physical, chemical and electrochemical properties of activated carbon (LAC) produced from lignin processed by standard carbonisation and KOH activation at a temperature of 950 C. They fabricated a highly porous carbon that had a BET surface area of almost 1946 m^2/g with 31% of the micropore volume comprising pores between 0.5 nm to 0.64 nm, that is, ultramicropores. The activated carbon possessed a high hydrogen storage capacity of 1.89 wt%. They suggested that high porosity with large micropores and small mesopores volume contributes positively to the hydrogen storage capacity.

The next publication of this group presented a schematic for a secondary battery that used the principle of a reversible electrolyser/fuel cell in an aqueous KOH electrolyte (Jurewicz *et al.* 2009). Figure 11 shows the schematic of the proposed system, which was named a ‘rechargeable fuel cell’.

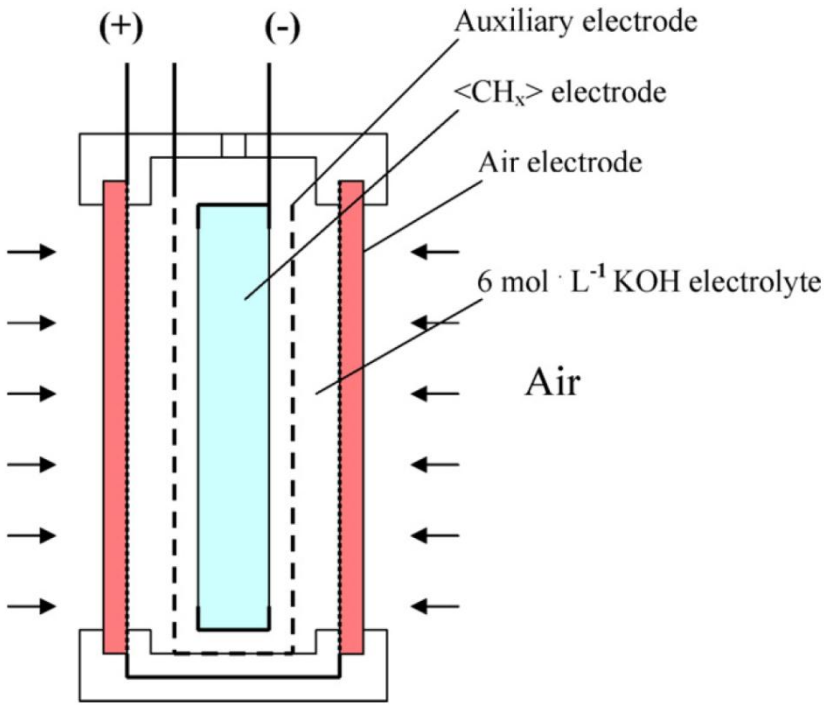

Figure 11: Schematic representation of the rechargeable fuel cell proposed by Jurewicz et al. (2009)

As can be seen in Figure 11, the carbon electrode is placed between two parallel diffusion air electrodes, which are electrically connected and form the cell walls. The carbon electrode was made of four layers of activated carbon. The auxiliary electrode was made from nickel gauze to avoid oxygen evolution, which can result in carbon oxidation.

Frackowiak (2010) investigates the bond between hydrogen and carbon. In her assumption carbon is considered as the host specie and hydrogen as the guest specie. She mentioned that the reversibility of the hydrogen within the carbon materials is guaranteed by a week chemical bonding H-C. She confirms that the binding energy of H-C about 110 kJ/mol and so electrochemical storage of hydrogen in carbon can be categorised as chemisorption.

In summary, this research group was one of first to demonstrate that hydrogen can be stored electrochemically in carbon media, with the focus on activated carbon. However, generally the majority of hydrogen produced in their studies was in the form of gas that was not stored in the solid media

Lota *et al.* (2011) studied the effect of charge parameters on hydrogen storage capacity. They used a new pulsed method of charging the electrodes, in which the carbon electrode is charged for few seconds, left to rest for few seconds, and then charged again. These pulse-

pause sequences were repeated several times. By using optimal parameters of 1 second pulses of 5 A/g and 0.5 second pauses for a total charging time of 9 minutes (6 min. charging + 3 min. pauses), the activated carbon was charged to about 60% of its total capacity (1.08 wt%). The authors concluded that the quick faradaic processes are the advantage for using in power devices. They investigated the effect of temperature on hydrogen storage capacity of activated carbon and show that a 10% improvement was achieved when temperature is elevated from 25°C to 60°C, confirming the result of Beguin *et al.* (2006). Figure 12 shows the proposed schematic of the system with a bonding reaction between carbon and hydrogen atoms (Lota *et al.* 2011).

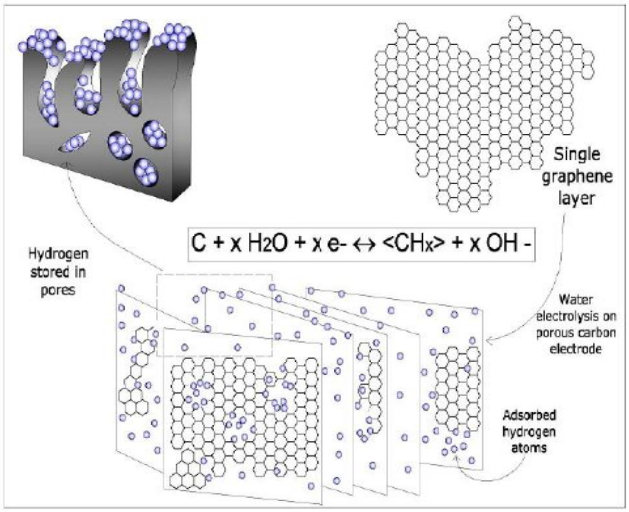

Figure 12: Illustration of hydrogen electrosorption in carbon material (Lota *et al.* 2011).

Candelaria *et al.* (2011) in their paper reviewed the structure of carbon for storing energy. They showed that highly porous carbon can be categorised into two forms: (1) derived from naturally occurring carbonaceous precursors such as coal, wood, coconut shells, fruit stones, and other agricultural byproducts; and (2) synthetic porous carbon. They showed that synthetic porous carbon can be used for supercapacitors. Based on their charge storage mechanism, there are two types of capacitors. The first one is electrochemical double layer capacitors (EDLC) based on activated carbon in which capacitance is proportional to porous surface area. For the EDLCs, the capacitance at one electrode interface is given by C=eA/4pt (where e is the dielectric constant of the electrical double-layer region, A the surface-area of the electrode, and t the thickness of the electrical double layer) (Candelaria *et al*. 2011).

Based on the high surface area of synthetic porous carbon, they are a suitable medium to be used in carbon electrode side in a fuel cell due to high capacitors for storing hydrogen.

Babel *et al.* (2012) investigated electrochemical hydrogen storage in several activated carbons from different precursors. They selected different types of activated carbon made from coconut shells, blackthorn stones, cellulose and lignin. The highest hydrogen storage capacity was obtained by using activated carbon made from blackthorn stone after 15 min activation at 950 C and a carbonisate/ KOH ratio of 1/5 around 2.31 wt%.

3.3.5 Proton conduction within electrodes for electrochemical hydrogen storage in activated carbons

3.3.5.1 Rationale

For electrochemical hydrogen storage in activated carbon, protons which have been produced from water electrolysis process need a proton conducting medium to provide the pathway into the storage material. In the following sections, solid-state and liquid-type of proton conductors are introduced.

3.3.5.2 Solid state – nafion

The idea of using an organic cation exchange membrane as a solid electrolyte and hence proton conductor in electrochemical cells was first proposed by Grubb (1959). A schematic of his polymer electrode fuel cell consisting of two electrodes and a solid polymer membrane is shown in Figure 13 (Grubb, 1959). The polymer electrolyte membrane is sandwiched between two platinum porous electrodes such as carbon paper. This polymer proton conducting media can be a solid membrane such as nafion, or a family of acids or a proton ionic liquid.

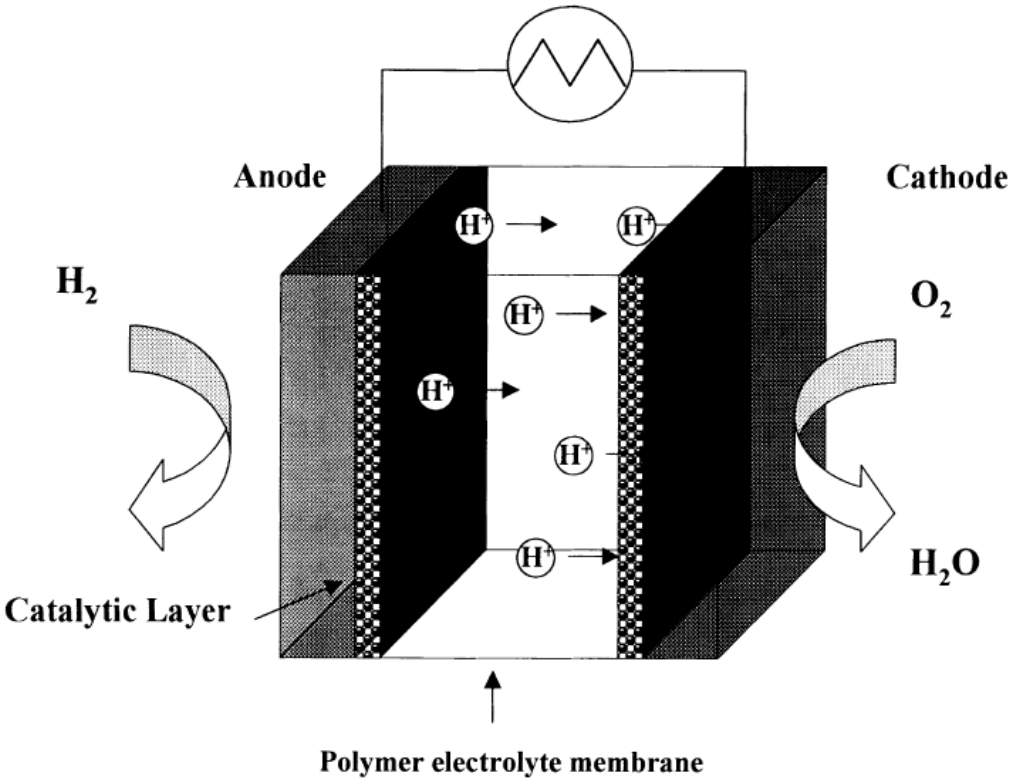

Figure 13: Schematic of a PEM membrane in a fuel cell, (Grubb, 1959).

Hofmann *et al.* (2007) investigated conduction on water molecules using molecular dynamics (MD). Water as one of the most important proton conductors has always been a point of interest in simulation and analysis. Hofmann *et al.* introduced a new reactive potential based on a radial distribution function. The results showed that the new potential described correctly the radial distribution functions of water over a wide range temperatures and pressures. The results of the MD simulations showed that the reactive potentials could reproduce the main features of structure and dynamical properties of water, including the geometry of water molecules and proton transfer on a classical level, in good agreement with the experiment

In their next paper this group performed a theoretical simulation of proton conductivity in nafion. The results further showed that the maximum proton diffusion in Zr-phosphate appears at pKa= 0.5. Similarly, in an idealised nafion tube it is found that conductivity also gets a maximum value with the rate of dissociation of sulphonate groups of 27%. This result

demonstrated that proton conduction in such tubes has some common features with topological solitons (Hofmann *et al.* 2010)

Another significant work has been done by Pisani *et al*. in 2008. The authors used molecular dynamic simulation and showed that protons in an acid solution form hydronium, H_3O^+ ions. The also identified the two main proton transport mechanisms in acid solution as:

1. migration of hydronium ions (vehicular diffusion)
2. Jumping of a proton from a hydronium ion to an adjacent water molecule (structure diffusion, or the Grotthus mechanism).

The first transport mechanism is classical and it encounters translational friction resistance. The second mechanism implies the breaking and formation of weak hydrogen–oxygen bonds.

Another significant work done in the field of theory of proton conduction in nafion is Choi *et al.* (2004). They presented their first analytical investigation on thermodynamics parameter and proton transport concept in nafion in 2004. They proposed a sorption model based on the thermodynamics analysis using the Flory-Huggins' activity model and Freger's elastic model. They showed for a given polymer system, the sorption amount per unit mass of dry polymer increased with acid strength.

In their next paper, they proposed a new method to represent proton conductivity and diffusion of protons in nafion. They showed that proton conductivity in nafion is highly dependent on its nanostructure and water content. For example, at low water content, the interaction of water molecules and hydrogen bonding is low, resulting in very low conductivity (Choi *et al.* 2004). The main transport mechanisms of protons in nafion were found to be:

- vehicular transport, that is, straight movement of hydronium ions
- the Grotthus mechanism, which is transfer of a proton from hydronium to a neighbouring water molecule thereby turning it into hydronium and leaving a water molecule behind, or
- hopping of protons along the surface of pores within nafion from one SO3- group to the next one.

At RMIT Unviversity, Jazaeri (2014), in his M Eng (by research) thesis, investigated the feasibility of a unitised regenerative fuel cell with a reversible carbon-based hydrogen storage electrode. He used various forms of activated carbon to test for reversible and direct hydrogen storage. He used three main activation methods, physical activation by CO_2 and steam, chemical activation by KOH, and replica method by silica templates. He also mixed activated carbon with nafion to provide a proton conductor within the electrode.

Jazaeri (2014) measured proton and electron conductivity by experiment in different relative humidity environments. He found that the proton conductivity of the aC-nafion composite materials (due the nafion) increased with increasing relative humidity and reached its maximum when the nafion in the composite had been fully hydrated. The values obtained for proton conductivity of the composite materials were between 0.044 and 0.11 S/cm at full hydration environment. The proton conductivity under dry conditions was much lower, between 0.005 to 0.031 S/cm (Jazaeri 2013). On the other hand, the electron conductivity of the composite materials decreased with increasing relative humidity. The values of the electron conductivity at 0% relative humidity were in the range of 0.93 S/cm to 28 S/cm for composite electrode.

A possible explanation of this lack of observed hydrogen storage is that the nafion medium could not penetrate into the porous structure of the activated carbon particles. Typically a basic nafion polymerised molecular unit has a main dimension of around 20 nm. The mesopores of activated carbons have diameters from 2 to 50 nm, while the ultramicropores where most hydrogen storage is expected to take place have typical diameters less than 0.7 nm. Hence it is most probable that nafion could not penetrate into even the mesopores, let alone the much smaller micro and ultramicropores (Jazaeri, 2014).

To address the problem of lack of nafion penetration into activated carbon identified by Jazaeri (2013), different types of proton conductors, such as acids and protic ionic liquids (Rana *et al.* 2012) that may penetrate into the porous carbon particles can be examined.

3.3.5.3 Liquid state– acid electrolytes

Another possible approach to proton conduction within porous carbon electrodes is to soak the electrode in a liquid acid as the proton conductor.

Bouchet and Siebert (1998) mixed PolyBenzImidazole (PBI) with H_3PO_4 , H_2SO_4 and HBr and measured the proton conductivity of this acidic liquid at a specific temperature, 300 K. The results showed that the best proton conductivity, 10^{-4} S cm^{-1} was achieved with H_2SO_4, It was suggested that the Grotthus hopping mechanism was the dominant contributor to proton conductivity.

Kawahara *et al*. (1999) continued Bouchet and Siebret's work a year later and mixed PBI with phosphoric, sulfuric, and hydrochloric acid separately .The mixture PBI/H_3PO_4 was thermally stable up to 500 C, while the proton conductivity reached 10^{-5} S cm^{-1} at 160 C.

He *et al.* (2003) prepared a mixture of PBI and phosphoric acid including zirconium phosphate (ZrP), ($Zr(HPO_4)_2 \cdot nH_2O$), phosphor-tungstic acid (PWA), ($H3PW_{12}O_{40} \cdot nH_2O$) and silico-tungstic acid (SiWA), ($H_4SiW_{12}O_{40} \cdot nH_2O$). The conductivity of the mixture (PBI/H_3PO_4) was measured at around 6.8×10^{-2} S cm^{-1} at 200 C and 5% relative humidity. The conductivity of the mixture was found to be dependent on the acid doping level, temperature and relative humidity.

Figure 14 and Table 1 classify different types of acid that can be used in polymer electrode membranes as a proton conductor as an alternative to the nafion used in conventional PEM fuel cells.

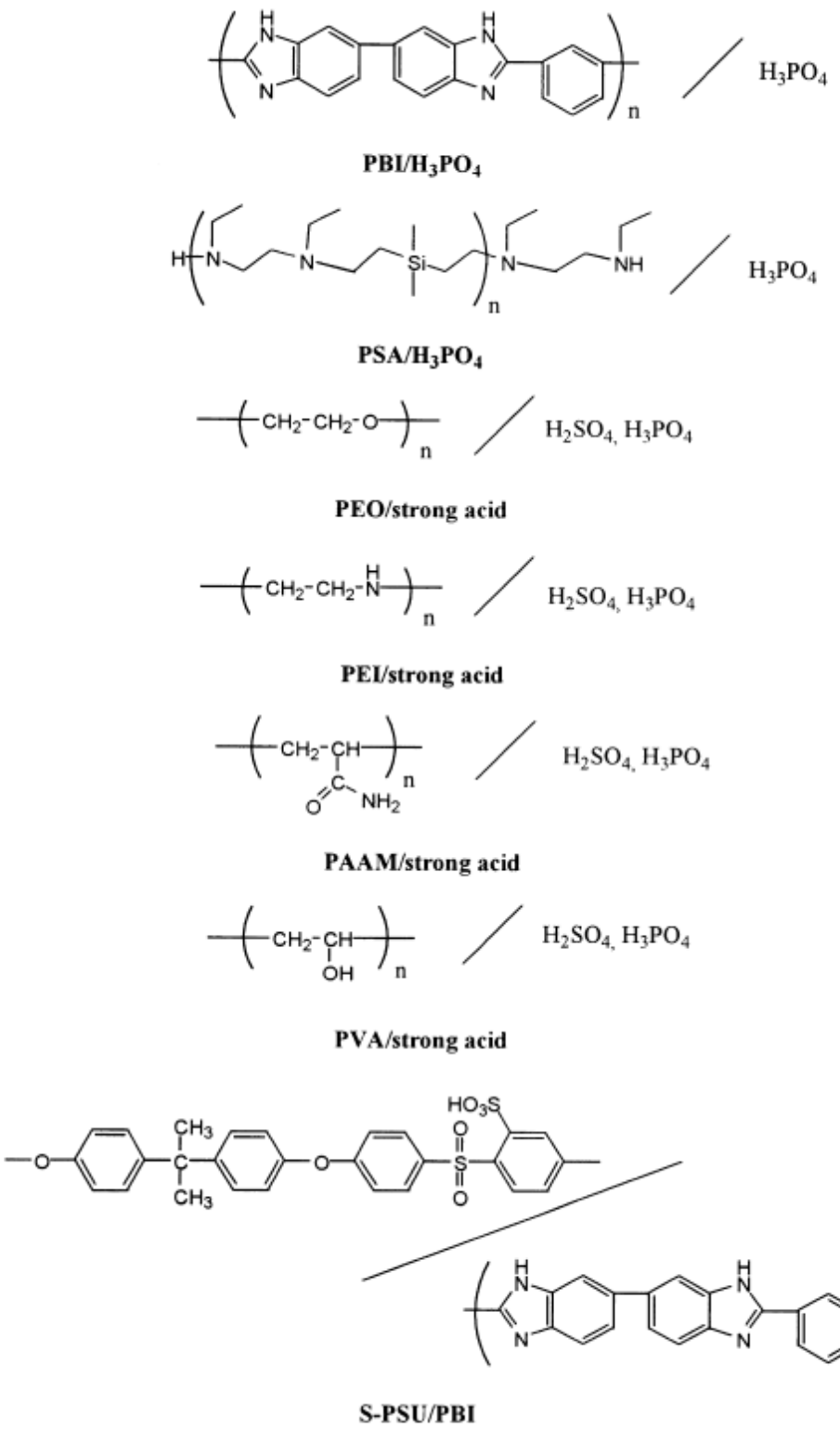

Figure 14: Chemical structures of polymer electrolytes based on acid-base polymer complexes (Rikukawa et al. 2000). poly (ethylene oxide) (PEO), poly(ethylene imine) (PEI), poly(acrylamide)

Table 1: The proton conductivity and thermal stability of different types of acid that can be used in polymer electrode membranes

Acid Type	**Proton conductivity (S/cm)**	**Thermal stability**	**Reference**
PBI/H3PO4	10^{-4} S	high	Bouchet 1998
PSA/H3PO4	10^{-4} S Cm^{-1}	high	Rikukawa *et al.* 2000
PEI/strong acid	10^{-4} S Cm^{-1}	poor	Bouchet 1997
PAAM/strong acid	10^{-4}-10^{-3} S Cm^{-1}	poor	Rikukawa *et al.* 2000
PVA/strong acid	10^{-3} S Cm^{-1}	poor	Gupa *et al.* 1996

At RMIT University Oberoi (2015) has recently investigated the use of a liquid acid as the proton conductor within porous activated carbon electrodes as the storage for hydrogen in both reversible electrochemical cells with liquid electrolytes and in the proton battery configuration. In his work he measured the reversible electrochemical hydrogen storage capacity of variety aC-PTFE sample electrodes in a three-electrode electrolytic cell. The reversible electrochemical hydrogen storage capacities of the fabricated aC-PTFE electrodes used in his experiment were found to be in the range of 0.36 – 1.6 wt% of equivalent hydrogen in carbon. The 'equivalent hydrogen' was the combination of electrochemical reaction between the hydrogen and carbon particles and the contribution of double-layer capacitance.

A candidate aC sample mesoporous carbon 1:7 KOH (supplied by CIC Energigune in Spain) showed the highest reversible capacity of 1.6 wt% in the electrochemical cell with dilute (1 mol) sulphuric acid as the electrolyte and proton conductor within the electrode. This sample then was selected to be used in a proton battery again soaked in dilute sulphuric acid for proton conduction to test the feasibility of this arrangement. Oberoi's (2015) work showed some potentially promising results in terms of hydrogen storage capacity, but some anomalies in terms of gas collections in electrolyser mode and the measured discharge capacities in fuel cell mode were identified, so that firm conclusions about the feasibility of a proton battery with a porous carbon electrode and liquid acid proton conductor could not be made.

3.4 Gaps in knowledge and understanding

It is clear from this review that, while considerable research has been conducted into the storage of hydrogen in gaseous form in various forms of porous carbon, relatively little work has been done on electrochemical storage of hydrogen in porous carbon media. The present thesis therefore focusses on electrochemical storage of hydrogen in carbon-based materials.

Among the limited research that has been done on electrochemical hydrogen storage in carbons, most has concentrated on liquid alkaline electrolytes. This thesis thus focusses on electrochemical hydrogen storage in acidic electrolyte environments. In particular, the emphasis in the present work is on the novel proton battery concept developed at RMIT University, based on a reversible PEM fuel cell with an integrated solid-state electrode for electrochemical hydrogen storage. To conduct protons directly into the pores of the carbon particles, the electrode is soaked in a liquid acid, a novel arrangement to provide an ionic bridge between the nafion electrolyte of the reversible PEM cell and the carbon-based storage medium. The present project continues the investigation of hydrogen storage electrodes for the novel proton battery from the stages where Andrews and Seif Mohammadi (2014), Jazaeri (2014) and Oberoi (2015) have reached.

This thesis also seeks to make a contribution towards developing an improved theoretical understanding of the processes of hydrogen diffusion through a liquid proton conducting medium into composite carbon-based electrodes, and subsequent bonding to surface carbon atoms within these porous media. Experiments are then conducted to test the theoretical predictions.

4 A THEORETICAL ANALYSIS OF AN ELECTROCHEMICAL CELL WITH AN INTEGRATED HYDROGEN STORAGE ELECTRODE

4.1 Overview

Electrochemical storage of hydrogen in activated carbon electrodes as part of a reversible fuel cell offers a potentially attractive option for storing surplus electrical energy from inherently variable solar and wind energy. In this chapter, a one-dimensional theoretical model is developed and presented of the process of H+ ion (proton, or more accurately, hydronium, H_3O^+) conduction through an acid electrolyte into a highly porous activated carbon electrode where it is neutralised and adsorbed on inner pore surfaces An analytical solution is obtained in the direction of the charge flow through the electrode assuming no variations in the plane of the active area of the cell (normal to this dimension).

A Butler-Volmer type equation is used to relate the rate of adsorption of hydrogen to the potential difference between the activated carbon surface and the electrolyte. This model for the hydrogen-storage electrode is then incorporated into a more general computer model based on MATLAB software of the entire electrochemical cell including the oxygen electrode. By running the model a theoretical voltage-current curve is generated for given input parameters for a particular activated carbon electrode. A parametric study is conducted to explore the influence of key input parameters on the resulting VI curves in both fuel cell and electrolyser modes.

The proposed model does not take into account any effect due to filling up of the variable hydrogen storage capacity. Here the case of a liquid acid electrolyte and an activated carbon hydrogen storage electrode is investigated. But it is important to note that the analysis can be generalised to any porous hydrogen storage material and any proton-conducting electrolyte. Later, in chapter 6, the model developed is applied to electrolyser-mode operation of an electrochemical cell with a liquid sulphuric acid electrolyte and activated carbon electrode.

4.2 A general model of a reversible electrochemical cell with a porous hydrogen storage electrode

4.2.1 The basic electrochemical cell considered

The schematic of the reversible electrochemical cell with a porous hydrogen storage electrode is shown in Figure 7. In this system, the protons produced during electrolysis diffuse straight into the solid-state storage to form a bond with the storage material, without combining with electrons to form hydrogen gas molecules and without this gas being compressed for storage. In fuel cell mode, this process is reversed, with hydrogen atoms being released from the storage and giving up an electron to become protons once again. These protons then re-enter the membrane and move back to the oxygen side where they combine with oxygen and electrons from the external circuit to re-form water.

The cell is comprised of the hydrogen storage electrode, the oxygen side electrode and an electron and proton conducting electrolyte between the oxygen and hydrogen electrode.

4.2.2 Charging (electrolyser) mode (E-mode)

4.2.2.1 Current flows and potential variation in E-mode

An equivalent circuit representing the electrochemical cell in E-mode with an integrated porous hydrogen storage electrode is shown in Figure 15. V_{cell} and I_{cell} are the voltage and the current of the cell respectively. η^H and η^O are the overpotentials on the hydrogen and oxygen electrode respectively. R_e^O and R_e^H are the electrode resistances (to electron flow) on the oxygen and hydrogen side respectively, and $R_m^{H^+}$ is the electrolyte resistance to proton flow. E_0^H and E_0^O are the reversible equilibrium potentials on hydrogen and oxygen sides respectively.

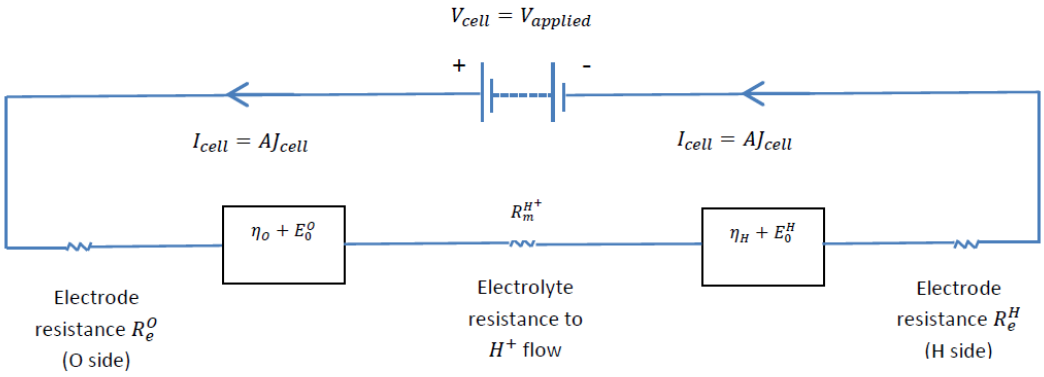

Figure 15: The equivalent circuit for the electrochemical cell in E mode

The general equation describing the total potential in the cell is equal to the summation of the entire potential drops element in the circuit as follows:

$$V_{cell} = (\eta^H + E_0^H) + (\eta^O + E_0^O) + I_{cell}(R_e^O + R_e^H) + I_{cell}R_m^{H^+} \qquad (1)$$

In the following sections the analytical model is presented based on the Butler-Volmer equation for O-side and H-side to relate the overpotentials to the corresponding current densities.

4.2.2.2 Oxygen-side reaction in E mode

The relationship between the current density and overpotential onn the oxygen side can be described by the Butler-Volmer equation (Doddathimaih and Andrews, 2008):

$$j_{cell}^O = j_0^O[\exp(\frac{\eta^O \alpha^O 2F}{RT}) - \exp(\frac{-\eta^O(1-\alpha^O)2F}{RT}] \qquad (2)$$

where j_{cell}^O is the current density in the oxygen electrode, j_0^O is the exchange current density on the oxygen side, η^O is the overpotential on the oxygen side, α^O is the charge transfer coefficient on the oxygen side, F is the Faraday constant, T is the temperature, and R is the gas constant.

By inverting equation (2), we can express the overpotential on the oxygen side in terms of current density and the other parameters as:

$$\eta^O = f^{-1}(j^O_{cell}, j^O_0, \alpha^O, T). \quad (3)$$

4.2.2.3 Hydrogen-side reaction

Figure 16 shows a schematic of the hydrogen storage electrode. It is assumed that the potential and current in the electrolyte and acid can vary in the direction x but are constant in the plane orthogonal to x. Hence, this is a simplified one-dimensional theoretical analysis.

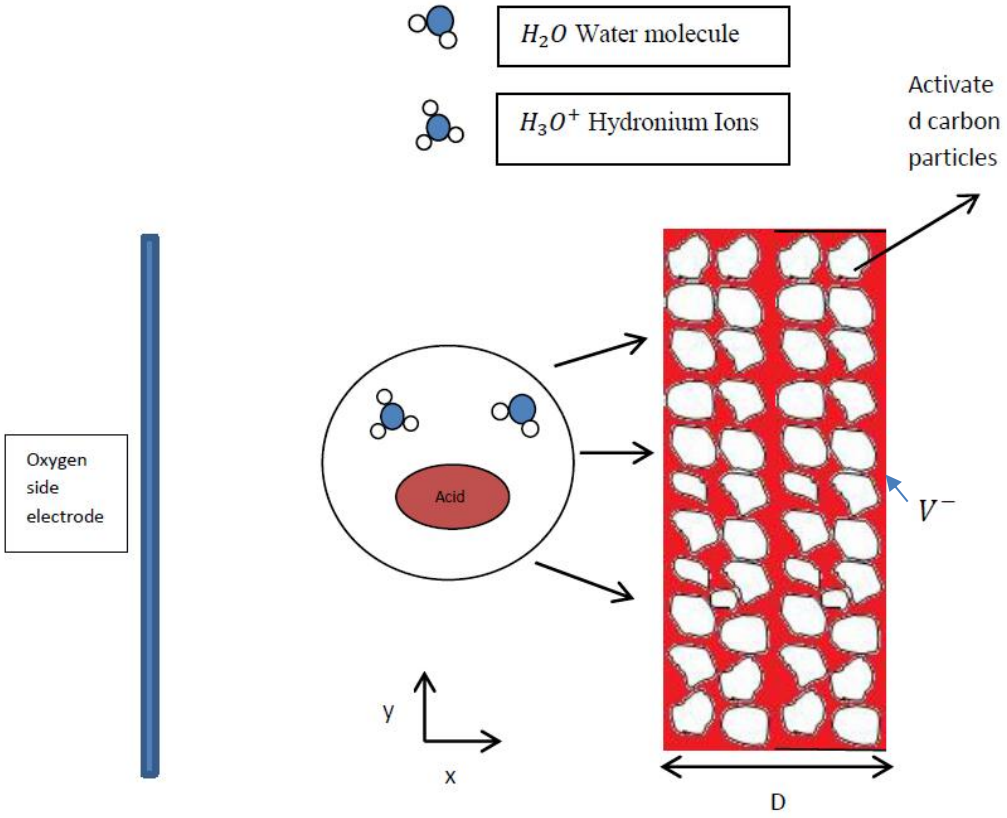

Figure 16: Schematic of hydrogen storage electrode, which has a negative potential applied during charging, with a positive potential applied to the oxygen electrode

The potential difference between the proton conducting medium and the H-storage medium within a layer of infinitesimal thickness δx at distance x from the boundary of the electrode with the membrane (or primary electrolyte) of the reversible fuel cell can be written as:

$$\varphi_{nc}(x) = \varphi_n(x) - \varphi_c(x) \qquad (4)$$

where $\varphi_c(x)$ is the potential of the H-storage medium in the layer, and $\varphi_n(x)$ is the corresponding potential in the proton conducting medium . By applying a negative charging electric potential to the right hand side of the electrode, both $\varphi_c(x)$ and $\varphi_n(x)$ will fall with increasing x.

According to the conservation of charge we have:

$$j_c(x) + j_n(x) = j_{cell} \qquad (5)$$

where $j_c(x)$ is the current density due to electron flow through the H-storage particles in the layer at x, $j_n(x)$ is the current density due to proton flow through the proton conducting medium, and j_{cell} (x) is the current density of the cell (relative to active area of the electrode).

The reversible reaction of charging and discharging process is:

$$nC + H^+ + e^- \Leftrightarrow [nC]H \qquad (6)$$

Let us assume the electrochemical current $\delta j(x)$ in this reaction can be described by a Butler-Volmer equation in the form of:

$$\delta j_{BV}^H = \delta x . j_0^H [\exp(\frac{\eta^H \alpha^H 2F}{RT}) - \exp(\frac{-\eta^H (1-\alpha^H) 2F}{RT}] \qquad (7)$$

where j_0^H is the exchange current density in hydrogen electrode, η^H is the overpotential on hydrogen side and α^H is the charge transfer coefficient on hydrogen side. The use of this equation assumes that the basic conditions of the charging reaction are constant over time. In other words, no account is taken of the effects of filling up the available storage sites with hydrogen. In actuality, as the available hydrogen storage capacity approaches being filled, both the exchange current density and the charge transfer coefficient for this reaction will progressively change with time. So this model holds as long as there are plenty of available storage sites left within the porous carbon material.

As $\delta x \to 0$ and given:

$$\delta j_{BV}^{H}(x) = -\delta j_n(x) = \delta j_c(x) \qquad (8)$$

Equation 7 becomes:

$$\frac{dj_c}{dx} = j_0^H[\exp(\frac{\eta^H \alpha^H 2F}{RT}) - \exp(\frac{-\eta^H (1-\alpha^H)2F}{RT}] \qquad (9)$$

The potential gradient within the H-storage medium can be expanded in terms of the electron current density and electron conductivity of the medium using Ohm's law as follows:

$$\frac{d\varphi_c(x)}{dx} = (\frac{-1}{\sigma_c}) j_c(x) \qquad (10)$$

where σ_c is the electron conductivity of the H-storage medium.

Similarly the potential gradient in the proton conducting medium within the storage electrode can be expanded as:

$$\frac{d\varphi_n(x)}{dx} = (\frac{-1}{\sigma_n}) j_n(x) \qquad (11)$$

where σ_n is the proton conductivity of this medium.

Knowing that $\eta(x) = \varphi_{nc}(x) - E_0$ (12)

and differentiating equation 12 yields:

$$\frac{d\eta^H}{dx} = \frac{d\varphi_n(x)}{dx} - \frac{d\varphi_c(x)}{dx} = -\frac{j_n(x)}{\sigma_n} + \frac{j_c(x)}{\sigma_c} , \qquad (13)$$

which on substituting for $j_n(x)$ from equation (5) becomes:

$$\frac{d\eta^H}{dx} = -\frac{1}{\sigma_n}(j_{cell} - j_c(x)) + \frac{j_c(x)}{\sigma_c} . \qquad (14)$$

Therefore $\frac{d\eta^H}{dx} = j_c(x)(\frac{1}{\sigma_c}+\frac{1}{\sigma_n}) - \frac{j_{cell}}{\sigma_n}$ (15)

Differentiating equation (15) gives:

$$\frac{d^2\eta^H}{dx^2} = \frac{dj_c(x)}{dx}(\frac{1}{\sigma_c}+\frac{1}{\sigma_n}) \qquad (16)$$

But from equation (9) $\frac{dj_c(x)}{dx}$ can be expanded as a function of η and hence by substituting for $\frac{dj_c(x)}{dx}$ in equation (16) a second order differential equation for η is obtained:

$$\frac{d^2\eta^H}{dx^2} = j_0^H[\exp(\frac{\eta^H\alpha^H 2F}{RT}) - \exp(\frac{-\eta^H(1-\alpha^H)2F}{RT}](\frac{1}{\sigma_c}+\frac{1}{\sigma_n}) \ . \qquad (17)$$

To solve equation 17 that is a second-order differential equation the following boundary conditions should be applied based on the physics and properties of the electrodes:

- referring to Figure 17, at x=D the proton current must fall down to zero since no proton can flow into the right-hand end plate.

  Hence:

  $$j_n(D) = 0 \qquad (18)$$

  and $j_c(D) = j_{cell}$ (19)

- At x=0 the electron current must similarly fall down to zero since no electron can pass into the electrolyte.

  Hence:

  $$j_n(0) = j_{cell} \qquad (20)$$

  and $j_c(0) = 0$ (21)

Knowing that:

$$\frac{d\eta^H}{dx} = -\frac{j_n(x)}{\sigma_n} + \frac{j_c(x)}{\sigma_c}$$

The following boundary conditions are obtained:

$$\frac{d\eta^H}{dx}(0) = -\frac{j_n(0)}{\sigma_n} + \frac{j_c(0)}{\sigma_c} = -\frac{j_{cell}}{\sigma_n} \qquad (23)$$

$$\frac{d\eta^H}{dx}(D) = -\frac{j_n(D)}{\sigma_n} + \frac{j_c(D)}{\sigma_c} = \frac{j_{cell}}{\sigma_c} \qquad (24)$$

4.2.3 Fuel cell mode

4.2.3.1 Current flows and potential variation

An equivalent circuit representing a proton flow battery in FC mode with an integrated activated carbon hydrogen storage electrode is shown in Figure 17.

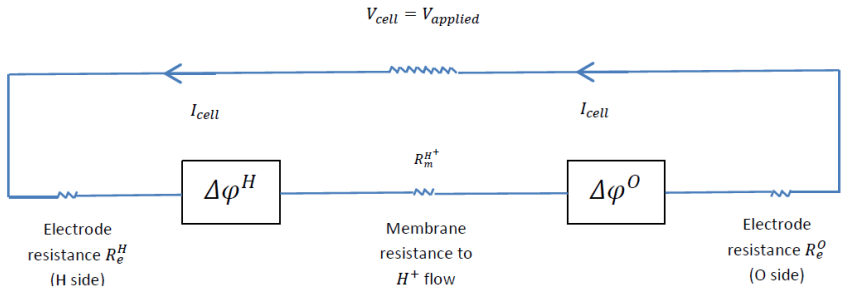

Figure 17: The equivalent circuit for a proton battery in E mode

The applied resistance across the cell in fuel cell mode is shown in figure above. V_{cell} and I_{cell} are the voltage and the current of the cell respectively. η^H and η^O are the overpotentials on the hydrogen and oxygen electrode respectively. R_e^O and R_e^H are the electrode resistances (to electron flow) on the oxygen side and hydrogen side respectively, and $R_m^{H^+}$ is the

resistance of the proton conducting medium. E_0^H and E_0^O are the reversible equilibrium potentials on hydrogen and oxygen electrodes respectively, similarly to E mode.

The general equation between voltage and current in FC mode can be written as:

$$V_{cell} = E_0^O + E_0^H + \eta^H + \eta^O - I_{cell}(R_e^O + R_e^H) - I_{cell} R_m^{H^+} \qquad (25)$$

It should be noted that in fuel cell mode, η^O and η^H are negative.

4.2.3.2 Oxygen-side reaction in FC-mode

The Butler-Volmer equation for the O-side reaction is again Eq. 2, the same as in E-mode but now in FC mode η <0 so the equation can be written as :

$$j_{cell}^O = j_0^O[\exp(\frac{-|\eta^O|\alpha^O 2F}{RT}) - \exp(\frac{+|\eta^O|(1-\alpha^O)2F}{RT}] \; . \qquad (26)$$

To solve equation 26 in FC mode the inverse function is use as we did in E mode.

So we have:

$$\eta^O = f^{-1}(j_{cell}^O, j_0^O, \alpha^O, T) \qquad (27)$$

It should be noted that for $\alpha^O = 0.5$, η^O has the same magnitude in FC mode as in E mode but is negative.

4.2.3.3 Hydrogen-side reaction in FC-mode

In the hydrogen-side electrode in FC mode, all the steps and the analytical solution are similar to those mentioned in section 2.2.1.3 but with a negative sign.

So the second-order differential equation derived by the analytical solution for FC mode can be written as:

$$\frac{d^2\eta^H}{dx^2} = j_0^H[\exp(\frac{-|\eta^H|\alpha^H 2F}{RT}) - \exp(\frac{+|\eta^H|(1-\alpha^H)2F}{RT}](\frac{1}{\sigma_c} + \frac{1}{\sigma_n}) \qquad (28)$$

The first term here has a negative sign for overpotential, while the second term has a positive sign. It should be noted that for $\alpha^H = 0.5$, η^H has the same magnitude in FC mode as in E mode but is negative.

4.3 Conclusion

In this chapter a one-dimensional theoretical analysis normal to the active surface of the electrodes in a reversible electrochemical cell has been developed. A Butler-Volmer type equation relates the rate of adsorption of hydrogen to the potential difference between the activated carbon surface and the electrolyte in hydrogen side electrode. By applying boundary conditions, a second- order differential equation has been derived that relates the potential between the proton conducting medium and the hydrogen-storage medium. In the next chapter a MATLAB program is developed to solve the developed equation numerically.

5 MATLAB SIMULATION OF AN ELECTROCHEMICAL HYDROGEN STORAGE CELL: BASE CASE AND PARAMETRIC STUDY

5.1 Overview

In this chapter, numerical solutions of the equations derived in chapter 4 relating the potential difference between the proton conducting medium and the hydrogen storage material, the oxygen-side overpotential, and the current density, in the reversible cell with an integrated H-storage electrode are found for both E- (hydrogen charging) and FC- (hydrogen discharging) modes using MATLAB software. Theoretical VI curves for the cell operating in E and FC modes are thus generated for the assumed base-case values for key input parameters. A parametric study is then conducted to explore the influence of these input assumptions on the resulting V-I curves.

5.2 Cell characteristic

The physical properties of the electrochemical cell modelled theoretically and with MATLAB are assumed to be the same as those of an actual cell used in the corresponding experimental procedure described later in Chapter 6.

Thus the oxygen electrode used is assumed to be a Pt wire, as shown in Figure 18. The oxygen gas generated on the wire surface is collected in the cylinder at the other end of the wire. The Pt wire diameter is 1 mm and the length of the wire is about 10 cm. Hence

$$A_{O-electtrode} = 3.14 \times 0.1 \times 10 = 3.14 \text{ cm}^2$$

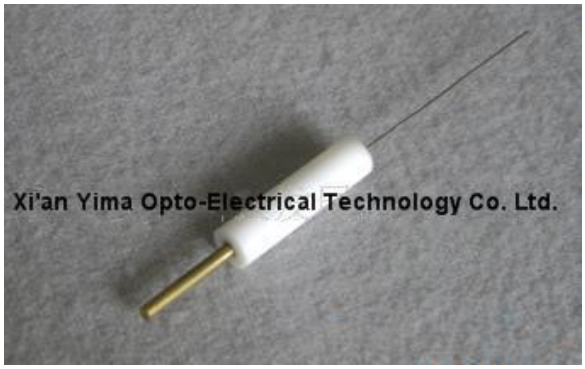

Figure 18: The oxygen-side electrode

The electrolyte used in the electrochemical cell is assumed to be dilute sulphuric acid with 1 molar concentration. The proton conductivity of the dilute sulphuric acid is taken as (Oberoi, 2015):

$$\sigma_n = 0.138 \text{ S/cm}$$

The properties of the hydrogen—storage electrode are assumed to be those of an activated carbon, named aCP and obtained from Oberoi's (2015) experiment as presented in Table 2.

It is important to mention that these are the bulk properties of an electrode made from aCP, with a 10 wt% PTFE binder. The electrical conductivity is measured for the electrode with the binder, and the proton conductivity is for the electrode soaked in dilute sulphuric acid as proton conducting medium, as used in the experimental electrochemical cell studied in chapter 6.

Table 2: Physical and electrical characteristics of the carbon electrode used in the theoretical model

Sample	Width (cm)	Length (cm)	Area cm²	Thickness (cm)	Proton conductivity (S/cm)	Electrical conductivity (S/cm)
Activated carbon	W	L	A = W x L	Th	σp	σe
aCP	2.4	2.4	5.76	0.2	0.0043	12.86

Other constant input parameters used in the mathematical model of the electrochemical cell are presented in Table 3, and again are the same as those of the experimental cell with and

aCP electrode investigated in chapter 6. These parameters are assumed to be the same in both E mode and FC mode.

Table 3: Constant input parameters used in simulation

Parameter	Description	Value	unit
F	Faraday constant	96485.3	Coloumb/mol
R	Gas constant	8.3145	j/mol K
T	temperature	298	K
σ_p	Proton conductivity of carbon electrode	0.0043	S/cm
σ_e	Electron conductivity of carbon electrode	12.86	S/cm
Th	Thickness of carbon electrode	0.2	Cm
A_O	Oxygen electrode area	3.14	Cm^2
A_H	Hydrogen electrode area	5.76	Cm^2
σ_n	Proton conductivity of bulk electrolyte	0.138	S/cm
W	Width of hydrogen electrode	2.4	Cm
L	Length of hydrogen electrode	2.4	Cm

5.3 Base case analysis

In the base case, the input parameters for the model are based on Dodathimmaiah's (2008) experiment on a URFC. The variable input parameters are j_0^H, j_0^O, α^H, α^O, E_0^H and E_0^O.

Table 4 shows the base-case parameter values.

Table 4: basic case variable input values

j_0^H (A/cm^2)	j_0^O (A/cm^2)	α^H	α^O	E_0^H (V)	E_0^O (V)
0.07	3e-5	0.5	0.5	0.2	1

In the oxygen-side electrode, the Butler-Volmer equation as given by earlier equation 2 is:

$$j_{cell}^O = j_0^O[\exp(\frac{\eta^O \alpha^O 2F}{RT}) - \exp(\frac{-\eta^O(1-\alpha^O)2F}{RT}] \quad (28)$$

Now considering the oxygen-side area equal to 3.14 cm^2, equation 2 can be written in the form of current as below:

$$I_{cell}^{O} = A_O j_0^O [\exp(\frac{\eta^O \alpha^O 2F}{RT}) - \exp(\frac{-\eta^O (1-\alpha^O) 2F}{RT}] \qquad (29)$$

Equation (29) is solved for overpotential on the oxygen side for different values of current.

For example, for I_{cell} =50 mA

$$50 \times 10^{-3} = 3.14 \times 3 \times 10^{-5} \left[e^{39\eta^O} - e^{-39\eta^O} \right]$$

Hence:

$$\eta^O = 0.1610 \text{ v}$$

Repeating the same procedure for the different current values gives in each case the corresponding overpotential in E mode. The results obtained are summarized in Table 5.

Table 5: Overpotential on O-side for diffent currents in E mode calculted using the theoretical model

I_{cell} (mA)	η^O (v)
50	0.1610
40	0.1551
30	0.1476
20	0.1371
10	0.1189
5	0.1020
1	0.0590
0.01	0
0.0001	0
0	0

Figure 19 shows the overpotential on O-side for the base case where α^O=0.5 and j_0^O=3×10^{-5} A/cm^2 for different current values in E mode.

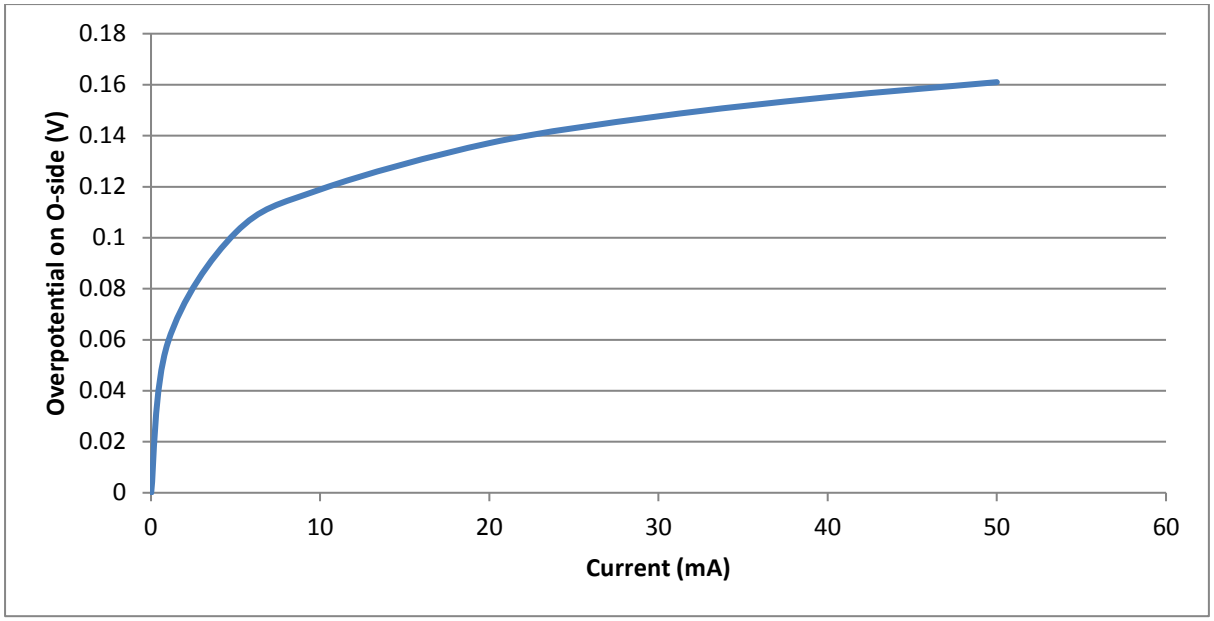

Figure 19: O-side overpotential vs current curve in E-mode

In the hydrogen-side electrode, putting the base-case parameter values into equation 17 and by applying boundary conditions 23 and 24:

$$\frac{d\eta}{dx}(0) = -\frac{j_n(0)}{\sigma_n} + \frac{j_c(0)}{\sigma_c} = -\frac{j_{cell}}{\sigma_n}$$

$$\frac{d\eta}{dx}(D) = -\frac{j_n(D)}{\sigma_n} + \frac{j_c(D)}{\sigma_c} = \frac{j_{cell}}{\sigma_c}$$

The results for the overpotential on the hydrogen side for different current values in E mode can be found by numerical solution of the equations using MATLAB. These are shown in Table 6.

Table 6: Overotential on hydrogen side for different currents calucalted using the theoretical model with numerical solution using Matlab

I_{cell} (mA)	η^H (v)
50	0.1069
40	0.095
30	0.081
20	0.062
10	0.032
5	0.0076
1	0
0.01	0
0.0001	0
0	0

Figure 20 shows the overpotential on H-side for different current values in E mode for the base case where α^O=0.5 and j_0^H=0.07 A/cm^2. For this exchange current density value the overpotential did not follow the expected trend at the beginning for the low value of current, that is, an increase but only slowly, so in the next simulation values for j_0^H>07 were chosen.

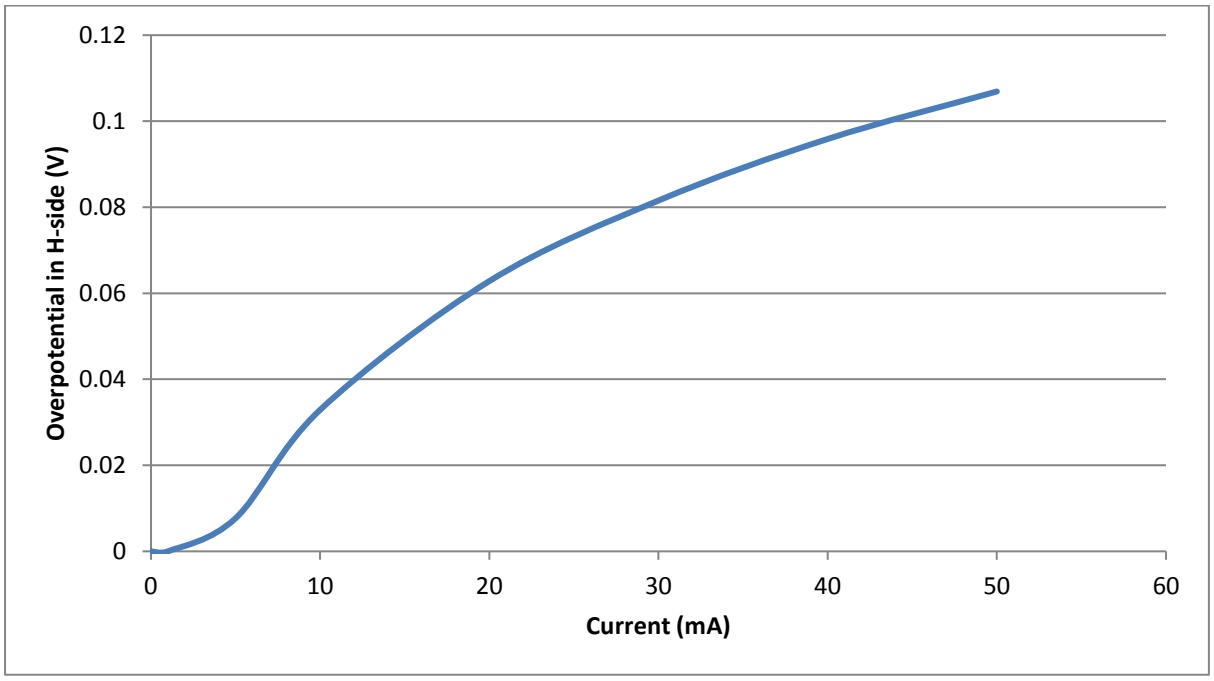

Figure 20: O-side overpotential vs current curve in E-mode.

One of the benefits of this new theoretical model is that the change in overpotential and current density can be computed through the thickness of the hydrogen-side electrode. This

relationship is plotted in Figure 21, which shows the overpotential on hydrogen side versus *x* (normal distance into electrode from its boundary with the electrolyte) for the base case and a current I=50 mA in E mode. It can be seen that the overpotential as the driving force in E mode for the hydrogen adsorption reaction decreases with increasing distance x into the electrode.

Figure 22 shows the current densities in the hydrogen-side electrode due to proton and electron flows. The proton current density, j_n, decreases with increasing distance x into the electrode, while the electron current decreases, in such a way that the total effective current at each *x* stays constant, in line with equation 30. $j_c(x) + j_n(x) = j_{cell}$ (30)

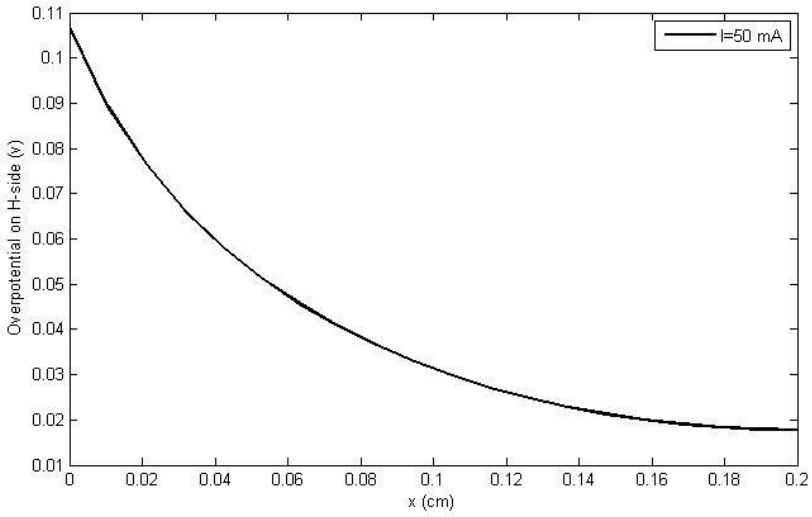

Figure 21: Overpotential in H-side electrode versus x, the normal distance into the electrode from its boundary with the electrolyte

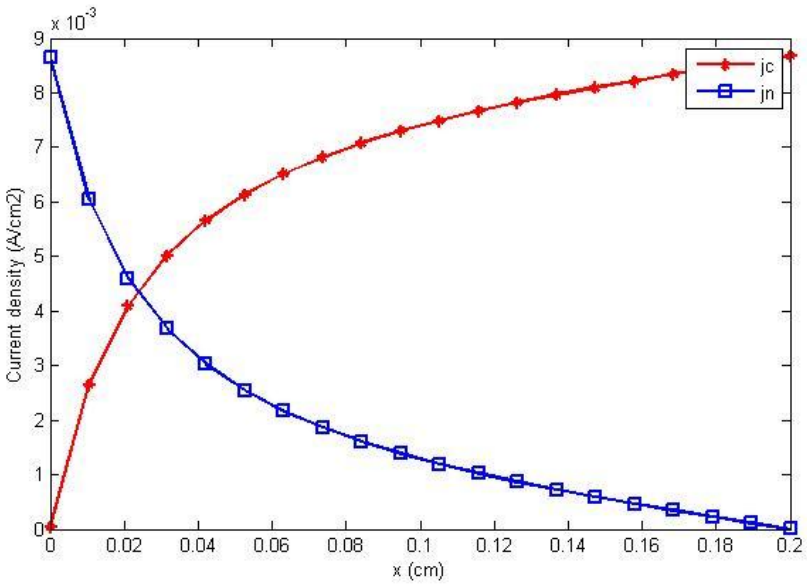

Figure 22: Current densities due to electron and proton flow in H-side electrode versus x

Another significant graph coming out of the simulation is the rate of proton adsorption in the hydrogen electrode, which here is defined as $\frac{dj_n}{dx}$. Figure 23 shows the variation of this rate through the electrode thickness. The rate of hydrogen adsorption is at a maximum in the first layer of the storage electrode, nearest the electrolyte, and falls at a decreasing rate moving towards the outer face of the electrode where it is zero.

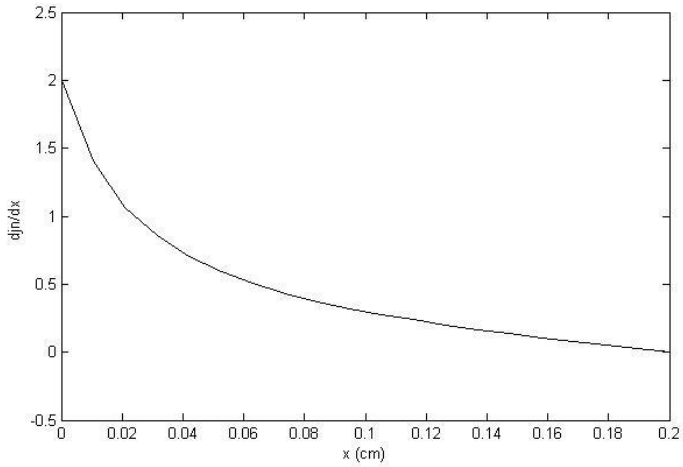

Figure 23: Proton adsorption rate within hydrogen electrode versus distance x into the electrode from the electrolyte boundary

Finally the outputs of the model for the base case for I_{cell}, the overpotentials on electrodes, E_0^O and E_0^H are shown in Table 7 and the corresponding VI curve is plotted Figure 24.

Table 7: input variable values for the base case analysis

I_{cell}	η^O	η^H	V_m	E_0^O	E_0^H	V_{total} E mode	V_{total} FC mode
50	0.1610	0.1069	0.12	1	0.2	1.61	-1.61
40	0.1551	0.095	0.094	1	0.2	1.57	-1.57
30	0.1476	0.081	0.067	1	0.2	1.52	-1.52
20	0.1371	0.062	0.04	1	0.2	1.47	-1.47
10	0.1189	0.032	0.2	1	0.2	1.41	-1.41
5	0.1020	0.0076	0.013	1	0.2	1.36	-1.36
1	0.0590	0	0.002	1	0.2	1.27	-1.27
0.01	0	0	0	1	0.2	1.2	-1.27
0.0001	0	0	0	1	0.2	1.2	-1.2
0	0	0	0	1	0.2	1.2	-1.2

Referring to equation 25, the VI curve in fuel cell mode is obtained and showed in Figure 24.

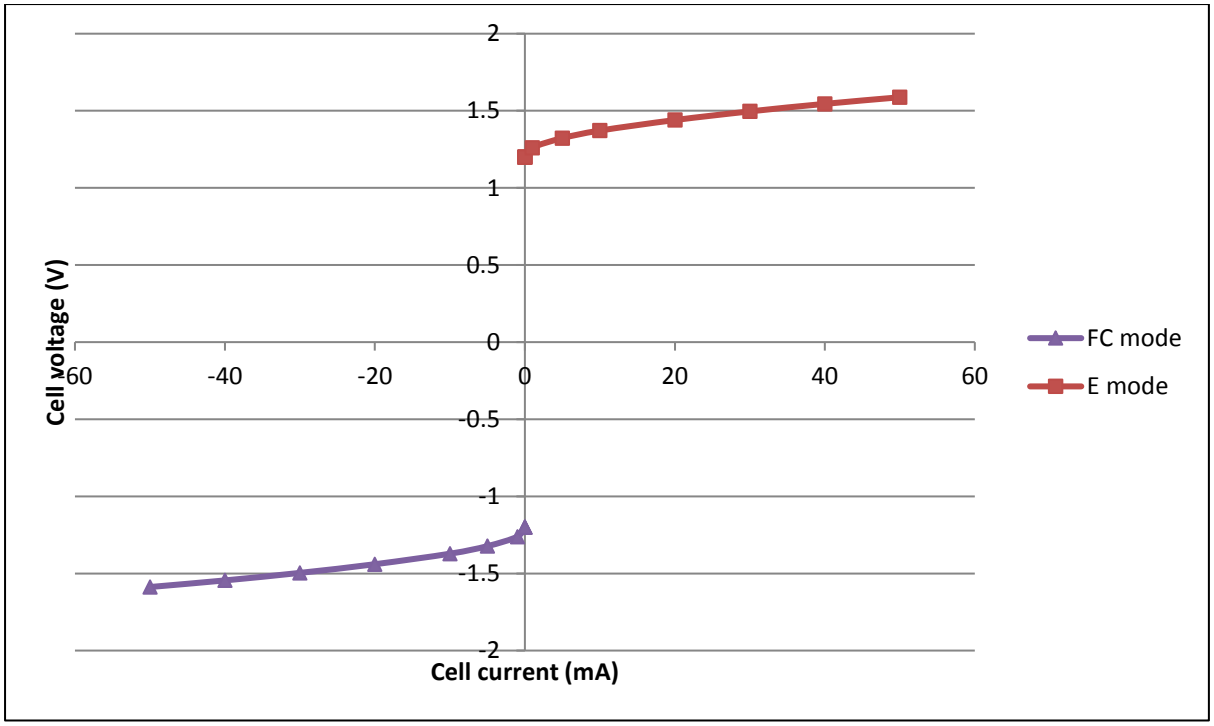

Figure 24: Voltage – current curves in E-mode and FC- generated by the new model when both charge transfer coefficients are 0.5

It can be seen in this case where $\alpha^O = \alpha^H = 0.5$ that the V-I curve in FC-mode is a reflection of the E-mode curve about the line $V_{cell} = E_0 = 1.2$ plus the sign change for I_{cell}, the latter reflecting the reversal of the direction of current flow on switching between modes. This case thus corresponds to an ideal reversible cell that performs equally well in both modes, so far as the increase in the absolute values of the electrode overpotentials with increasing cell current is concerned.

5.4 Parametric analysis: effect of varying key input parameters

In this section, the influence of changing the charge transfer coefficients and exchange current densities on the relationships between overpotentials on each electrode and current, and between cell voltage and current, in both E-mode and FC mode are investigated. Also the effect of reversible potential on hydrogen side electrode as a barrier for storing hydrogen is evaluated.

5.4.1 Changing charge transfer coefficients

5.4.1.1 Charge transfer coefficient α^O

In the first case, all the input variables are held constant while the charge transfer coefficient α^O is varied between 0.4 and 0.7, as in Table 8.

Table 8: Input values for the case where α^O changes

Run number	Parameter					
	j_0^H (A/cm^2)	j_0^O (A/cm^2)	α^H	α^O	E_0^H (V)	E_0^O (V)
1	0.07	3e-5	0.5	0.5	0.2	1
2	0.07	3e-5	0.5	0.4	0.2	1
3	0.07	3e-5	0.5	0.6	0.2	1
4	0.07	3e-5	0.5	0.7	0.2	1

Figure 25 shows the overpotential on O-side versus current for different values of α^O in both E mode and FC mode.

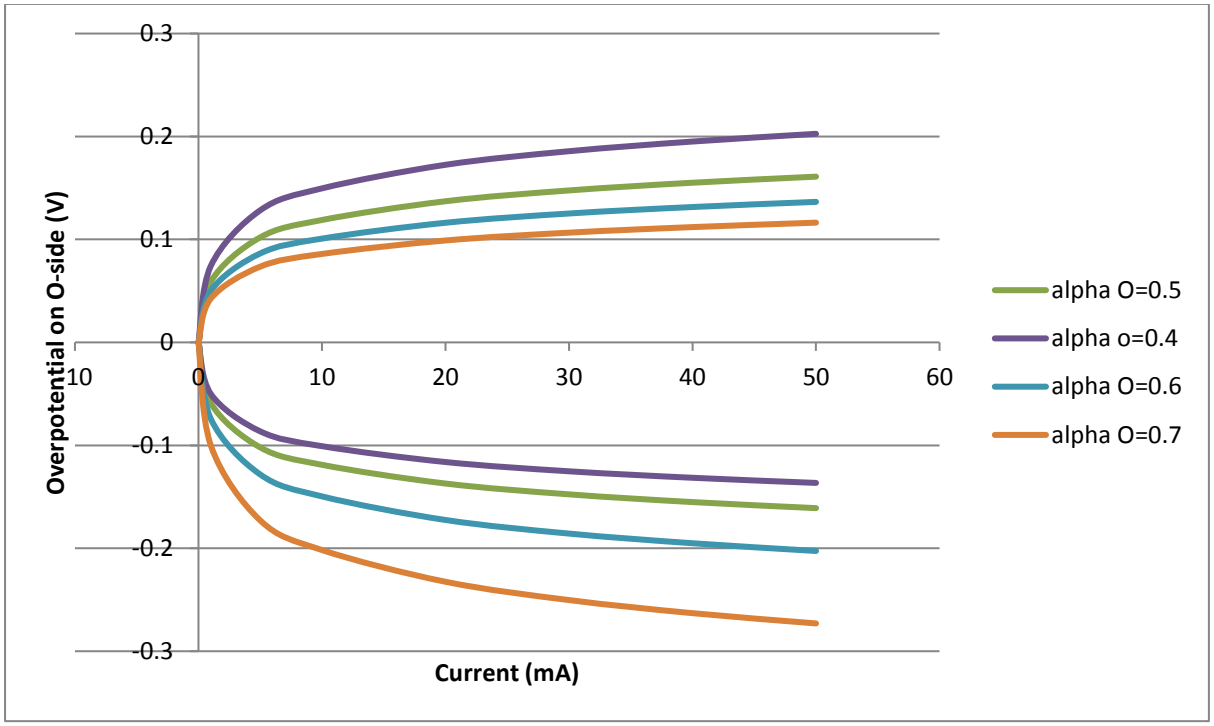

Figure 25: O-side overpotential vs current curves in E-mode and FC-mode generated by the model for the different values of O-side charge transfer coefficient, αO

If α^O is increased above 0.5 towards 1 while all other input parameters are held constant, the O-side overpotential at each current decreases progressively in E-mode, as seen in Figure 25. In FC-mode, the increasing value of α^O above 0.5 towards 1 increases the magnitude of the overpotential in FC-mode. It means that for the values above 0.5, the E mode reaction is favoured in rather than FC mode. Similarly for decreasing values of α^O below 0.5, the magnitude of the overpotential in FC-mode decrease, as also shown in Figure 25. Thus, it can be noted that the performance in FC-mode will improve for decreased values of α^O.

Figure 26 shows the family of V-I curves obtained by varying α^O while keeping other input parameters constant (as in Table 8).

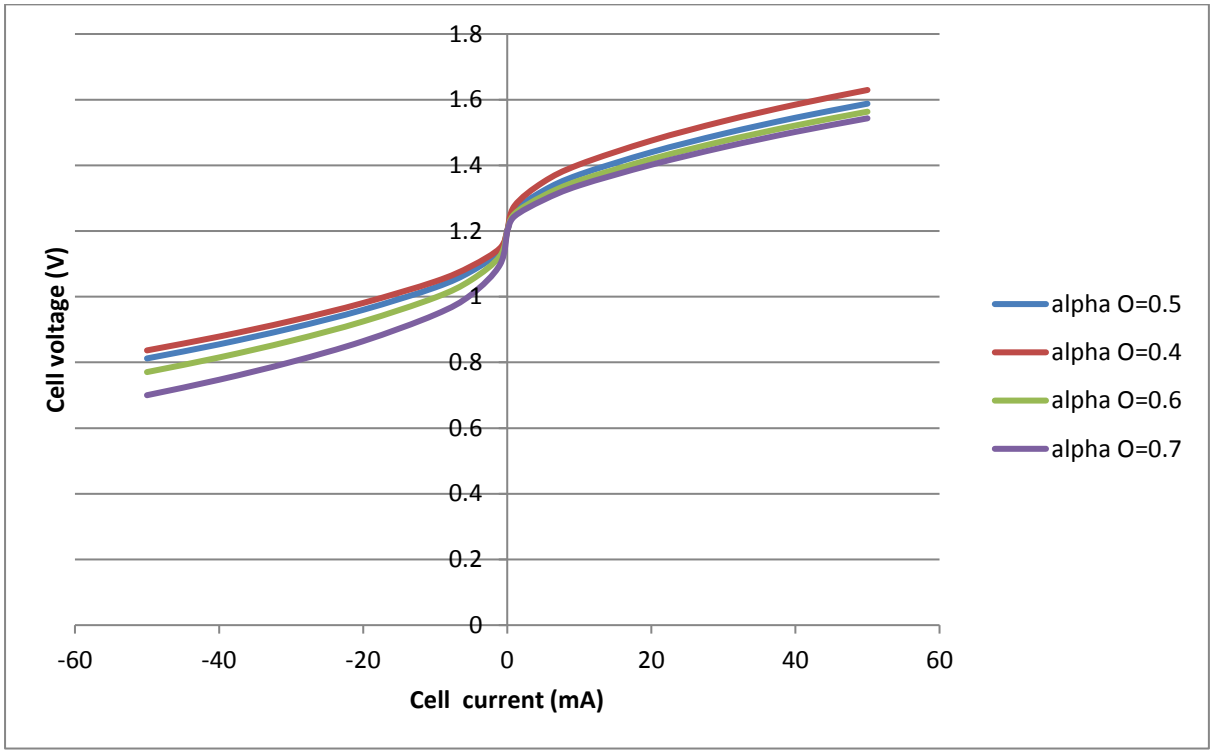

Figure 26: V-I curves obtained by varying αO while holding other input values constant (see Table 8)

It can be seen that, as long as the charge transfer coefficient increases, the overall cell potential decreases in E mode. On the other hand, in FC mode the cell potential compared to the reversible potential increases.

5.4.1.2 Charge transfer coefficient α^H

Next, all the input variables are held constant while the charge transfer coefficient α^H is varied between 0.4 and 0.7, as in Table 9.

Table 9: Input values for the case where α^H changes

Run number	Parameter					
	j_0^H (A/cm^2)	j_0^O (A/cm^2)	α^H	α^O	E_0^H (V)	E_0^O (V)
1	0.007	3e-5	0.5	0.5	0.2	1
2	0.007	3e-5	0.4	0.5	0.2	1
3	0.007	3e-5	0.6	0.5	0.2	1
4	0.007	3e-5	0.7	0.5	0.2	1

Figure 27 shows the overpotential on H-side versus current for different values of α^H in both E mode and FC mode, and Figure 28 the corresponding family of V-I curves.

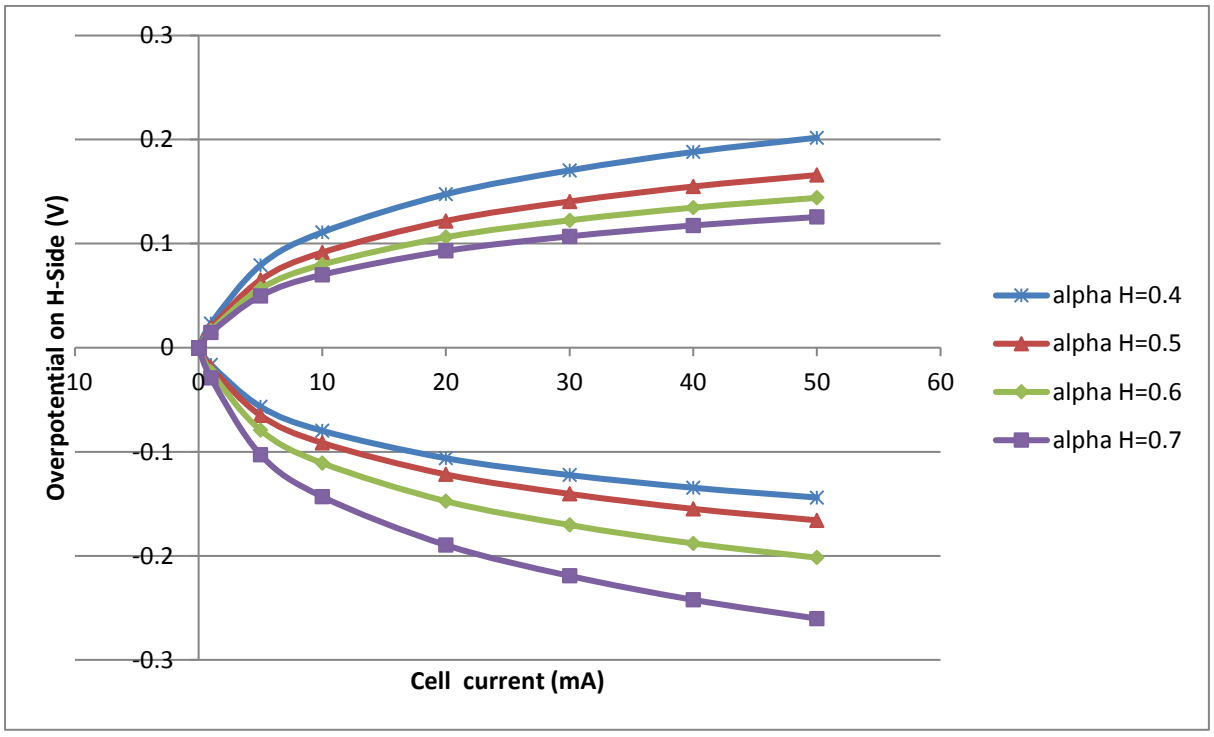

Figure 27: H-side overpotential vs current curves in E-mode and FC-mode generated by the model for the various values of H-side charge transfer coefficient, αH

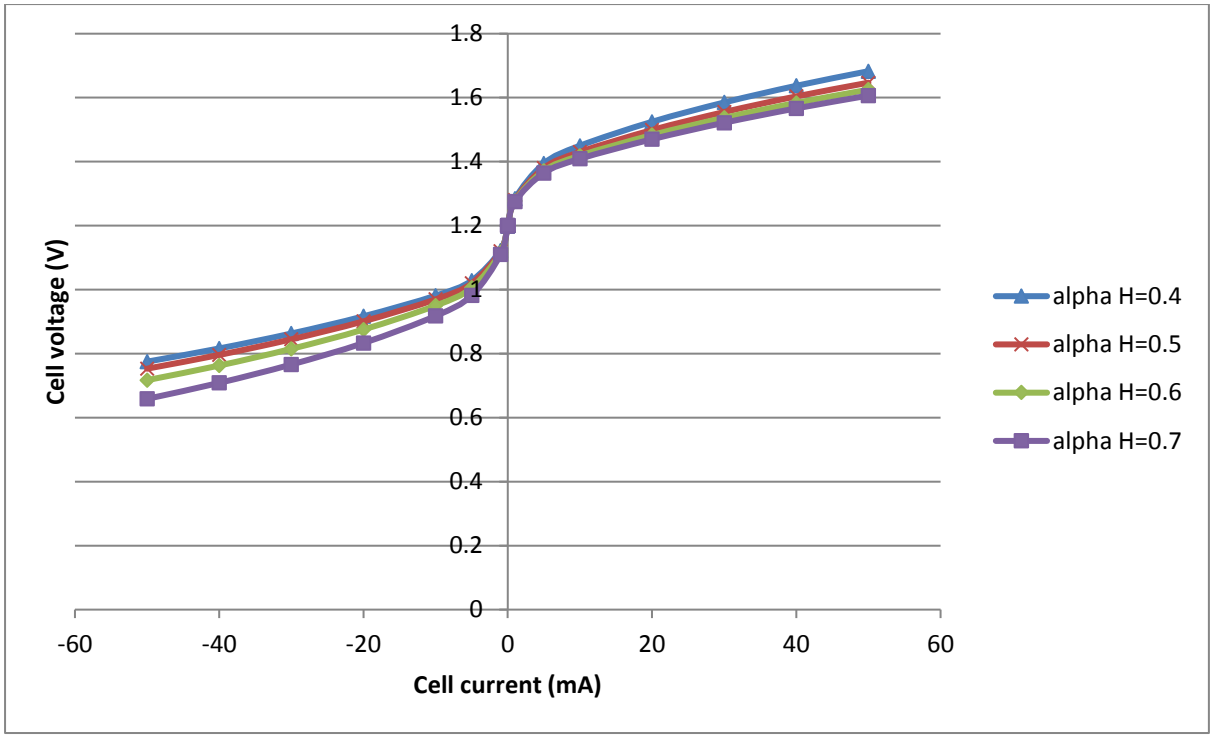

Figure 28: V-I curves based on input values from Table 9

On the basis of this analysis, the influences of varying α^H and α^O can be summarised as follows:

- α^H, α^O = 0.5 means that electrode is fully reversible, functioning as well in FC mode as in E-mode (so far as the increase in overpotential with increasing current is concerned). (Figure 28, α^H=0.5)
- α^H, α^O > 0.5 means that electrode performs better in E-mode than in FC mode. (Figure 28, α^H=0.6)
- α^H, α^O < 0.5 means that electrode performs better in FC-mode than in E mode. (Figure 28, α^H=0.4).

5.4.2 Exchange current density

The variation of current with overpotentials and V-I curves for different values of exchange current density in both E-mode and FC mode, is investigated in this part. Both charge transfer coefficients, α^O and α^H, will be held at 0.5 so that the effects specifically attributable to changes in exchange current density can be isolated. The values of other parameters assumed are given in the following table.

5.4.2.1 Exchange current density on O-side

Next, all the input variables are held constant while the exchange current density j_0^O is varied between 3×10^{-5} and 3×10^{-7} A/cm^2, as in Table 10.

Table 10: input values for the case where j_0^H changes

Run number	Parameter					
	j_0^H (A/cm^2)	j_0^O (A/cm^2)	α^H	α^O	E_0^H (V)	E_0^O (V)
1	0.007	3e-5	0.5	0.5	0.2	1
2	0.007	3e-4	0.5	0.5	0.2	1
3	0.007	3e-6	0.5	0.5	0.2	1
4	0.007	3e-7	0.5	0.5	0.2	1

Figure 29 shows the overpotential on O-side versus current for different values of j_0^O both E mode and FC mode.

As j_O^O is decreased, the O-side overpotential (a positive potential) increases progressively in E-mode, thus reducing the performance of the URFC. In FC-mode, the O-side overpotential is negative and becomes increasingly negative as j_O^O is decreased, again reducing FC-mode performance. Conversely, increasing j_O^O improves performance of the URFC in both modes.

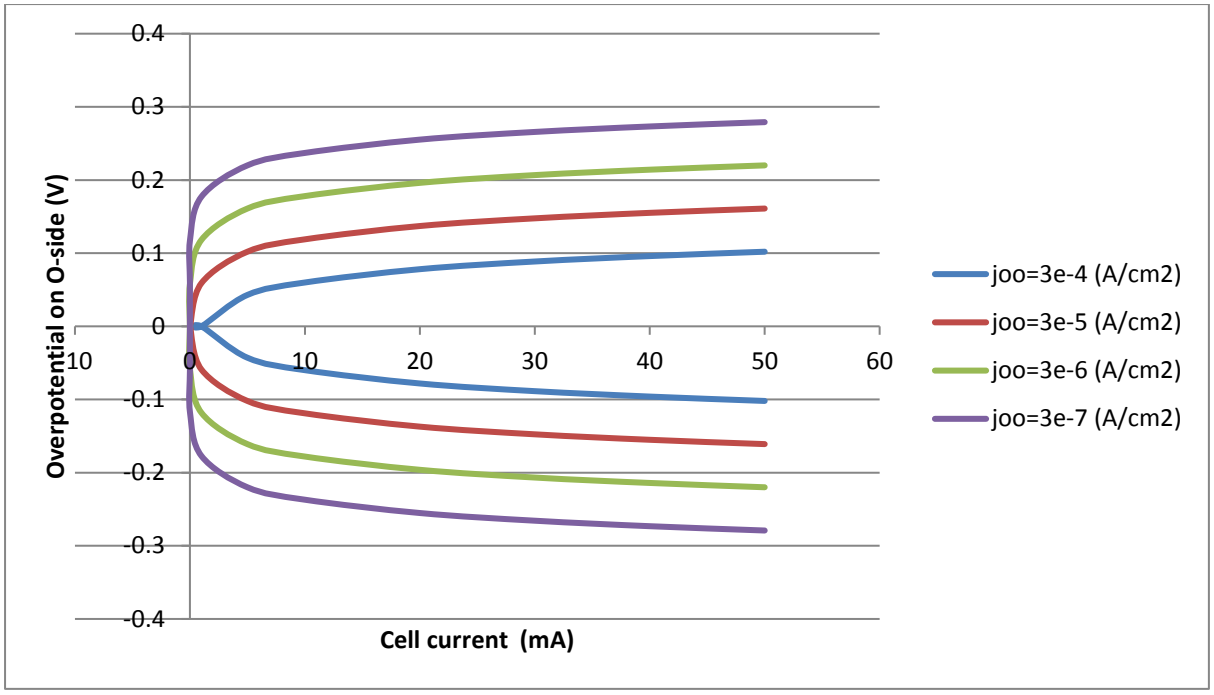

Figure 29: Current and overpotential variations for decreasing values of exchange current density on O side while holding all other parameters constant.

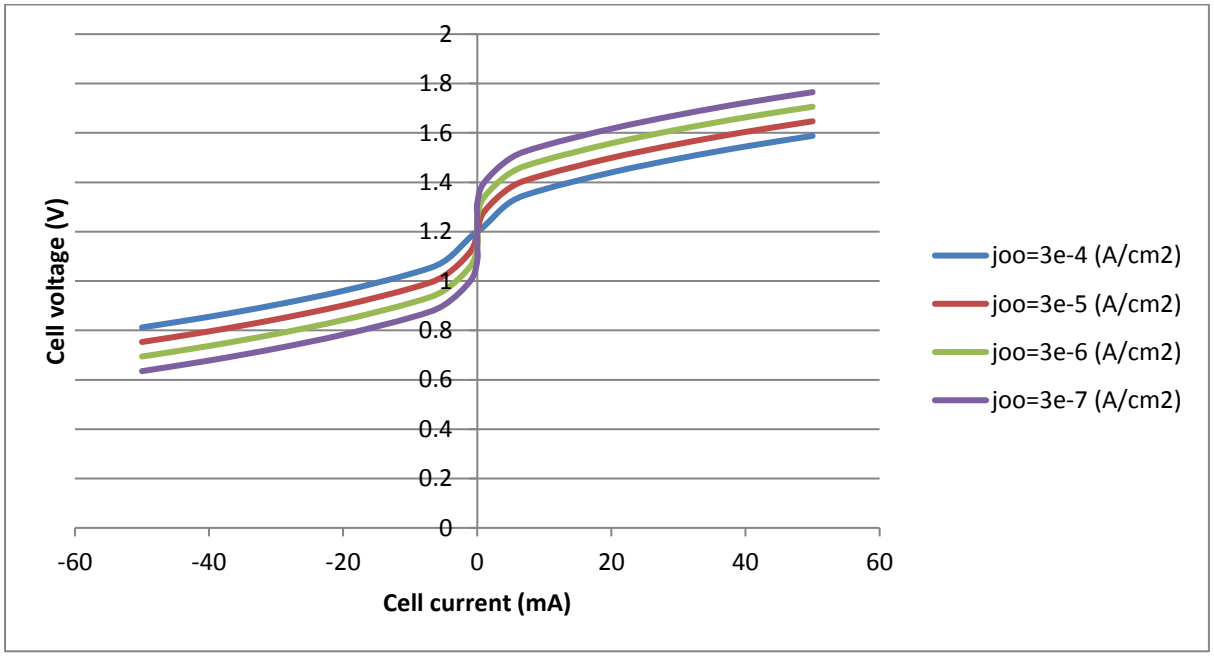

Figure 30: V-I curves based on input values from table 9 changing only j_0^O

It can be seen from the Figure 30 that by decreasing the exchange current density on O-side for a specific cell current, cell voltage increases and the performance of the cell in both sides

decreases as well. Conversely increasing the exchange current density on O-side decreases the cell voltage and the performance of the cell is increased.

5.4.2.2 Exchange current density on H-side

Next, all the input variables are held constant while the exchange current density j_0^H is varied between 0.00007 and 0.07 A/cm^2 as in Table 11.

Table 11: input values for the case where j_0^H changes

Run number	Parameter					
	j_0^H (A/cm^2)	j_0^O (A/cm^2)	α^H	α^O	E_0^H (V)	E_0^O (V)
1	0.007	3e-5	0.5	0.5	0.2	1
2	0.07	3e-5	0.5	0.5	0.2	1
3	0.0007	3e-5	0.5	0.5	0.2	1
4	0.00007	3e-5	0.5	0.5	0.2	1

Figure 31 shows the overpotential on H-side versus current for different values of j_0^H in both E mode and FC mode.

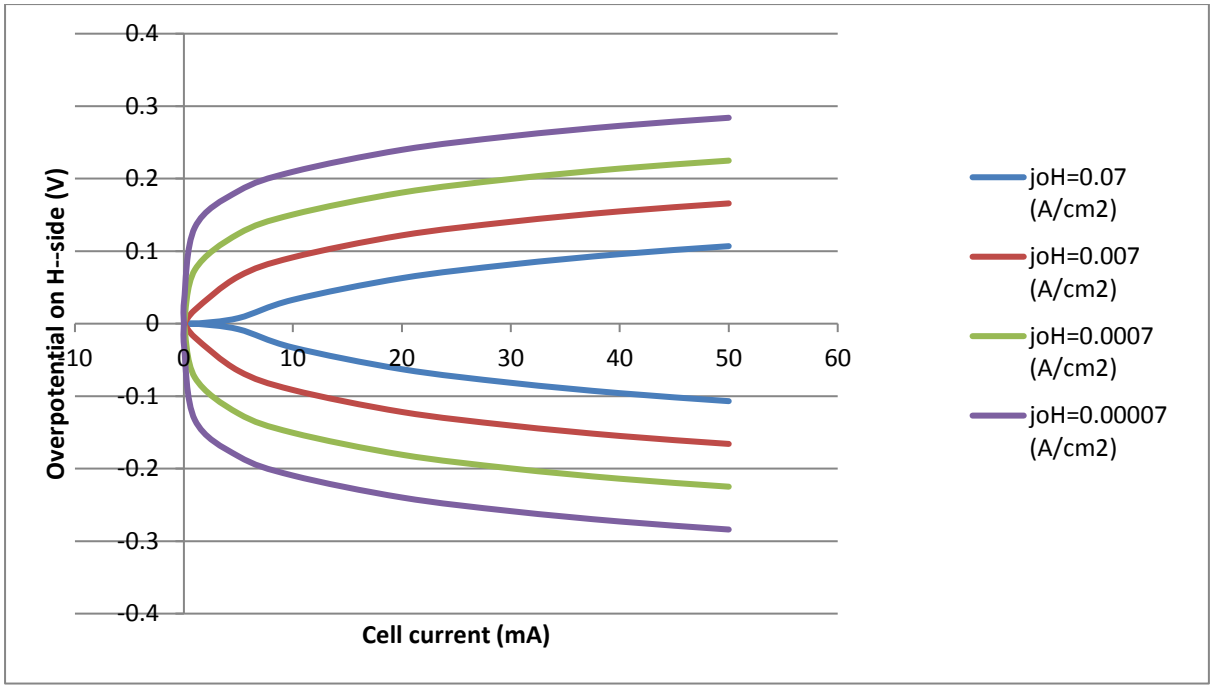

Figure 31: overpotential on H-side for different values of exchange current density

As j_O^H is decreased, the H-side overpotential (a positive potential) increases progressively in E-mode, thus reducing the performance of the URFC. In FC-mode, the H-side overpotential is negative and becomes increasingly negative as j_O^H is decreased, again reducing FC-mode performance. Conversely, increasing j_O^H improves performance of the URFC in both modes.

Figure 32 shows the family of V-I curves obtained by varying α^O while keeping other input parameters constant (as in Table 11).

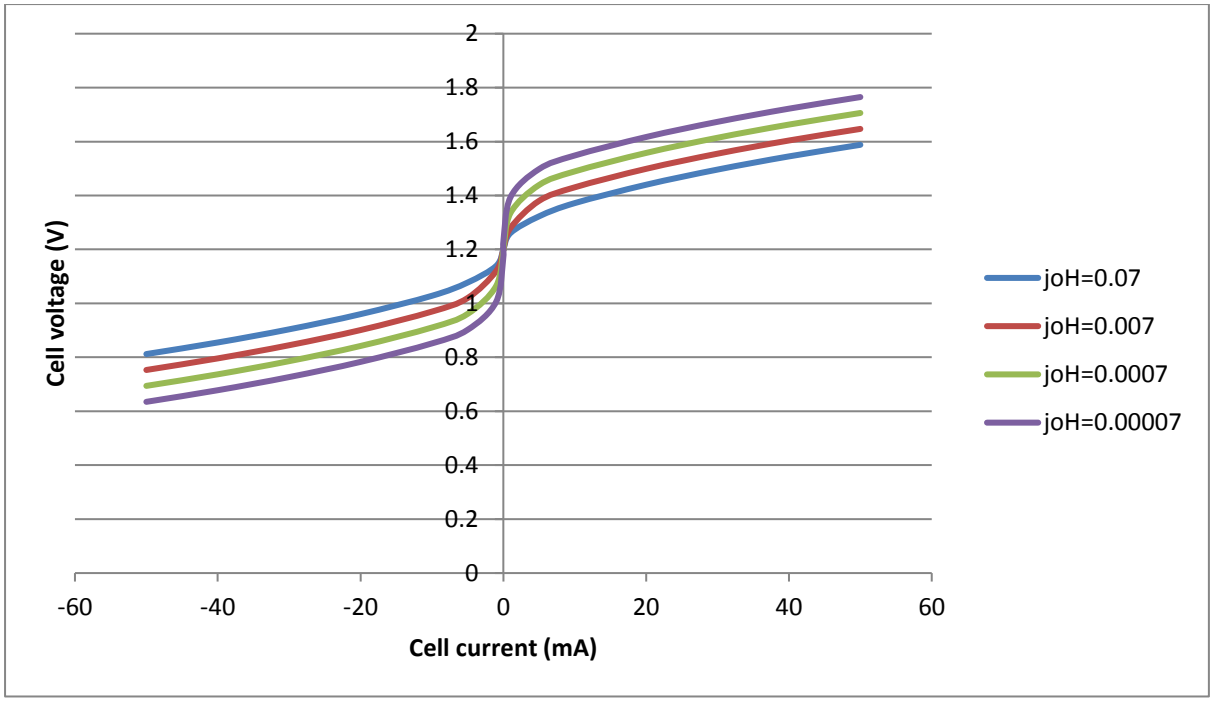

Figure 32: V-I curves based on input values from Table 11

It can be seen from Figure 32 that by decreasing the exchange current density on H-side for a specific cell current, cell voltage increases and the performance of the cell in both sides decreases as well.

5.4.3 Reversible potentials

In this part of the study the effect of varying the reversible potential in hydrogen side electrodes is investigated. In this case, all the input variables are held constant while the reversible potential E_0^H is change between 0.1 and 0.4 V, as in Table 12.

Table 12: Input values for the case where E_0^H changes

Run number	Parameter					
	j_0^H (A/cm^2)	j_0^O (A/cm^2)	α^H	α^O	E_0^H (V)	E_0^O (V)
1	0.007	3e-5	0.5	0.5	0.1	1
2	0.007	3e-5	0.5	0.5	0.2	1
3	0.007	3e-5	0.5	0.5	0.3	1
4	0.007	3e-5	0.5	0.5	0.4	1

Figure 33 shows the family of V-I curves obtained by varying E_0^H while keeping other input parameters constant (as in Table 12).

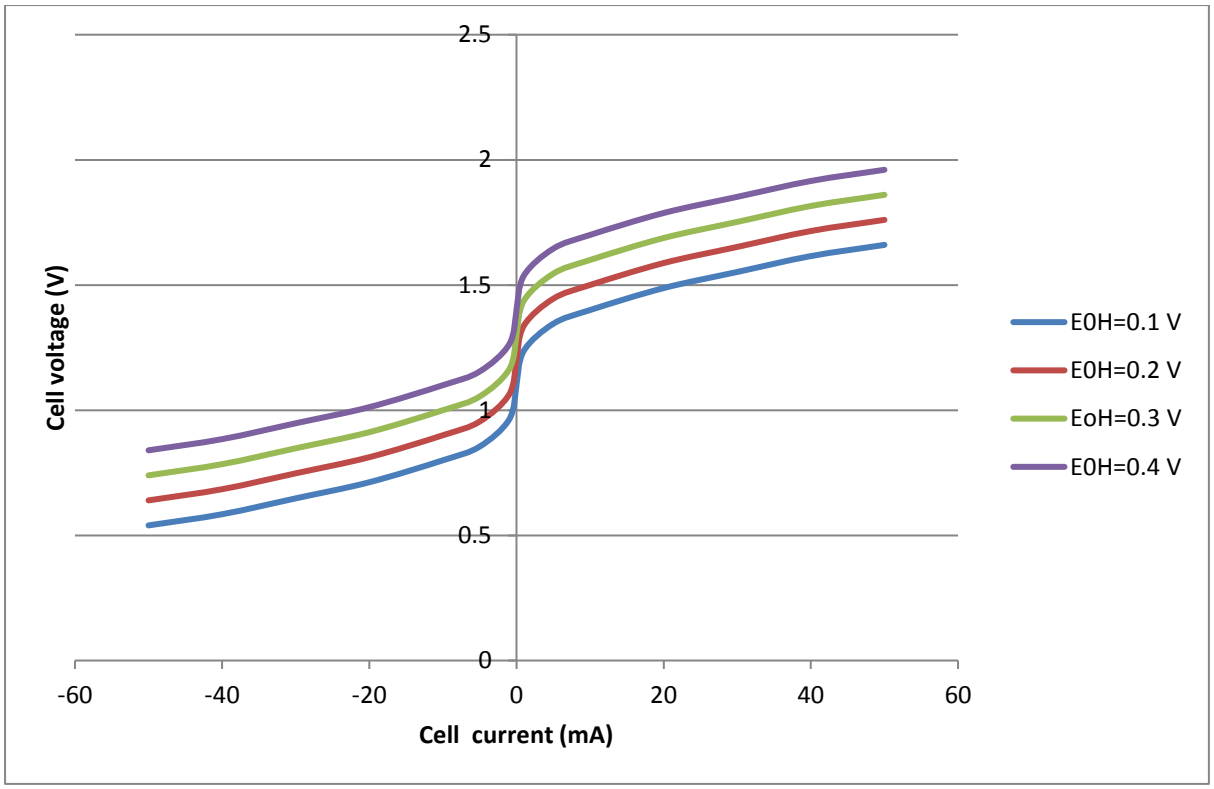

Figure 33: V-I curves based on input values from table 11

It can be seen from the figure 33 that increasing and decreasing the reversible potential on H-side electrode will shift the cell potential up and down respectively. The same results can be obtained for varying the reversible potential on O-side electrode as well.

5.5 Conclusion

In this chapter a numerical solution has been developed by using a set of MATLAB codes for the electrochemical cell voltage and current. The effects of each variable values have been studied and various V-I curves and overpotential curves for different currents have been obtained. It can be seen that a change of the charge transfer coefficient on both sides changes the slope of both overpotential and V-I curves, while changing the exchange current density

shifts the overpotential and V-I curves up and down. Increasing the exchange current density decreases the overpotential in charging mode since it is acting as a driving force. The reversible potential affects the cut-in value of voltage at which current starts to increase on the V-I curve. Later in section 6.7.1, the effect of reversible potential on the V-I curve based on the physical parameter and characterization of carbon electrode will be investigated.

In chapter 6 an experimental study is conducted and the experimental VI curves are compared with the theoretical ones.

6 AN EXPERIMENTAL STUDY OF ELECTROCHEMICAL HYDROGEN STORAGE IN SELECTED CARBON-BASED MATERIALS

6.1 Introduction

Electrochemical storage of hydrogen in carbon electrodes as part of a reversible fuel cell offers a potentially attractive option for storing surplus electrical energy from inherently variable solar and wind energy. Activated carbon has been used for this purpose and has shown promising potential for storing hydrogen and then releasing it working in fuel cell mode (Oberoi, 2015). In this chapter four different types of carbon material have been investigated as the hydrogen-storage electrode in a reversible cell with a liquid acidic electrolyte. Two samples were the graphitic carbon based namely spherical conductive graphite and graphene platelets. The other two were forms of activated carbon: one a commercial sample named aCN 99; and the other synthesised from phenolic resin with KOH activation.

The electron conductivity of electrodes made from these four forms of carbon material was measured in a small button cell using direct voltage and current measurements and Ohm's Law. The proton conductivities of the electrodes soaked in acid were calculated from the protonic resistance measured using Electrochemical Impedance Spectroscopy (EIS). The double-layer capacitances of the sample electrodes soaked in acid were measured by cyclic voltammetry. The hydrogen storage capacities of the electrodes were measured in an electrochemical cell with a dilute sulphuric acid electrolyte by galvanostatic charging and discharging. The best-performing carbon electrodes among these samples for reversible electrochemical hydrogen storage were identified. Possible explanations of the relative hydrogen storage capacities are offered in terms of physical characteristics of the samples such as pore sizes and available internal surface areas as sites for bonding to hydrogen.

6.2 Carbon samples and their physical properties

6.2.1 Selection of carbon materials

In the present work different carbon samples have been chosen based on different morphology and structure of the particles, and availability, to gain a better understanding of the process of proton conduction and bonding in these various materials. The selection remains a relatively restricted one, and thus constitutes a starting point in this form of analysis rather than any attempt at being more comprehensive.

The carbon materials used to prepare electrodes are listed in Table 13 along with data on their physical characteristics.

Table 13: physical characteristics of selected carbon samples

Sample	Particle size(micron)	Pore volume(cm^3/g)	Bulk density(g/cm^3)	Source
aCN Norit 99	~20	600	0.42	Sigma-Aldrich Co. LLC
1:7 KOH phenolic resin	N/A	1450	0.16	Monash University, Dr Mamun Mullah
Graphene platelets	~15-20	Not applicable, since particles are not porous	0.11	Dr Shuying Wu from RMIT University
Spherical graphite	~5-40	Not applicable, since particles are not porous	0.83	Triton Minerlands LTD

6.2.2 Activated carbon samples

Two types of activated carbon have been tested, aCN Norit 99 and phenolic resin activated with KOH (Table 12).

The aCN Norit 99 sample was a commercially-available activated carbon, also called ‘activated charcoal’. Figure 34 shows the morphology of this sample.

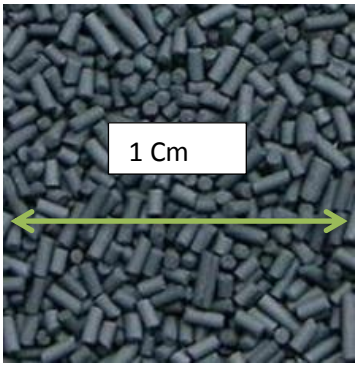

Figure 34: The morphology of charcoal sample

As can be seen in figure 34, this sample was supplied in the form of relatively large particles (3 mm diameter), which were then ground using a mortar and pestle into a powder of much smaller particles (20 micron) (Figure 35).

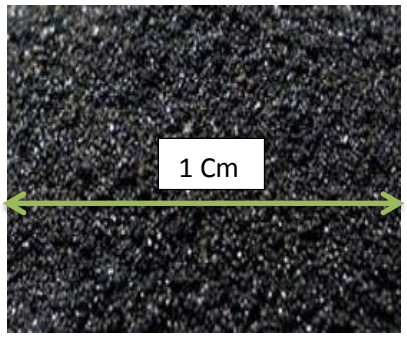

Figure 35: Activated carbon Norit 99 in powder form

The SEM machine available in Australian Microscopy and Microanalysis Research Facility (AMMRF) at RMIT University was employed for imaging the carbon samples used in this research project. High vacuum was used when imaging the carbon samples with a high accelerating voltage of 20 kV. A sticky double-sided conductive carbon tape was used to mount the carbon samples on stubs in the SEM. An SEM image for aCN 99 is shown in Figure 36. The average particle size distribution is around 5 micron.

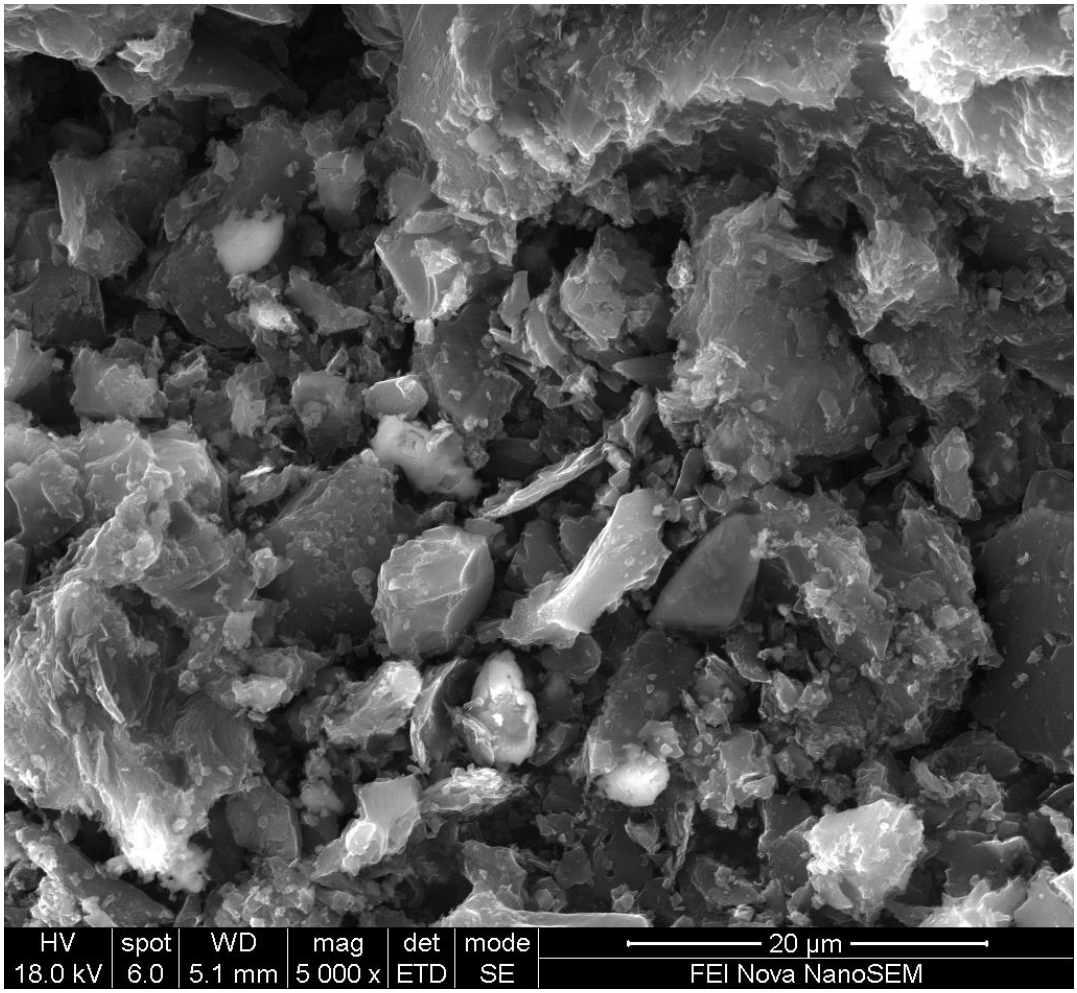

Figure 36: SEM image of activated carbon Norit 99 powder

Another activated carbon used in the electrochemical cell and proton battery experiment was made from phenolic resin activated with KOH 1:7. This activated carbon from phenolic resin activated KOH 1:7 has mesoporous and microporous porosity, which is suitable for storing hydrogen. The properties of this sample are shown in Table 14.

Table 14: Properties of the aC KOH 1:7 (Mamun Mollah Monash University)

sample	BET surface area (m^2/g)	Micropore volume (cm^3/g) Co_2 Adsorption	Mesopore volume (cm^3/g) N_2 Adsorption	Total pore volume (cm^3/g)	Bulk density (g/cm^3)
aC KOH 1:7	3870	0.56	0.82	1.38	0.16

6.2.3 Graphene platelets

The third sample used in this project for electrochemical hydrogen storage measurement was a powder of graphene platelets supplied by Dr Shuying Wu from RMIT University (School of Engineering) and made in the RMIT University Composites Lab (Shuying Wu *et al.* 2015). Figure 37 shows the graphene platelets powder.

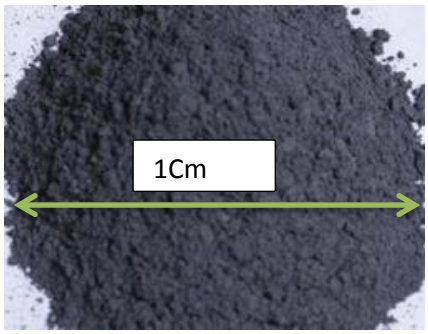

Figure 37: graphene platelets powder

An SEM image of a thin layer of graphene platelets resting on a glass surface is shown in Figure 38. Each graphene platelet was formed by stacking in the order of 20 layers of graphene with ~0.35 nanometre spacing between each layer (Shuying Wu *et al.* 2015). For a typical platelet 15 µm x 10 µm and 10 nm thick, the surface area of the top and bottom planes is 600 times that of the edge planes.

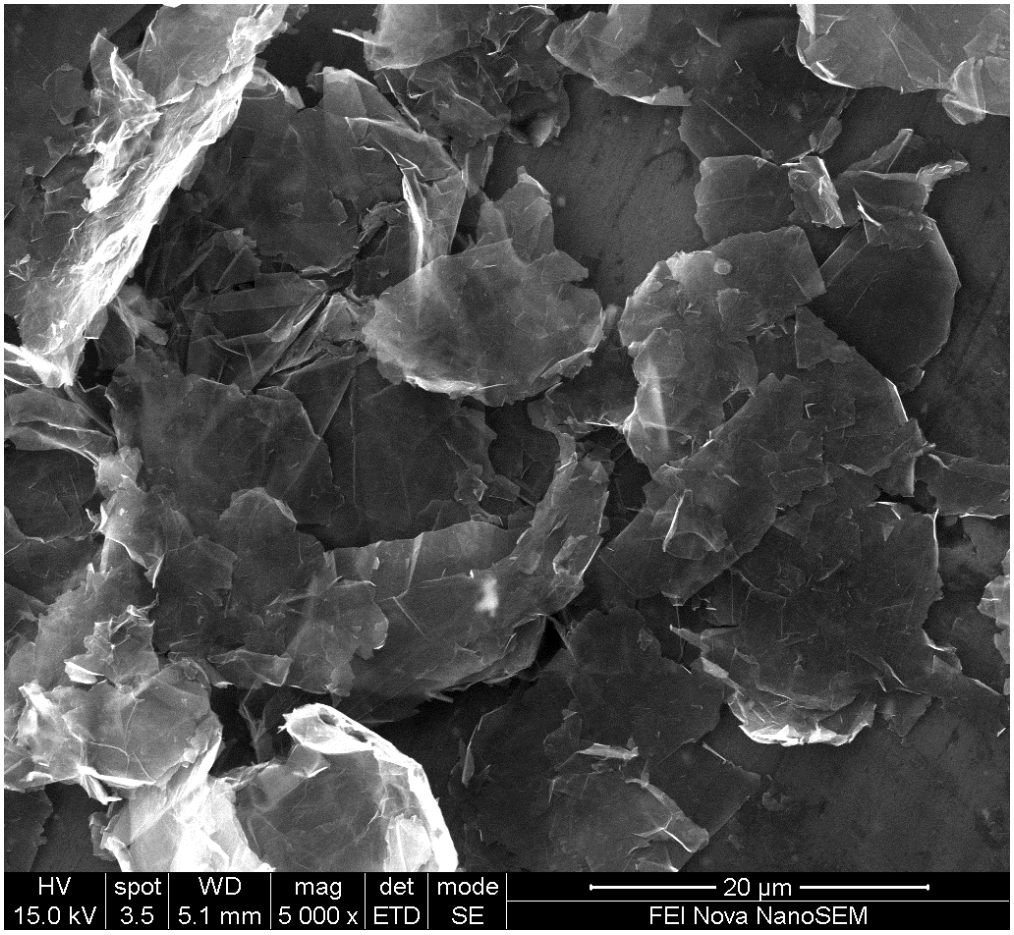

Figure 38: SEM image of graphene platelet sample

6.2.4 Spherical conductive graphite

The final sample used in this project was a powder of spherical conductive graphite. This material is the same as that used in Li-ion batteries in which lithium ions intercalate between the graphene layers that for the graphite. So using this material for electrochemical hydrogen storage promised an interesting comparison in terms of storage and reversibility.

Figure 39 shows the SEM image of this sample. The typical particle sizes varied from 5 to 40 micron. According to data from the supplier, the spherical graphite consisted of an average of 90% distribution at <35 microns, 50% distribution at <13 microns and 10% distribution at <4.5 microns (Triton Minerlands LTD).

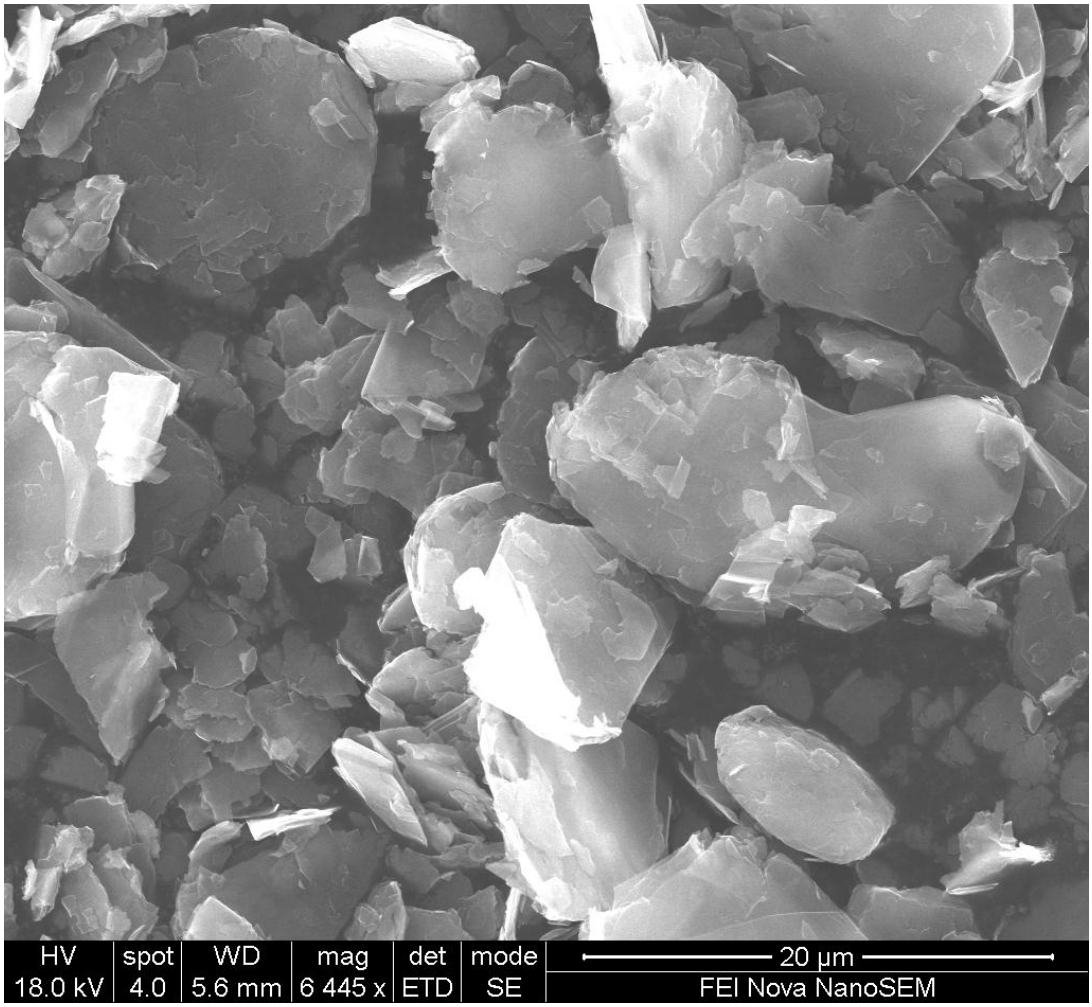

Figure 39: SEM image of the conductive graphite powder

6.3 Fabrication of carbon-PTFE electrodes

6.3.1 Weighing and mixing

All the carbon samples were weighed by using a digital weighing scale to measure their mass, density, and the required amounts needed to fabricate electrodes (Figure 40). The selected carbon samples weight varies from 1 to 1.8 grams in the square shape and from 0.3 to 0.7 grams in circular shape.

Figure 40: Digital weighting scale used in this work (source: www.weigh.com.au)

The next step is to add PTFE to the carbon powder to make electrodes. A commercial polytetrafluoroethylene (PTFE) solution was added into already-weighed carbon powder and mixed in a magnetic stirring device (Figure 41) to get a uniform distribution. The mass of PTFE solution added was set to achieve a 10% proportion of the total electrode mass after evaporation of the solvent in which the PTFE was dissolved. For example, for the sample electrode made from spherical conductive graphite had a total mass 1.8 g, comprised of 0.18 g PTFE and 1.62 g of the graphite powder.

Figure 41: Magnetic stirring device used to mix PTFE and carbon

6.3.2 Moulding

The slurry of carbon particles and PTFE solution was then poured into an aluminium mould of dimensions 25 mm x 25 mm x 2 mm to obtain the desired shape of the electrode, as shown in Figure 42.

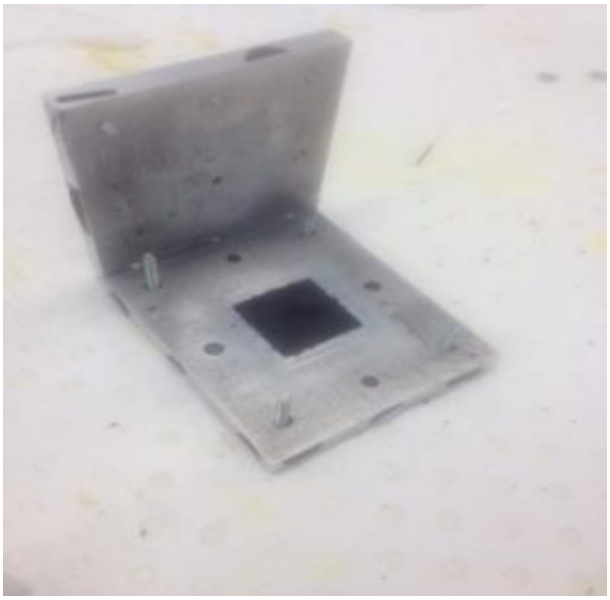

Figure 42: The mould used to fabricate square carbon-based electrodes with PTFE binder

After filling with the carbon-PTFE mixture, the mould was put in an oven and heated for two hours at a temperature of 110º C to evaporate all the solvent from the mixture. The resulting solid electrode was then removed from the mould and was ready to be used, as shown in Figure 43.

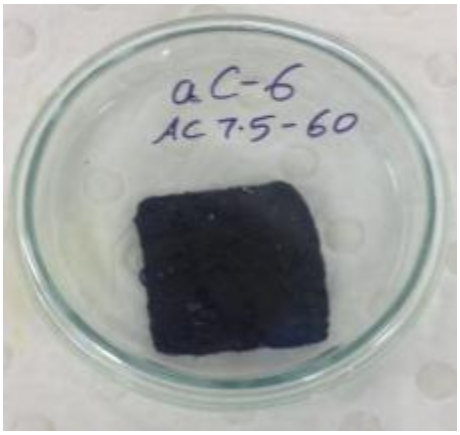

Figure 43: Fabricated activated carbon-PTFE solid electrode

6.4 Proton and electron conductivity measurements

6.4.1 The nature of the electron and proton conductivities within a carbon electrode soaked in acid

Proton and electron conductivities are electrical properties of a material. Electron conductivity measures the material's ability to conduct electrons, while proton conductivity

shows how porous is the material based on the proton movement inside the material porosity. In the present work proton conductivity of all selected carbon-based material has been measured within an electrode soaked in dilute acid. So it should be noted that the proton conductivity values obtained represent the movement of proton in the bulk electrolyte (Figure 44) and also the electrolyte which penetrate within the porosity of selected materials (Figure 45).

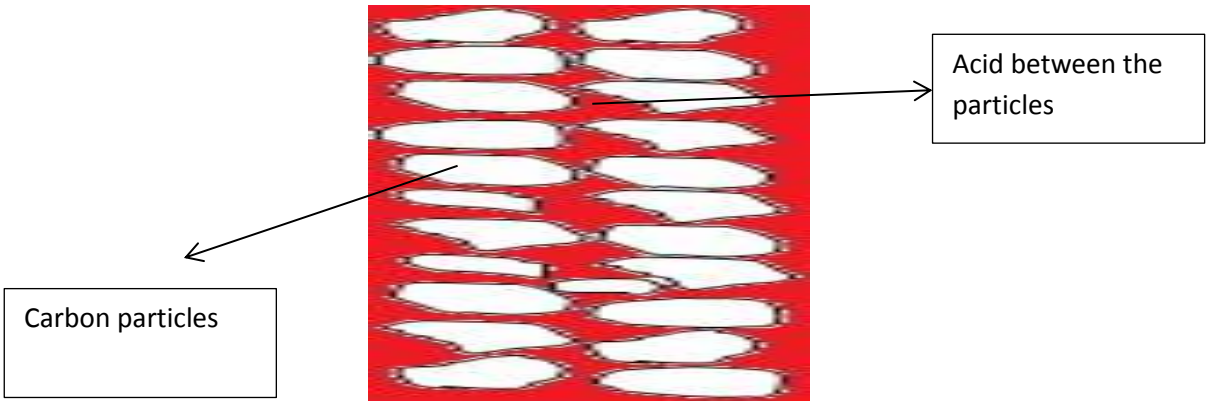

Figure 44: Presence of acid in the bulk electrolyte between the particles

Figure 45: Acid penetrated within the porosity of activated carbon particles

It should be noted that the electron conductivity is obtained from the solid medium of the electrode and the value measured here is bulk property of the electrode reflecting its porosity.

On the other hand, the proton conductivity of the electrode arises when acid fills the pores in the solid medium, both between particles and within particles. Proton conductivity as measure here is thus also a bulk property of the electrode plus acid, and not just the proton conductivity of the acid itself.

6.4.2 Electrochemical impedance spectroscopy

The proton conductivity of a porous electrode with pores filled by acid, as in the present case, can be measured by using electrochemical impedance spectroscopy (EIS). EIS is a characterisation and diagnostic technique that can be used in battery and fuel cell technology and devices (S. Buller et al. 2005). Electrochemical impedance is usually measured by applying an AC potential to an electrochemical cell and then measuring the resulting AC current through the cell. The impedance is then calculated and represented as a complex number on a Nyquist diagram where in the horizontal axis is the real part of the impedance and the vertical axis is negative of the imaginary part. A sample EIS output the spherical graphite is shown in Figure 46 (M. Tliha *et al.* 2010). The intersect of the Nyquist plot at the beginning which is at high frequency indicates the total resistance of the cell including the electrode. Then by subtracting the resistance of the holders and the membrane in between, what is left is the proton conductivity of the electrode.

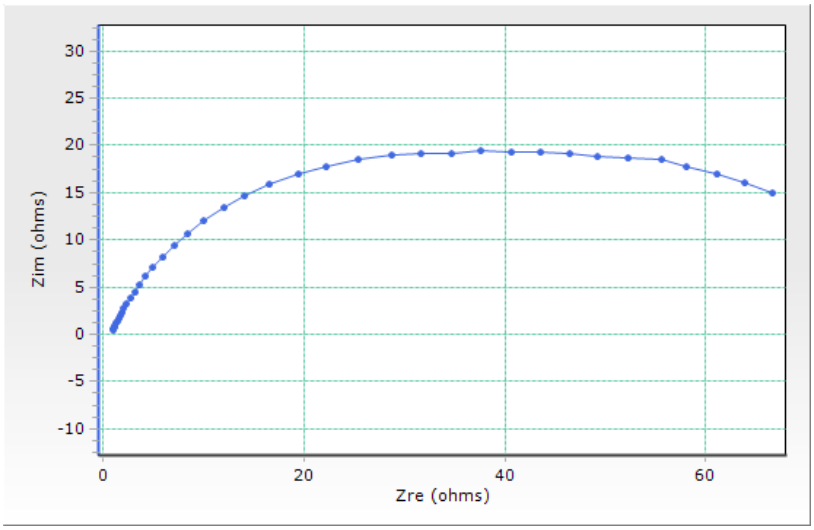

Figure 46: Nyquist plot for the spherical graphite sample obtained using Electrochemical Impedance Spectroscopy.

In the present work a Versastat 3 workstation machine was used to apply EIS. All the EIS tests were performed in the Sustainable Hydrogen Energy Lab, at RMIT University, Bundoora east campus, by the author.

6.4.3 Design and manufacture of the test cell for EIS method

In this study a split flat coin cell was used to perform the EIS test to measure the proton conductivity of the carbon electrodes soaked in 1 M sulphuric acid. The arrangement of the cell was such as the carbon electrode is sandwiched between two nafion-117 membranes. The nafion membranes are good proton conductors by very poor electron conductors. Hence the only current that can pass through the carbon electrode as an AC potential is applied across the whole cell is due to proton conductivity. So we can be sure that the resistance measured by the EIS test is due to proton movement.

To model the response of the EIS test, an equivalent circuit is shown in Figures 47 and 48.

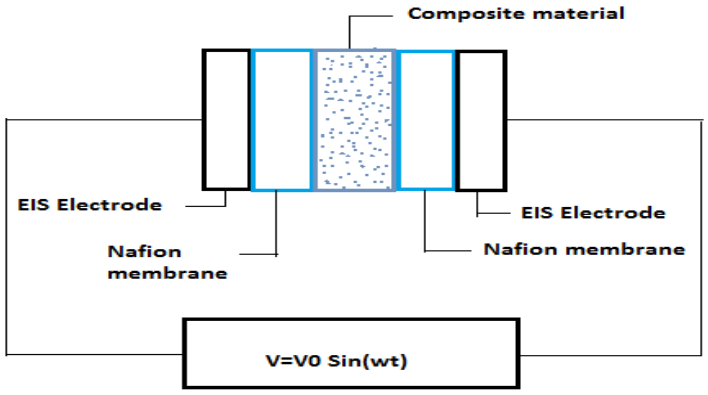

Figure 47: Test configuration for measurement of proton resistance with EIS (J. Jazaeri 2013).

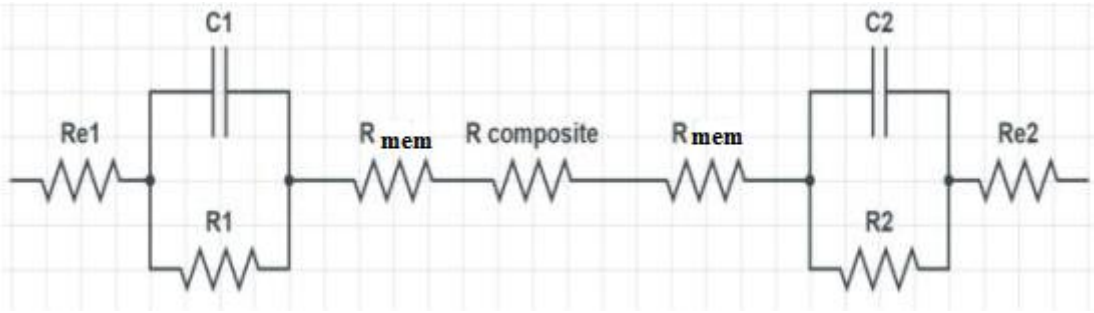

Figure 48: Equivalent circuit for measurement of proton resistance with EIS (J. Jazaeri 2013).

The electrical resistance of the metal electrodes are represented as Re1 and Re2 in Figure 7. The double-layer capacitances phenomena at the interfaces of the nafion membrane and the metal electrodes are represented by two sets of straight capacitors and resistances in parallel. The resistance of the nafion membrane to ion (H^+) transfer is R_{mem}. The total effective impedance for the equivalent circuit shown in Figure 48 is given by the following equation:

$$Z = R_{e1} + \frac{R1 \times \frac{1}{j\omega C1}}{R1 + \frac{1}{j\omega C1}} + R_{mem} + R_{electrode} + R_{mem} + \frac{R2 \times \frac{1}{j\omega C2}}{R2 + \frac{1}{j\omega C2}} + R_{e2} \qquad (31)$$

so as:

$$\omega \to 0, \quad Z \ \to R_{e1} + R_1 + R_{mem} + R_2 + R_{e2}$$

and as:

$$\omega \to \infty, \quad Z \ \to R_{e1} + R_{mem} + R_{e2}$$

At the high frequency limit, the total resistance measure on the real axis of the Nyquest plot represents the total proton resistance of the electrode, membranes and the plates (V. Ijeri *et al.* 2010).

So the final equation at high frequency for the equivalent circuit is simplified to:

$$Z(\omega \to \infty) = R_{e1} + R_{mem} + R_{electrode} + R_{mem} + R_{e2}$$

Where R_{e1} and R_{e2} are the ohmic resistances of the endplates due to electron flow, R_{mem} is the nafion resistance and $R_{electrode}$ is the carbon electrode resistance due to proton flow.

The total series ohmic resistance of the test rig includes the resistance of the stainless steel plates and the connecting wires to the EIS cell, that is introduced as R_{e1} and R_{e2}. This total series DC resistance to electron flow of the EIS set-up was measured separately simply by connecting together the EIS electrodes as shown in Figure 47. The Nyquist plot obtained for the corresponding EIS test is shown in Figure 49.

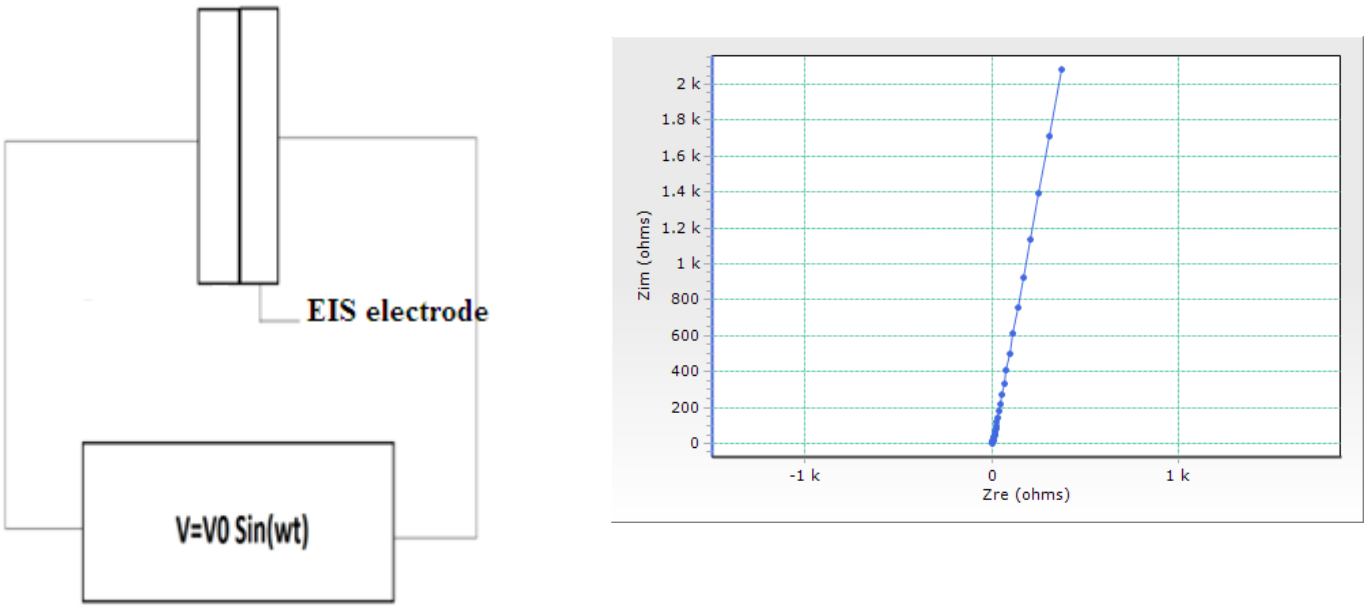

Figure 49: Equivalent circuit for measurement of proton resistance with EIS (J. Jazaeri 2013).

The results from EIS test for the two end plates shows that the total ohmic resistance for the outer plates was equal to 0.354 ohm (which is 0.177 ohm for each plate).

The proton conductivity of the nafion-117 used was measured earlier by Amandeep Obreoi and was equal to 0.1 S/cm (Obreoi, 2015).

6.4.4 Proton conductivity of the carbon electrodes soaked in acid

The EIS test was run for the whole circuit (Figure 48) and the total series resistance of the carbon electrode, nafion membranes and the end plates read from the high-frequency intercept on the real axis in the Nyquist plot. Knowing the ohmic resistance of the plates and the proton resistance of the nafion membranes the proton resistivity of the carbon electrode can be obtained from the equation:

$$R_{comp} = R_{EQ} - R_{e1} - R_{e2} - 2R_{mem} \qquad (32)$$

where R_{EQ} is the total resistance of the set up.

Then the proton conductivity of the carbon electrode is calculated from:

$$\sigma_{comp} = \frac{t}{R_{comp}A} \qquad (33)$$

where t is the thickness and A is the area of the carbon electrode. The measured proton conductivities of electrodes made from the four carbon samples are shown in the Table 15.

6.4.5 Electron conductivity of the carbon electrodes

The bulk electron conductivities of the carbon electrodes were measured simply by using a multimeter and a split flat coin cell. In this configuration the carbon electrode was sandwiched between two stainless-steel plates and the total ohmic resistance of the set up was measured. Subtracting the ohmic electron resistance of the end plates from the total resistance measured gave the effective bulk resistance of the carbon electrode (R_E), assuming contact resistances are negligible. The electron conductivity (σ_E in S/cm) can then be calculated from:

$$\sigma_E = \frac{t}{R_E A} \qquad (34)$$

where t and A are respectively the thickness and the area of the sample material in cm. The experimentally-measured electron and proton conductivities of electrodes made from all the carbon samples are shown in Table 15.

Table 15: Experimentally measured proton and electron conductivities of the aC-PTFE electrodes.

Sample	t (cm)	A (Cm2)	Proton conductivity of the sample in S/cm (σ_p)	Electrical conductivity of the sample in S/cm (σ_e)
aC'N 99	0.2	0.017	0.009±0.0004	7.8±0.3
Graphene platelets	0.2	0.017	0.005±0.0002	10.2±0.5
Flake graphite	0.2	0.017	0.001±0.0001	3.7±0.1
Spherical graphite	0.2	0.017	0.016±0.0008	12.1±0.6

6.5 Double-layer capacitance of carbon electrodes

6.5.1 Overview

The double-layer capacitance and reversible hydrogen storage capacity of the composite carbon electrodes with PTFE binder were measured using a liquid dilute sulphuric acid (1 M) electrolyte with this acid also penetrating into the spaces between carbon particles in the electrode, and into the internal pores of particles for the activated carbon electrodes. This capacitance is formed on the interfaces between the surfaces of carbon particles and the sulphuric acid that penetrates through the electrode, and between the inner pore surfaces and the acid. The influence of an electric field across the cell, protons in the form of hydronium ions move towards the surfaces of carbon particles (outer and inner). This surplus positive charge attracts electrons within the carbon towards the same surfaces. Hence the system acts like a capacitor, generating so-called double-layer capacitance. This capacitance thus contributes to the measured hydrogen storage potential of the carbon electrodes since the positively-charged hydronium ions (and the protons within them) are held electrostatically near the negatively-charged surfaces of pores within the carbon particles (in the case of porous activated carbon), or near the outer surfaces of the carbon particles in the case of the other samples.

6.5.2 Experimental setup to measure double-layer capacitance

A split flat coin cell for battery R & D supplied by MTI (Figure 50) was used to measure the double-layer capacitance of all the fabricated carbon electrodes.

Figure 50: Split flat coin cell for battery R & D of 15 mm diameter, used to measure double-layer capacitance

This coin cell comprised two end plates or metal electrodes with attached terminal clips for electrical connections (Figure 51). One of the end plates had a cavity of 15 mm diameter to accommodate the electrodes to be tested. The two identical test electrodes were separated by an electrical insulator made from filter paper.

Figure 51: Exploded view of split flat coin cell, diameter 15 mm

The end plates of the split flat coin cell were fastened by four screws and wing nuts. The electrolyte used was 1 M dilute sulphuric acid.

6.5.3 Double-layer capacitance of the carbon electrodes

Cyclic voltammetry was employed to measure the double-layer capacitance of the carbon electrodes using a VERSASTAT 3 electrochemical workstation.

Cyclic voltammetry (CV) is a very useful tool in the field of electrochemistry that has been applied to measuring the double-layer capacitance of supercapacitors, fuel cell and batteries (Hainan Wand and Laurent Pilon 2012). In such applications, only ions can access the electric double-layers formed at the electrode/electrolyte interfaces and there is no net electronic current due to presence of an electric insulator in between the two endplates of the cell. In CV an electric potential is applied between the two end plates of the cell and varied with time linearly and periodically the current generated over time is measured.

The shape of the cyclic voltammogram can be used to analyse the electrochemical charging and discharging process (Hainan Wand and Laurent Pilon 2012). At the beginning of the cyclic voltammetry test, the current increases by increasing the potential from zero to the maximum in charging of the carbon composite electrode, followed by decrease in voltage due to which the current goes negative.

Pairs of circular electrodes were fabricated for each carbon sample using the bottom cell mould shown in Figure 51 and the process described earlier in section 6.3.2

Each pair of electrodes was electrically separated in the cell by a porous filter paper serving as the electric insulator. The split flat coin cell was then closed and connected to the electrochemical workstation through terminals as shown in Figure 52.

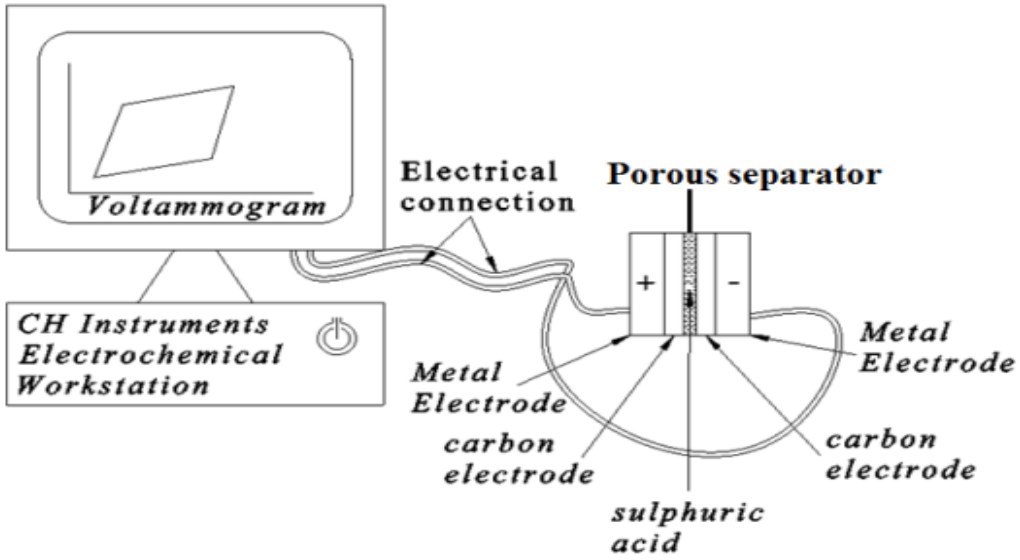

Figure 52: A schematic of the split flat coin cell connected to the electrochemical workstation for cyclic voltammetry (Amandeep Obreoi, 2015)

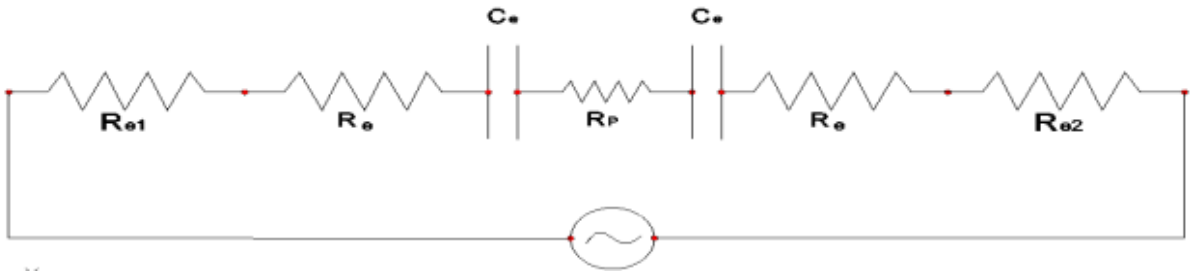

Figure 53: Equivalent circuit for capacitance measurement in a bottom cell set up

The equivalent circuit associated with the capacitance measurement arrangement is shown in Figure 53. In this Figure, R_{e1} and R_{e2} represent the resistances of the end plates, R_e represents the resistance of the electrode, and R_p is the bulk resistance between its two faces, to proton transport. The electrochemical workstation was set to perform cyclic voltammetry or the linear sweep of potential (from 0 volts to 1.5 volts) with respect to time was applied and voltage was increased in equal incremental steps.

Figures 54 to 57 show the linear sweep voltammogram for selected carbon samples.

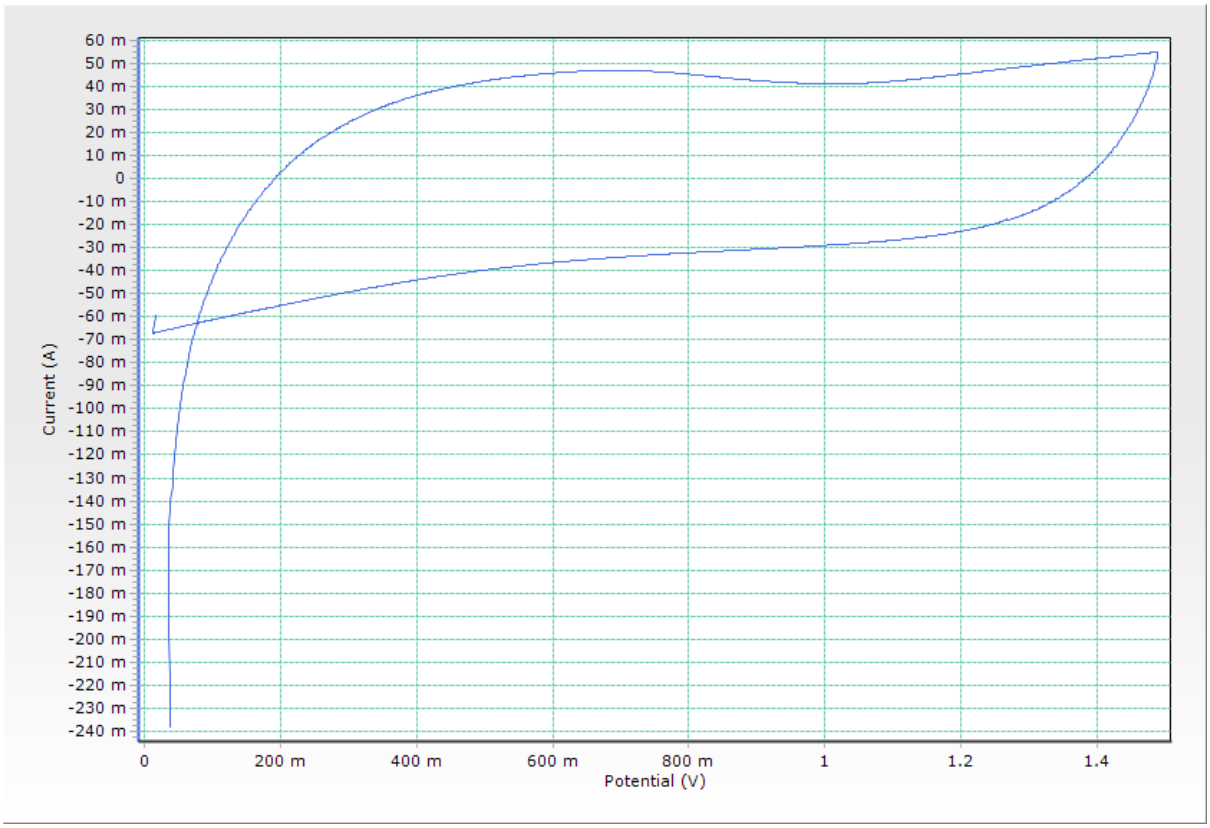

Figure 54: Cyclic voltammogram for graphite-PTFE sample electrode, Scan rate 2mV/s

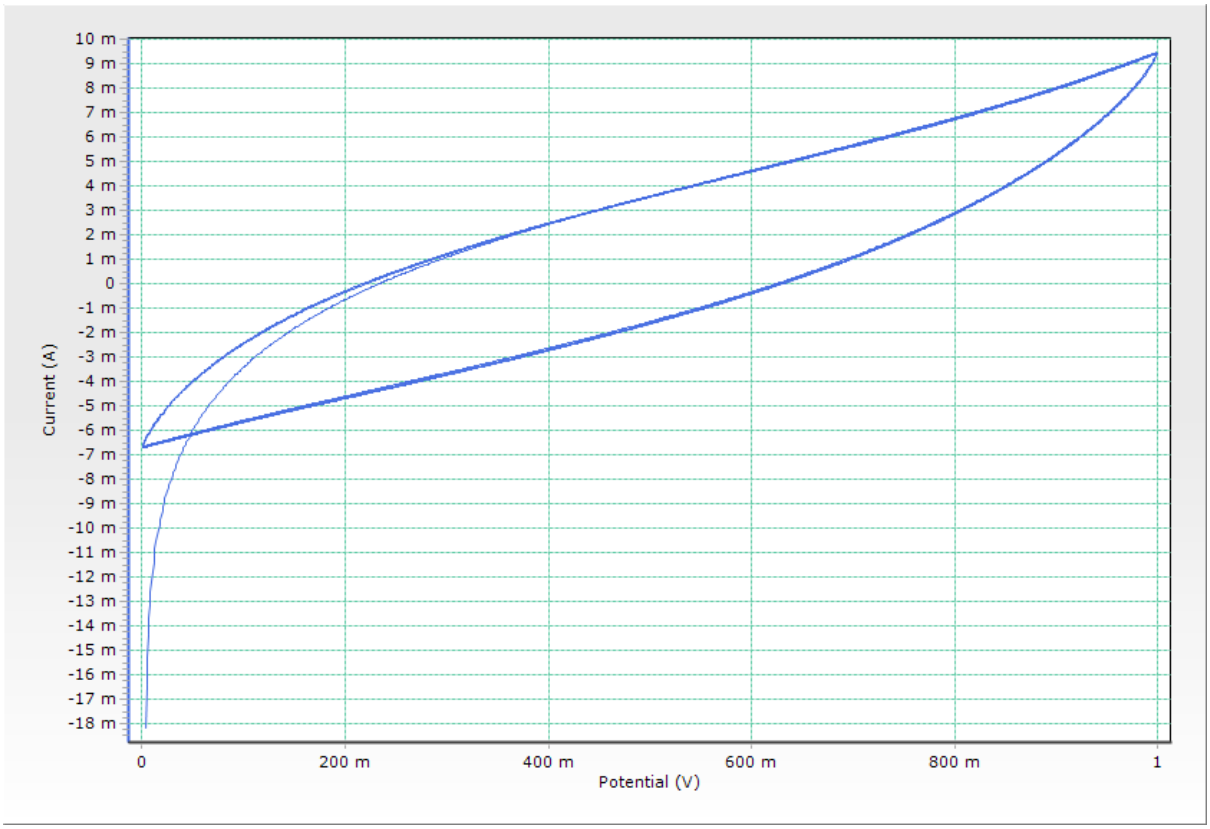

Figure 55: Cyclic voltammogram for flake graphite-PTFE sample electrode, Scan rate 2mV/s

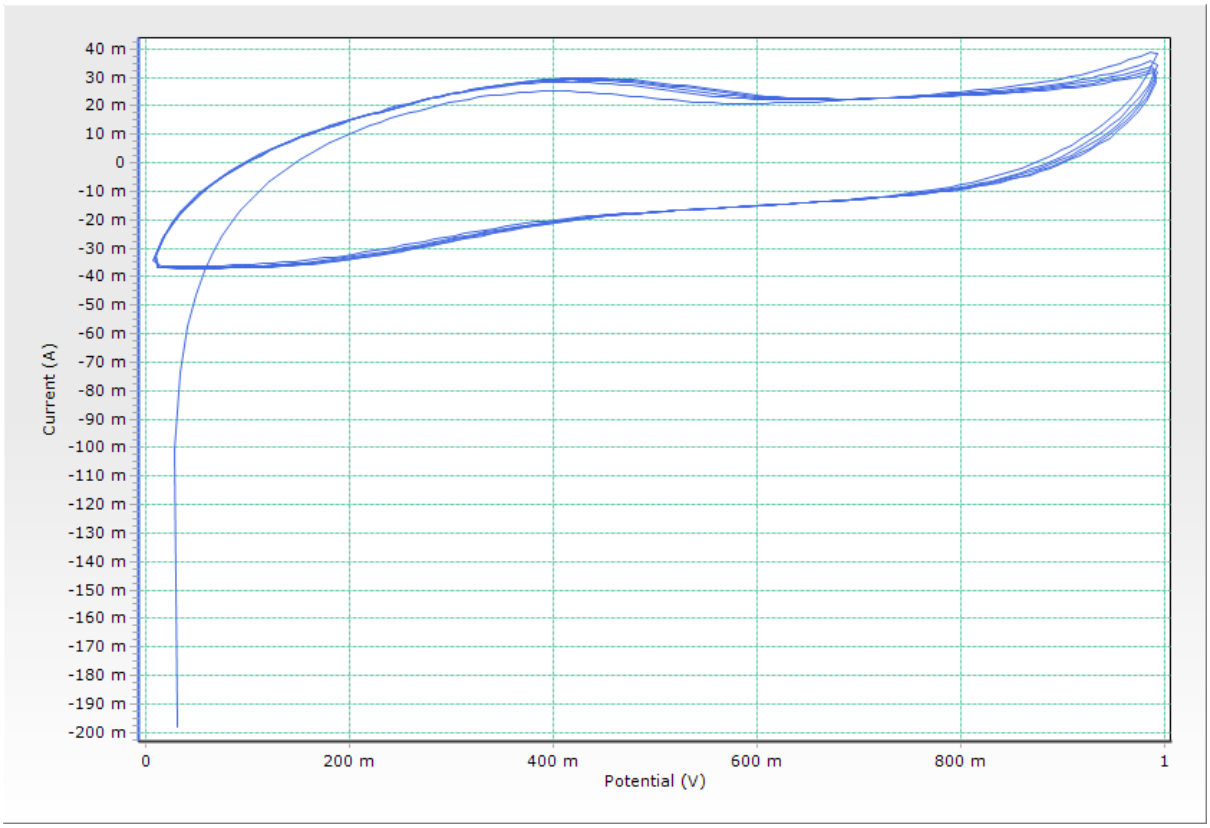

Figure 56: Cyclic voltammogram for graphene-PTFE sample electrode, Scan rate 2mV/s

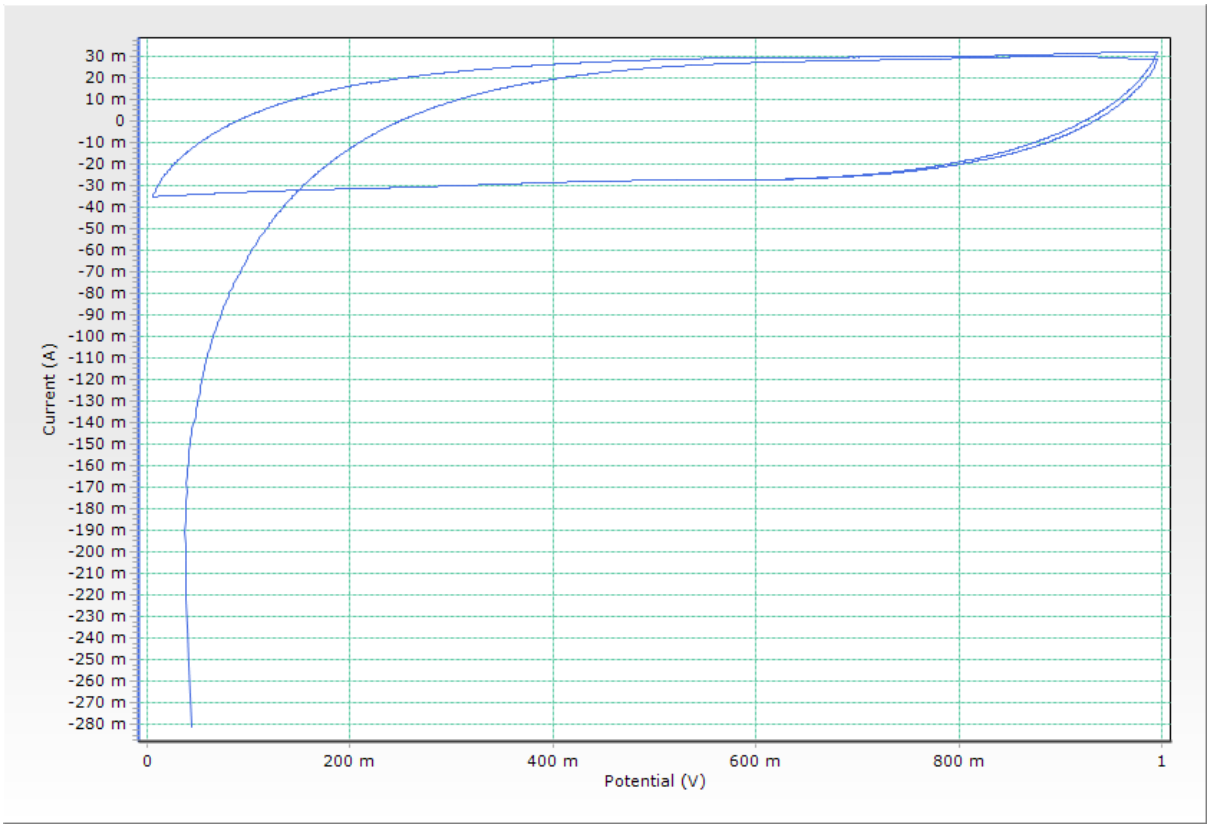

Figure 57: Cyclic voltammogram for aC'N99-PTFE sample electrode, Scan rate 2mV/s

The peak current where the graph tends to horizontal line was estimated from the voltammogram to calculate the double-layer capacitance per unit mass of carbon composite in the electrodes using the equation (A. Velikonja 2014).

$$C = \frac{I_{peak}}{V_t \times M_c} \qquad (35)$$

where

C → capacitance in F/g

I_{peak} → peak current in mA (the highest identified value of current from Figure 39)

V_t → scan rate in mV/s

M_c → mass of carbon in gram.

In the present study the scan rate applied in linear sweep experiment for all carbon samples has been set to 2 mV/s. In the present study, the scan rate applied in linear sweep experiments for all carbon samples was set to 2 mV/s. Higher scan rates up to 50 mV/s were also tried, but the results indicated that at the higher scan rates there was no plateau characteristic of double layer capacitance effect observed.

The values for double-layer capacitance per unit mass of all fabricated carbon composite-PTFE sample electrodes obtained from the experimental voltammograms and using this calculation method are presented in Table 16.

Table 16: Double-layer capacitance of all fabricated carbon sample electrodes

Sample	Peak current (mA)	Scan rate (mV/s)	Mass of carbon powder (grams)	Total mass of electrode (grams)	Capacitance considering total mass of the electrode (F/g)	Capacitance considering mass of carbon powder (F/g)
aC-N 99	20±2	5	0.3	0.35	11.42±1	13.3±1
Graphene platlets	30 ±2	5	0.65	0.73	8.2±0.8	9.2±0.9
Flake graphite	10 ±2	5	0.33	0.4	5±0.5	6.06±0.6
Graphite	50 ±2	5	0.7	0.78	12.98±1	14.28 ±1

The double-layer capacitance of all selected carbon samples varies between 9.2 F/g to 14.28 F/g. The highest value 14.28 F/g is obtained for the spherical graphite while the lowest one 9.2 F/g was for the flake graphite sample.

6.6 Electrochemical hydrogen storage in carbon-based electrodes

6.6.1 Overview

Carbon materials have been researched extensively as energy storage media for electrical devices like supercapacitors (Jurewicz and Vix Guterl *et al.* 2004). Electrochemical hydrogen

storage by electrolysis of water is one of the potential electrochemical applications of carbon materials. This process consists of storage of electrical charge through electro-reduction of water and formation of weak chemical bonds between hydrogen and carbon. Various types of carbon material such as activated carbons, carbon nanotubes (CNT), and lately graphene-based materials have been explored by scientists for this application. Various forms of graphite have already been used for storing Li+ ions in Li-ion batteries.

In this section, the experimental apparatus to measure the electrochemical hydrogen storage capacity of the four carbon materials selected is first described. The results obtained for the storage capacities of the samples with a liquid dilute sulphuric acid electrolyte using galvanostatic charging discharging are then reported

6.6.1 Experimental set up to measure electrochemical hydrogen storage

6.6.1.1 Preparation of dilute (1 M) sulphuric acid as the electrolyte

Dilute sulphuric acid was chosen as the acid electrolyte for the present project since it is easily available and a good proton conductor. The first step in preparation of 1 M dilute sulphuric acid from the concentrated acid was to calculate the molarity of the concentrated acid. In the present project the molarity (number of moles contained in 1 litre of reagent) of the 98% concentrated sulphuric acid used was 18.4. The volume of concentrated sulphuric acid required to prepare 1 litre of dilute sulphuric acid of 1M molarity was calculated from equation 36:

$$\frac{1\ ml}{0.0184\ moles} = \frac{x\ ml}{1\ mole} \qquad (36)$$

where

x → is the required volume.

Solving for 'x' in equation 36 gave the value of 54.3 ml. This volume of the acid was slowly added into 945.7 litres of distilled water to obtain 1 litre of 1 M dilute sulphuric acid solution in total. For safety reasons, it is essential for the concentrated acid to be added slowly into the

much larger volume of distilled water, since the reaction is exothermic. The container was stood in cold water and the mixture continuously stirred to dissipate the heat evolved from the exothermic reaction. This dilute acid was then used to fill the electrolytic cell to act as the electrolyte in the electrochemical experiments.

In the present study no examination of the effect of varying this molarity was studied. But it may be worthwhile to conduct this investigation in the future to find the optimal molarity for this application. There will be an upper limit to the molarity employed to avoid chemical attack on the electrode materials themselves, and materials in the experimental apparatus.

6.6.2 Designs for experimental set-up considered

6.6.2.1 Overview

Three different designs for the experimental set up for the galvanostatic charge-discharge measurements were evaluated:

- A standard two-electrode electrochemical cell
- A modified Hoffman voltammeter
- A combination of a two-electrode electrochemical cell and Hoffman voltammeter for gas collection.

These three set-ups are now described in turn and their advantages and disadvantages are discussed.

6.6.2.2 A standard two-electrode electrochemical cell

The two-electrode electrolytic cell considered in the present project was custom-made on request of the author by Xi'an Yima Opto-electrical Technology Co. Ltd. located in China (Figure 58). The specifications of the two-electrode electrolytic cell are listed in Table 17.

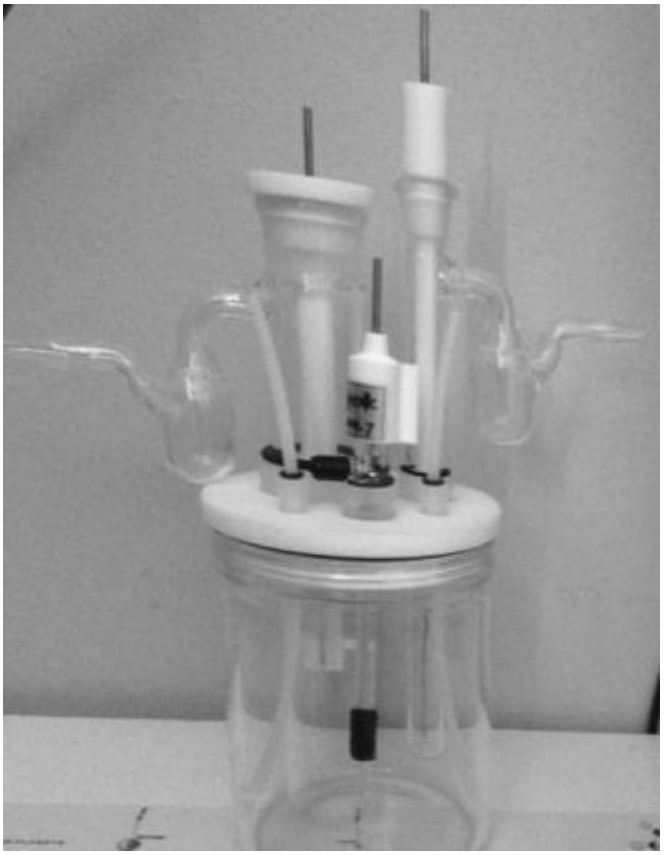

Figure 58: Two electrode-electrolytic cells used to measure the electrochemical hydrogen storage capacity

Table 17: Specifications of the Xi'an Yima Opto-electrical Technology Co. Ltd C001 electrolytic cell

Name	Description
Type	3-electrode sealed electrolytic cell
Model	C001
Volume	250 ml
Diameter	60 mm
Height	90 mm
Sealing	PTFE cover
Auxiliary/Counter electrode	Platinum wire of 0.8 mm diameter and 50mm length
Reference electrode	Hg/HgO
Working electrode	Fabricated aC-PTFE electrodes
Gas collection	Glass tube housings on counter and working electrode

The working electrode holder supplied by the manufacturer is shown in Figure 59, and the other two electrodes made from stainless steel (counter and reference) in Figures 60 and 61.

Figure 59: Expanded working electrode holder for C001 electrolytic cell

Figure 60: Counter electrode (platinum wire) for C001 electrolytic cell

Figure 61: Reference electrode (Hg/HgO) for the C001 electrolytic cell

The final configuration of the set up with gas collection cylinder connecting to the device is shown in Figure 62.

Figure 62: Graduated cylinders connected to working and counter electrodes of the 3-electrode electrolytic cell

After connecting the set up to the electrochemical workstation and starting the charging it was noticed that this set-up is not accurate enough. The first problem observed was the gap between the fluid in the cylinder and the connection tubes (distilled water), and the fluid in the electrochemical cell, which is dilute acid. This gap is filled by air. To avoid mixing the distilled water in the collection cylinder and the connection tubes with the acid in the electrochemical cell it was impossible to get rid of air trapped in the middle. So at the beginning of the experiment air is mixed with oxygen and the hydrogen gas generated, which is clearly not desirable.

The other problem observed was how to balance the pressures, and the levels of acid, in the hydrogen and oxygen side tubes. At the beginning of the experiment, as expected, the rate of hydrogen gas production is much lower than that for oxygen gas, since the majority of the protons liberated enter the storage material and bond with the carbon particles after neutralisation by electrons. So the pressure build up on the oxygen side is greater than on the hydrogen side. Consequently, in the first hour of the experiment the level of acid in the oxygen-side tube was decreasing and in the hydrogen-side tube it was increasing. So progressively the acid in the oxygen side tube was pushed out by the gas and the experiment had to be stopped.

To overcome with this problem, one solution was to separate the oxygen side and hydrogen side tube with a membrane, then the pressure in each side does not affect the other side. Hence in the next experimental set up a Hoffman voltammeter apparatus with some modification was used.

6.6.2.3 Hofmann voltameter apparatus for electrochemical hydrogen storage

The picture of the normal Hofmann apparatus cell is shown in Figure 63. As can be seen it contains two collection cylinders with a header in between to balance the level of liquid in each tube. Here the header balances the pressure in the columns and then the pressure built up in each tube does not affect the other one.

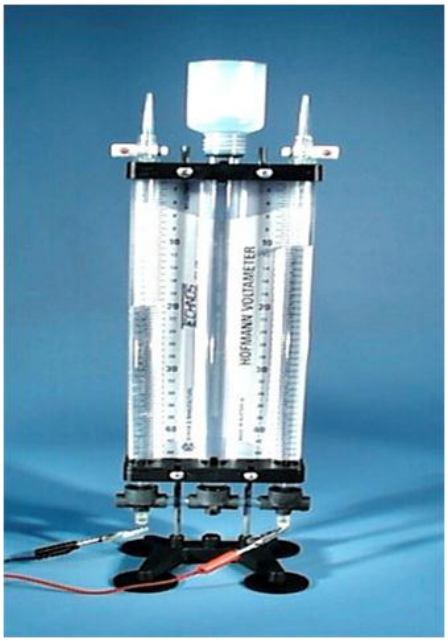

Figure 63: Hofmann voltameter apparatus

For the present experiments, some modifications to the usual Hofmann apparatus were made as follows.

In the first modification to the apparatus, the diameter (outer) of one of the electrode tubes was changed to 1 cm, so the carbon electrodes to be tested (dimensions 7 mm x 25 mm x 2 mm) could fit into the tube lengthways with an electrical conductor attached and passing through the end plug of the tube to the outside to allow electrical connection to a power source. Figure 64 details the modification made.

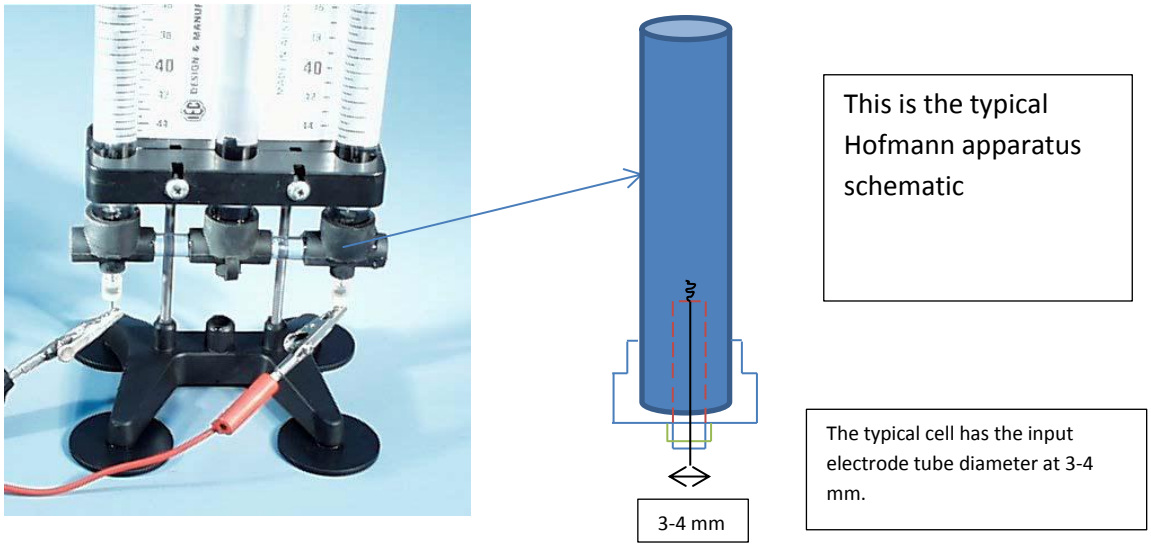

Figure 64: schematic of the electrode in the cell, on right the schematic of the electrode connection to the platinum wire is shown

As the carbon electrode had to be fitted inside the tube (diameter 1 cm), it was cut in half to a width of 7 mm, as shown in Figure 65. Also to hold the carbon sample at the end of the electrode inside the tubes a stainless steel clip as shown in Figure 66 was designed.

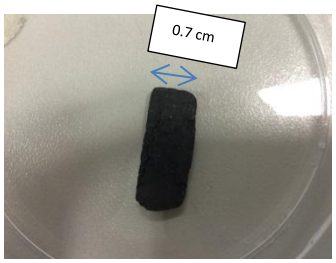

Figure 65: Reduced width of the electrode after being cut in half so that it fitted in the tube of the Hofmann voltammeter

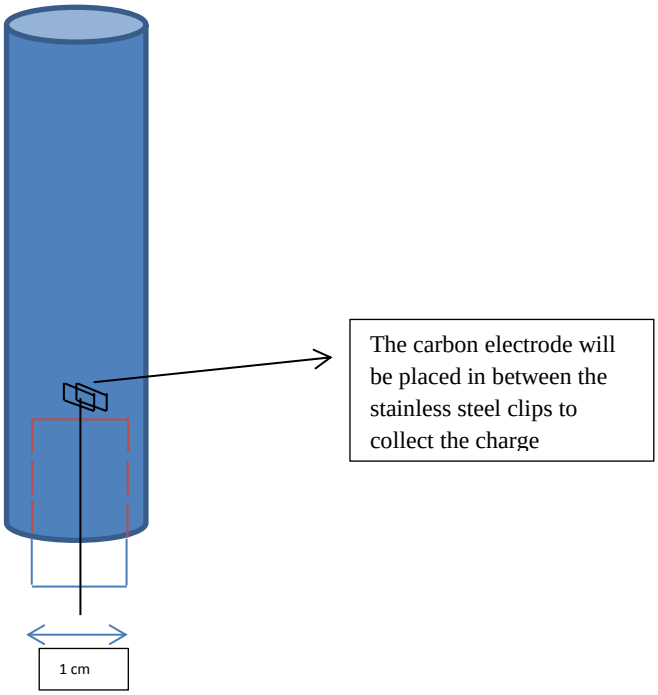

Figure 66: Stainless steel clips designed to hold the electrode on the hydrogen side

In the second modification to the apparatus, in the oxygen electrode side an additional small tube passing through the end plug was designed to allow oxygen from an external gas bottle to be blown onto the platinum electrode in the form of bubbles.

The resulting configuration is shown in Figure 67.

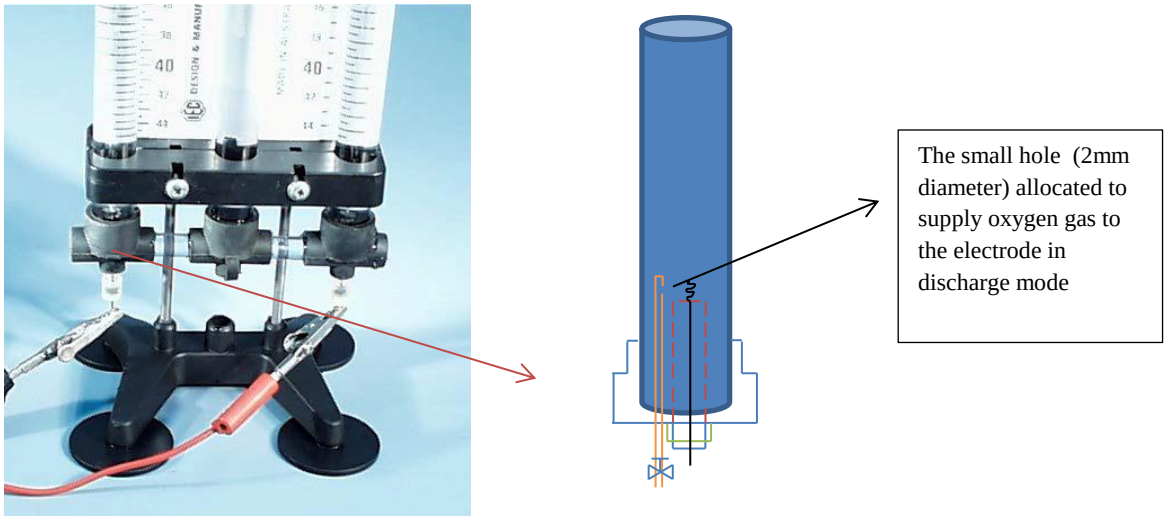

Figure 67: The modified oxygen-side electrode with a small hole for oxygen supply in discharge mode

The modified Hofmann voltameter apparatus was then trialled for galvanostatic charging and discharging of a sample electrode. However, a very high voltage (up to 4.2 V) across the cell was needed to obtain even a relatively low charging current of 40 mA. Figure 68 compares the initial V-I curve obtained during charging for the earlier two-electrode electrochemical cell and that obtained with the same sample with the Hofmann cell. At a voltage such as 2 V, the obtained current in the Hofmann cell was much lower than the two-electrode electrochemical cell. As was observed, to achieve a certain current at 40 mA the required voltage in the Electrochemical cell is about 1.7 while in the Hofmann cell the voltage was measure as 4.2 V.

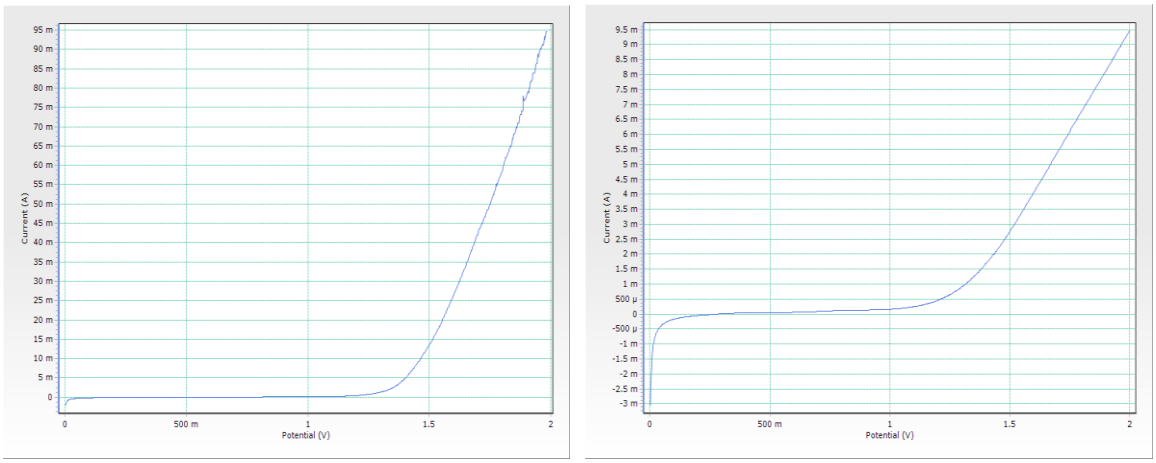

Figure 68: initial V-I curve for graphite sample in electrochemical cell (on left) and Hofmann cell (on right)

An EIS test was therefore conducted on both cells to measure the total series resistance.

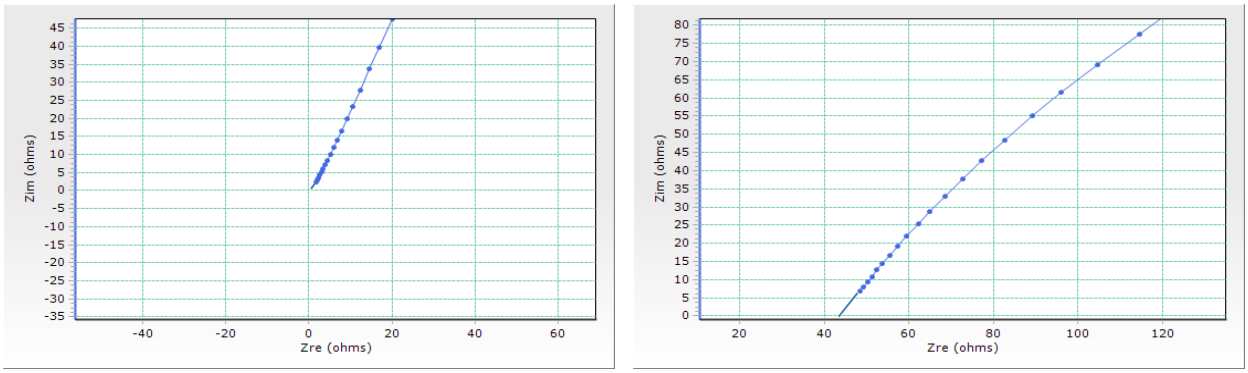

Figure 69: EIS for 3electrodes electrochemical cell (on left) and Hofmann cell (on right)

The results from EIS test show the overall resistance in the both cell (Figure 69). Then by subtracting the resistance in the electrodes, what is left is the resistance between the two electrodes. Figure 69 shows that the resistance between the two electrodes in two-electrode electrochemical cell is about 1.1 ohm and in the Hofmann cell is 42.5 ohm. This big difference between two cells is due to the distance between the two electrodes in the Hofmann cell compare to the electrochemical cell.

A high voltage during charging is not desired since in increases the relative proportions of hydrogen gas production versus storage of H within the carbon electrode. Moreover after two hours charging at 4.2 V some corrosion of the hydrogen-side electrode was observed (Figure 70). Such corrosive electrochemical reactions are much more likely at higher charging voltages.

Figure 70: Hydrogen-side electrode damaged due to higher voltage during charging

A further problem in using the Hofmann cell is that its relatively high series resistance substantially inhibits the fuel cell mode reaction, since the cell voltage falls to below 0.5 V at even a very low discharge current.

For these reasons, a third experimental set-up was designed, incorporating the favourable features from the first two set-ups.

6.6.2.4 Combined two-electrode electrochemical cell and Hofmann apparatus for gas storage

The final set up that was designed consisted of a two-electrode electrochemical cell similar to the first electrochemical cell, with Hofmann-type inverted burettes used for gas collection (Figure 70). The two-electrode electrochemical cell had a relatively small gap between the two electrodes and hence low series resistance, making it suitable for charging and discharging. The Hofmann burettes and header allowed gas collection while balancing the pressures and levels over the two electrodes this set up was thus found to permit charging without excessive voltages, as well as effective discharging in fuel cell mode, while providing enough accuracy in volumes of gas collected.

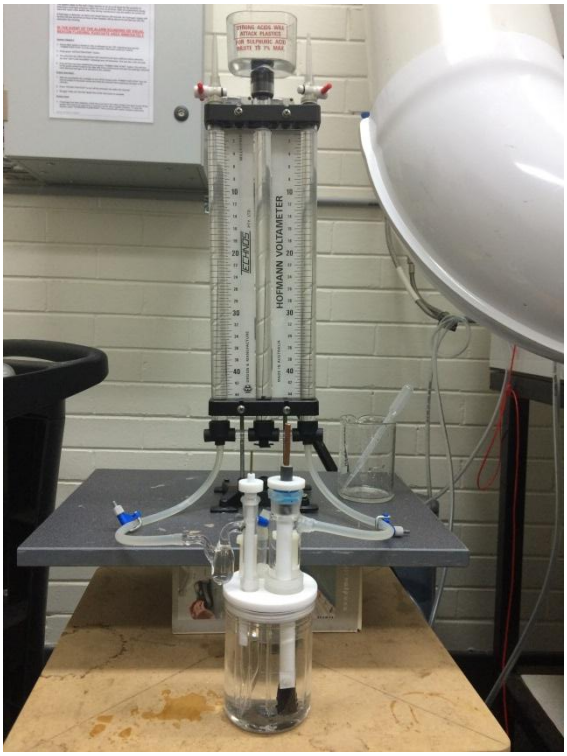

Figure 71: Combined electrochemical cell –Hofmann apparatus

6.6.2.5 VI curves

The first measurement to be done was to get a V-I curve for each sample before charging to choose an appropriate charging current. Figure 72 shows the V-I curve for the selected samples. The charging current chosen was dependent on the voltage and the rate of the hydrogen gas production. As the voltage increases, the current increases as well, but at higher voltages there is a higher propensity to produce hydrogen gas, which is not desirable. So the current chosen was in the safe zone wherein there was a reasonably high charging current without formation of hydrogen gas as well.

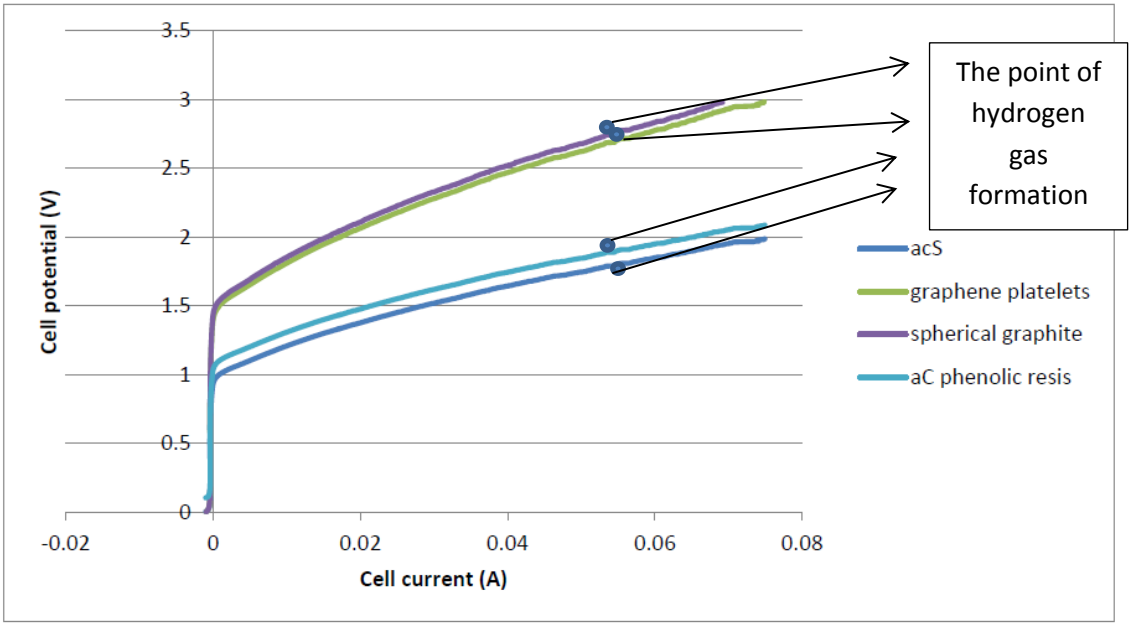

Figure 72: The experimental V-I curve for all selected samples

The point of gas formation is shown on Figure 72 for each sample. Hence if in charging mode the voltage reaches this value, the hydrogen produced will be in the form of gas rather than staying as hydronium and bonding electrochemically to the carbon in the electrode. So to avoid hydrogen gas production with all the samples, a charging current of 40 mA (0.04 A) was chosen.

6.6.2.6 Galvanostatic charge and discharge

A preliminary test of simple electrolysis was run on all the fabricated carbon electrodes with 1 mol dilute sulphuric acid as electrolyte to mark the voltage and current values on a VI curve where H_2 gas formation started, as explained in the previous subsection. To avoid the hydrogen gas generation the charging voltage and hence current and in galvanostatic charging were kept below the critical value of 40 mA. The carbon-PTFE sample electrodes were then charged (galvanostatic charging or electrolyser mode) at this constant charging current, until a sudden rise in hydrogen gas generation was observed, indicating that the storage had reached its maximum capacity. The total charging time recorded was 5 hours. The water was

split into hydrogen and oxygen ions on the counter electrode with the usual water electrolysis reaction:

$$H_2O \rightarrow 2\ H^+ + 0.5\ O_2 \qquad (37)$$

The oxygen gas liberated by reaction at the counter electrode was collected in the graduated cylinder and the volume of gas was recorded. This amount was later used in the calculations to estimate the quantity of hydrogen produced electrochemically. The hydrogen gas formed at the working electrode was collected in another graduated cylinder and its volume was recorded.

After galvanostatic charging of the cell, the system was allowed to rest for 1 hour before switching to galvanostatic discharging. Thereafter, the electrolytic cell was set for discharging (fuel cell mode) at constant discharge current. The time for discharging was recorded.

The entire process of galvanostatic charging and discharging of the cell during both cycles was recorded in the form of potential versus time curves for all the electrodes. These curves are shown in Figures 73 and 74.

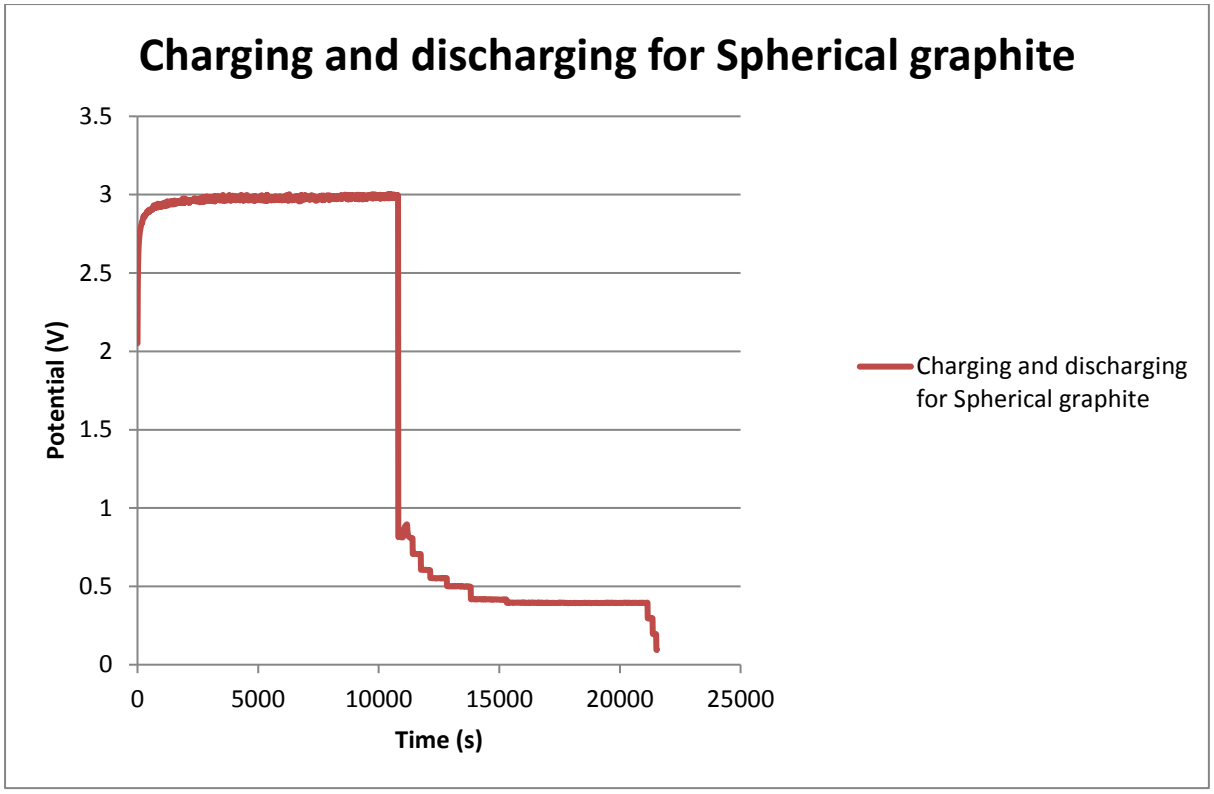

Figure 73: Galvanostatic charge-discharge curves for sample spherical conductive graphite in 1 mol sulphuric acid. Charge 40 mA during 5 hours, discharge: 2 mA, until open circuit potential.

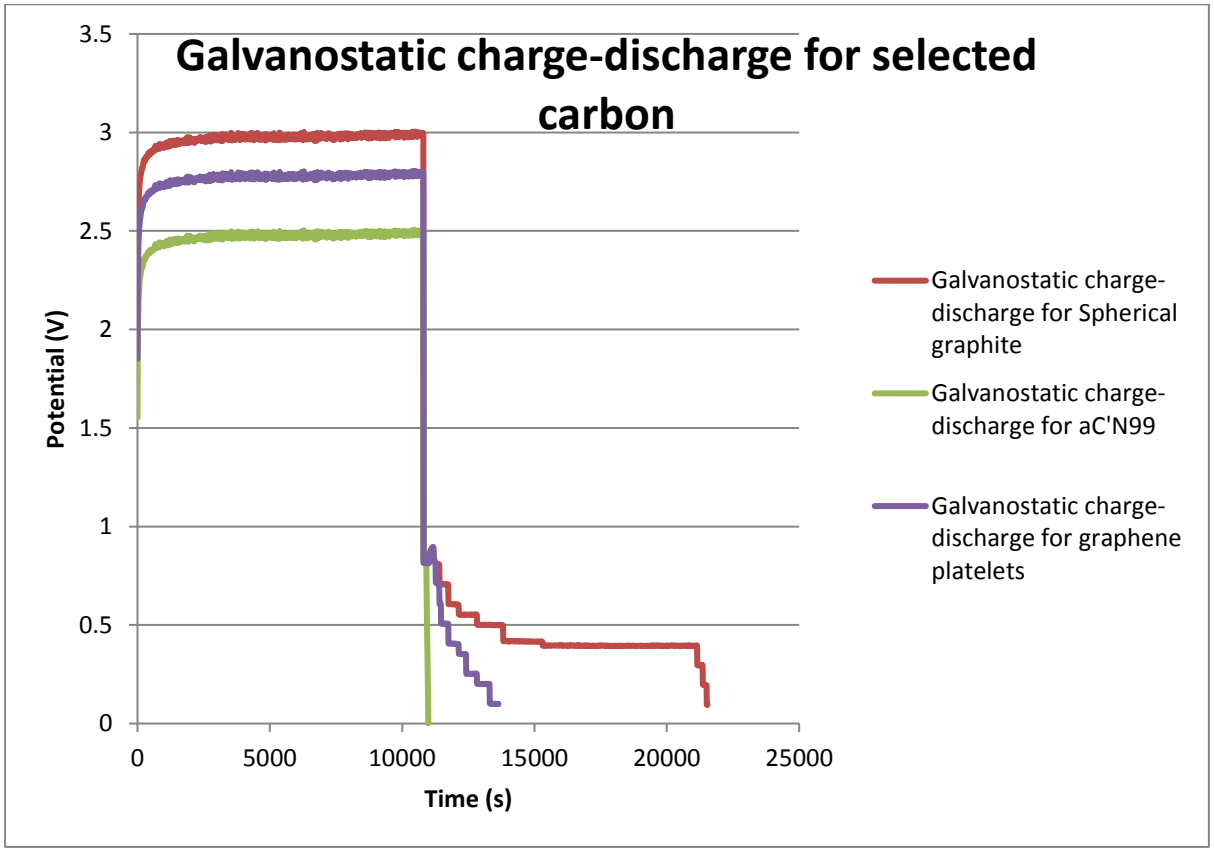

Figure 74: Galvanostatic charge-discharge curves for selected carbon in 1 mol sulphuric acid. Charge 40 mA during 5 hours, discharge: 2 mA, until open circuit potential

In the process of galvanostatic charging, hydrogen was stored electrochemically in the carbon electrode under the influence of the charging current (40 mA during 5 hours). The amount of hydrogen reversibly stored was assessed by subjecting the cell to the discharge current of 2 mA until a near zero potential was reached. It is important to note that oxygen gas has also been collected from the beginning of the experiment. At the end of the charging experiment the amount of oxygen gas collected has been completely in agreement (with less that 1% error) with the theory from the Faraday's law.

In galvanostatic charging the total hydrogen stored was calculated as the difference between the total theoretical hydrogen production using Faraday's law, and the amount of hydrogen gas collected. The amount of hydrogen (M mols) produced at I amps for t seconds is given by:

$$M = \frac{I.t}{F} \qquad (38)$$

where F is the Faraday constant (96485 C). Therefore the hydrogen produced at 40 mA for 5 hours electrolysis is equal to 0.0074 mol.

Table 18 shows weight percentage of hydrogen stored during charging for the selected carbon samples, calculated from the experimental data by this method.

Table 18: Weight percentage of hydrogen stored during charging for the selected carbon samples. The error ranges are estimated from instrumental measurement errors

Name of carbon material	**Hydrogen mol produced (mol)**	**Volume of hydrogen collected (cm^3)**	**Mass of hydrogen stored (g)**	**Wt% hydrogen stored**
aC'N99	0.0074	85±1	0.000518	0.051±0.005
Graphene	0.0074	82.8±1	0.00147	0.147±0.001
Flake graphite	0.0074	90±1	0.000148	0.014±0.001
Spherical graphite	0.0074	71.76±1	0.002951	0.2951±0.003
aC phenolic resin	0.0074	46±1	0.00191	0.62±0.006

All the error ranges in this chapter have been measured by considering the fraction errors that may occur due to the limits in precision of instrumental measurements.

During galvanostatic discharge, the total charge flow (in coulombs) was calculated using equation below.

$$Q_{discharge} = I \, . \, t \qquad (39)$$

where,

I → current (A)

t → discharge time (s).

The mass of hydrogen released from the electrode was calculated by using equation 40.

$$M = \frac{I \, . t}{1000 \, . F} \qquad (40)$$

where

M → mass of hydrogen generated in kg.

I → discharge current in mA

t → discharge time in sec.

F → Faraday's constant (96 485 C mol^{-1})

Hence, the amount of hydrogen released from carbon was calculated by applying equation 41:

$$M\ \% = \frac{M}{M + M_C} \qquad (41)$$

where

M → mass of hydrogen in kg

M_C → mass of activated carbon in kg

The hydrogen mass % released in the carbon electrodes as measured and estimated in the discharge part of the cycle are listed in Table 19.

Table 19: Equivalent mass of hydrogen released in carbon sample in discharge

Name of the sample	Galvanostatic discharge current [mA]	Time of discharge (second)	Equivalent mass of hydrogen released in carbon [mass %]
aC'N99	2	60	0.00024±0.00001
Graphene	2	3650	0.015±0.001
Flake graphite	2	100	0.001±0.0001
Spherical graphite	2	10000	0.0296±0.001

Table 20 shows the comparison of equivalent mass of hydrogen stored and released for all selected carbon samples.

Table 20: equivalent mass of hydrogen stored and released

Name of the sample	Wt% hydrogen stored	Equivalent mass of hydrogen released from carbon [mass %]
aC'N99	0.051±0.005	0.00024±0.00001
Graphene	0.147±0.001	0.015±0.001
Flake graphite	0.014±0.001	0.001±0.0001
Spherical graphite	0.2951±0.003	0.0296±0.001
aC KOH 1:7 with 30% PTFE	0.6125±0.006	0.2026±0.002

6.7 Comparing experimental and theoretical VI curves in E-mode

6.7.1 Fitting theoretical to experimental VI curves

A theoretical V-I curve was obtained for each carbon-based electrode in the electrochemical cell using the theoretical analysis presented in chapter 4 and the associated MATLAB model of chapter 5. To find the best-fitting theoretical V-I curve to the experimental curve for each sample, the experimental V-I curve was set as the target, and the input parameters in the model such as exchange current density, reversible reaction potential and charge transfer coefficient varied to minimise the differences between experimental and the modelled curve.

It is important to mention that even the best fit curves obtained has an error of around 2% as can be seen in Figure 76.

Figure 75 shows how the modelled V-I curve was progressively fitted to the experimental curve for the aCS sample by changing the charge transfer coefficient and exchange current densities input to the model.

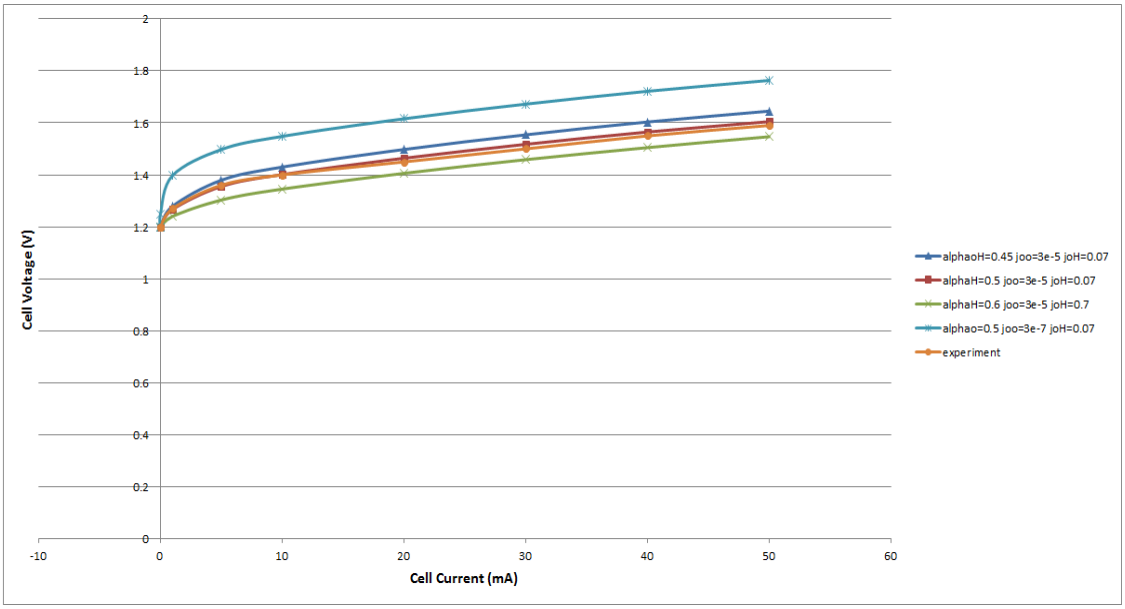

Figure 75: The best fitting theoretical VI curve to the experimental curve for aCS

In the present work, all the variable values on the oxygen side are fixed based on the concept of the oxygen gas evolution reaction (Doddathimmaiah, 2009).

Figure 76 shows the fitted V-I curve from the theory and the experiments for all selected carbon-base materials.

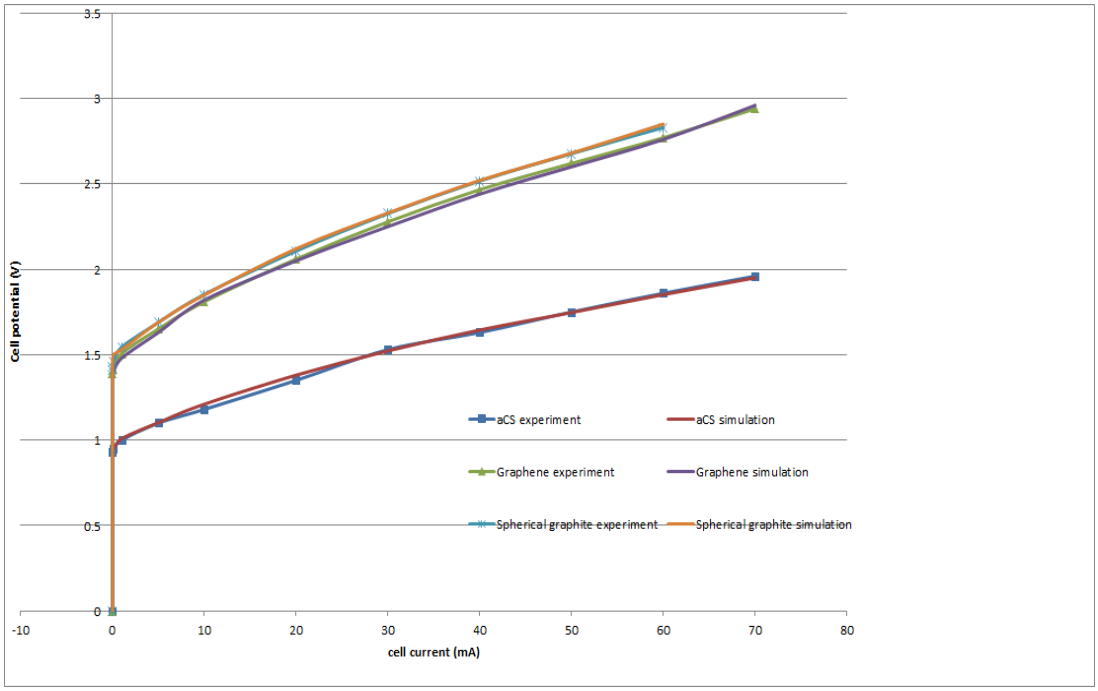

Figure 76: Best-fitting theoretical and experimental V-I curves for activated carbon, graphene and graphite sample

The fitted variable values obtained are shown in Table 21.

Table 21: best fitting parameters value in the model for the experimental values

Samples	Parameter				
	j_0^H (A/cm^2)	j_0^O (A/cm^2)	α^H	α^O	E_0 (V)
aCS	0.0072	3e-5	0.53	0.50	0.8
Graphene platelets	0.00065	3e-5	0.68	0.50	1.3
Spherical graphite	0.00082	3e-5	0.7	0.50	1.4
aC KOH 1:7	0.054	3e-5	0.52	0.50	0.9

6.7.2 Discussion

The H-side exchange current densities for all carbon samples varied between 0.00065 and 0.054, which the smaller values are obtained for graphitic sample and the larger value for activated carbon (Table 19). The exchange current density indicates the rate of the charging reaction for a given overpotential for different samples, so a higher value shows that the reaction at a given rate takes place at a lower potential. The H-side charge transfer coefficient found for aCS was 0.53, which suggests that the reaction of hydrogen and carbon in charging and discharging mode is almost reversible (section 5.3). Consistent with this finding, the results of the electrochemical hydrogen storage using the electrochemical cell also showed that the equivalent hydrogen stored and released using aCS were about 0.58 and 0.55 wt% respectively, that is, the charge - discharge reaction was relatively reversible (Amandeep Obereoi, 2015). The values for charge transfer coefficient obtained for the graphene platelet electrode was 0.6, and that for the graphite electrode was 0.7, indicating that the hydrogen charging reaction in these samples is to some degree more favoured than discharge mode. The results from the electrochemical hydrogen storage for the graphene platelet and graphite electrodes presented in chapter 6 also shows that their equivalent hydrogen storages were 0.3 and 0.14 wt% respectively, while the corresponding amounts of hydrogen released on discharge were 0.029 and 0.014 wt% respectively. Once again these relative values are consistent with the findings of the best-fit values for the H-side charge transfer coefficients for these samples, which were both greater than 0.5.

Another notable finding from the best-fit parameters pertains to the reversible reaction potentials. For the aCS sample and aC KOH 1:7, the reversible reaction potentials were found to be 0.8 V and 0.9 V respectively, but for the graphene platelet and graphite electrodes they were much higher at 1.3 V and 1.4 V respectively. The higher value of reversible reaction potential indicates that a proton in the form of hydronium needs a higher voltage as the driving force to get into the layers of graphene and graphite. This higher potential required is probably due to the structure of the graphene platelets and graphite. In another words, as the hydronium ions reach the edge plane of the graphene and graphite, a weak hydrogen-carbon bond (or attraction) is formed due to the charge attraction. These hydronium ions located on the edge planes block the movement of other hydronium ions into the gap between the graphitic layers in graphite and graphene platelets. Hence, while the other hydronium ions are trying to reach the centre of the electrode, the potential as the driving force increases, and

thus leads to formation of hydrogen gas. This higher potential is another possible explanation for the larger values obtained for charge transfer coefficient too. As the potential in charging mode increases to attract the hydronium in between the graphene layers in both the platelets and the graphite, there is a lower chance for the proton to be released in discharge mode, when the potential encouraging this release is much less than 1 V. Thus the equivalent hydrogen released in discharge mode is lower than the amount stored for graphene sample.

The charging voltage is higher for a given current for the graphene platelet and graphite electrodes compared to the aCS and aC KOH 1:7 samples. Hence the possibility of forming hydrogen gas increases during charging, and this may lead to a lower hydrogen wt% stored in the electrode itself. In the experiment it was found that the wt% of H stored for the graphene platelet and graphite electrodes was only around third that stored in the activated carbon sample electrode.

The calculated equivalent mass of hydrogen stored in carbon ranged from 0.014 wt% to 0.6 % for the three forms of carbon used in these experiments. The fabricated carbon sample named activated carbon from phenolic resin KOH 1:7 with 30% PTFE binder showed the highest electrochemical hydrogen storage capacity at 0.6% during the galvanostatic charge among all the fabricated sample electrodes whereas the flake graphite showed the lowest capacity.

A notable point observed during galvanostatic charging for the spherical graphite at a constant current of 40 mA was the relatively high voltage of just less than 3 V reached after just an hour of charging. A possible explanation of this increased voltage may simply be that storage sites close to surfaces of the electrode had become largely filled with hydrogen by this time. Then additional hydrogen can only be stored by movement of hydrogen atoms from these sites to unfilled sites on the same graphene plane further into the body of the material, thus freeing up more storage sites nearer the surface. This additional movement of H atoms into the body of the material may require a higher potential.

A comparison between a reversible hydrogen fuel cell and a Li-ion battery is a point of interest here. As the literature shows, the charging voltage in Li-ion batteries starts from low potential and hence the battery is getting full it can increase to 3.6 V maximum. In the experiments reported in this thesis, it was observed that a relatively high potential was

required to encourage protons to penetrate between the layers of graphite. But this potential increase also increases the rate of hydrogen gas production. So an advantage in Li-ion battery electrochemistry is that lithium does not form a gas even at high voltages, while hydrogen gas can be more readily generated during a charging process.

6.8 Conclusion

The experimental components in this chapter involved measuring the hydrogen storage capacities of carbon-based electrodes with a liquid acidic electrolyte. Four different forms of carbon were used to make sample electrodes: a commercial activated charcoal (Norit); an activated carbon made by treating phenolic resin with KOH at high temperature; spherical graphite, as used in lithium ion batteries; and 'graphene platelets' comprising around 20 stacked layers of graphene. Solid electrodes from these carbons were fabricated using a PTFE binder. Their bulk electron and proton conductivities, double layer capacitance, and reversible electrochemical hydrogen storage capacity when soaked in a dilute sulphuric acid electrolyte (as 'internal' proton conductor) were then measured. The electron conductivity of the samples was found to be in the range 4 to 12 S/cm, which compares to 16 S/cm for pure graphite. Their proton conductivities, due to the acid filling the pores, was found in the range 0.001 – 0.016 S/cm, compared, for example, to that of 1 M dilute sulphuric acid and fully hydrated nafion of ~0.1 S/cm . The double layer capacitance of the carbon electrodes was found to be in the range of 6 – 15 F/g, which compares to 200 F/g for supercapacitor materials. The total reversible electrochemical hydrogen storage capacities of the carbon electrodes immersed in 1 M dilute sulphuric acid were in the range of 0.01– 0.6 mass%.

The theoretical V-I curves in charging mode was then compared to the experimental one for each sample and the variable values on the hydrogen side electrode was obtained by fixing all the variable values on the oxygen side. These variable values on hydrogen side can help us to understand better the process of hydrogen movement and storage into the storage material. For example, an exchange current density for the sample ac KOH 1:7 was obtained at around 0.054 A/cm^2 which indicates the reaction of carbon and hydrogen takes place for this sample in a lower potential. The charge transfer coefficient varies from 0.53 to 0.7 which shows the hydrogen storage within activated carbon sample aCS is reversible. However, for graphite and graphene this value is greater than 0.5 which leads to irreversibility.

The experiments on the spherical conductive graphite and graphene platelets electrode showed promising results in terms of understanding the process of hydrogen storage related to the structure of these graphitic materials. It appears that, as the proton (as hydronium) moves towards these materials, a carbon-hydrogen bond is formed on the first layer of the edge plane close to the boundary and then block the pathway of the other protons. This process pushes the next proton into the next available site for hydrogen storage, the charging potential as the driving force increases which lead to hydrogen gas formation.

The spherical graphite is used commercially as the negative electrode in Li-ion batteries. In such batteries an organic electrolyte is employed and there are no chemical routes for hydrogen gas formation even at high voltages. So different methods of making electrode considering different configuration and deposition graphite which could help the proton to enter and exit of the storage material should be considered.

7 EXPERIMENTAL INVESTIGATION OF A PROTON BATTERY WITH SELECTED BEST-PERFORMING CARBON-BASED ELECTRODES

7.1 Overview

In this chapter the best-performing electrode in the electrochemical cell and that reported in chapter 6 of this thesis (section 6.7) is used in a proton battery (PB) device to evaluate its charging-discharging process and the equivalent reversible hydrogen storage capacity. The PB device used in this project is the same as described in previous work at RMIT (Andrews and Seif Mohammadi, 2014). The latter used metal hydride as the hydrogen storage electrode while in the present work activated carbon soaked in dilute sulphuric acid is employed.

7.2 Design and construction of the experimental proton battery

7.2.1 Introduction

The proton battery is a reversible PEM fuel cell (URFC) with an integrated solid-state hydrogen storage electrode (as described in Chapter 3, section 3.2).

In the present work a porous carbon-based material is used instead of a metal hydride as used in the previous work (Andrews and Seif Mohammadi, 2014) for the hydrogen storage. (Figure 77 shows the schematic of the proton battery with carbon-base electrode used hereThe oxygen side of the proton battery is similar to a PEM fuel cell including titanium felt instead of GDL and iridium oxide catalyst. on the hydrogen side nafion membrane is used as the proton conductive media and the other side of nafion carbon-base electrode is located as the hydrogen storage material.

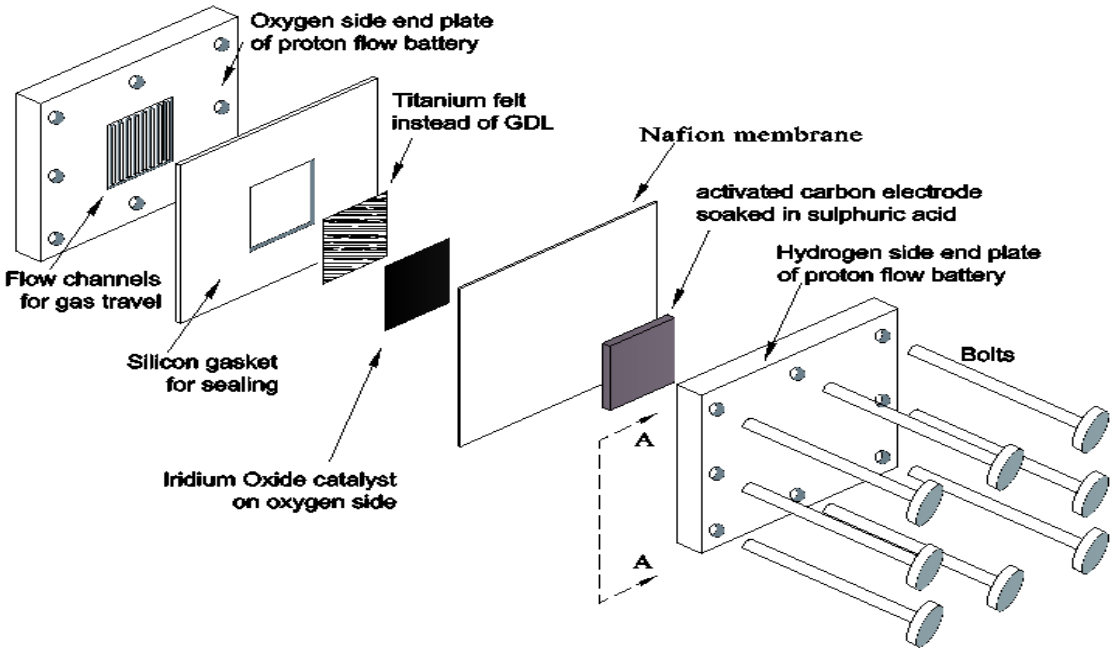

Figure 77: Schematic diagram of the experimental proton battery (Oberoi, 2015)

The proton battery device was used in E-mode to split water into proton and oxygen gas. Oxygen gas is collected in the measurement gas collection cylinder and protons are transported to the carbon-base material which is negatively charged. Then in the FC mode the stored hydrogen is released and travel to the oxygen side electrode and reform water.

7.2.2 End plates

This device contains two end plate made from stainless steel (SS316), in order to properties such as high electrical conductivity, high thermal conductivity, and high resistance to chemical corrosion (Yuan *et al.* 2005).

The length and width of both oxygen and hydrogen side end plates are 72 mm and 84 mm respectively but the thickness is different. The oxygen side end plate has a thickness of 7 mm while on the hydrogen side it is 9 mm to accommodate the carbon storage electrode with thickness around 2 mm. Figure 78 shows the actual oxygen and hydrogen end plate used for PB in this work.

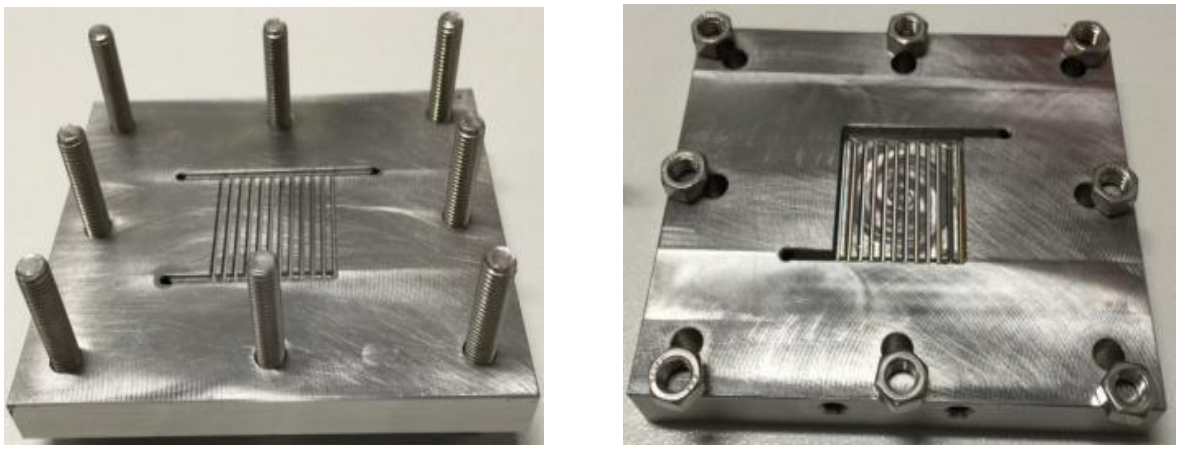

Figure 78: Actual oxygen side (left) and hydrogen (right) end plate of the proton battery

In Figure 78 the gas flow channel configuration is shown. In the hydrogen side end plate, the ribs of the gas flow channels are recessed 2 mm below the main inner surface of the end plate to accommodate the carbon hydrogen-storage electrode.

7.2.3 Silicone gasket for sealing

Silicone rubber is the most commonly material used for sealing in fuel cell industry because of low cost of material, flexibility and easy to cut in different shapes. A silicone gasket of 1 ± 0.02 mm thickness was used covering the active area of the PB, that is, 25 mm x 25 mm. Prior to the experiment, the whole PB was placed inside a tank of distilled water with all inlets and outlets blocked, and completely immersed to test the gas tightness of the internal volumes. Air was blown in around 1 barg from one channel while all the other channels were blocked on both oxygen and hydrogen sides.

7.2.4 Porous sintered titanium felt as GDB

To provide an electrically-conductive pathway between the catalyst layer of the membrane electrode assembly and the oxygen-side end plate, and supply of oxygen from the flow channels through to the catalyst particles, a gas diffusion layer (GDL) should be used in a PB, as in a standard reversible or conventional PEM fuel cell. In a PEM fuel cell, this GDL is

usually made of a porous material such as a bunch of carbon fibres (Jong-Won Lee *et al.* 2012).

In earlier work on URFCs (Jong-Won Lee *et al.* 2012), and in the previous work at RMIT, while it was observed that carbon-based GDL on the O-side is attacked by oxygen in electrolyser mode. Hence as in other experimental URFCs (H.Tang *et al*, 2011, Amandeep Oberoi, 2015), in the present work we used a porous sintered titanium felt as the O-side GDL instead of carbon fabric. The sintered titanium felt used, made by the Belgian company Baekert, is shown in Figure 79. The catalyst loading on the oxygen side is a mixture of 2 mg per cm^2 of iridium oxide and 2 mg 2 mg per cm^2 of platinum black.

Figure 79: Porous sintered titanium felt used as the GDL

On the hydrogen electrode side, the porous carbon H-storage electrode replaced a GDL. The carbon-based electrode is located in the cavity in the hydrogen-side end plate, while dilute sulphuric acid is employed as the proton conduction medium. Dilute sulphuric acid can easily penetrate within the porous activated carbon particles and is used as the proton conductive media to transport protons within the carbon-base material. The carbon-based electrode is then pressed directly against the nafion 117 membrane, which in E-mode conducts the protons (as hydronium) generated by the splitting of water molecules on the O-side electrode. It should be noted that, since the nafion is flexible enough for sealing, there is no silicone rubber used on the hydrogen side.

7.2.5 Activated carbon electrode

On the hydrogen-side electrode the best-performing electrode in the electrochemical cell and that reported in chapter 6 of this thesis (section 6.7) was selected. As the results in his work

showed, this activated carbon from phenolic resin activated KOH 1:7 has mesoporous and microporous porosity, which is suitable for storing hydrogen.

The electrode made procedure from this sample for PB is similar to the one used for the electrochemical cell in chapter 6 (section 6.3). The detail of fabrication is given in subsection 6.3.2.

The physical properties of the electrode made for the PB are shown in Table 22.

Table 22: physical properties of the electrode used in PB

sample	Width of the sample (cm)	Length of the sample (cm)	Thickness of the sample (cm)	Area (cm^2)
aC KOH 1:7	2.2	2.5	0.2	5.5

7.3 Experimental set up

The proton battery experiments were all conducted under a fume hood inside a cabinet in the Sustainable Hydrogen Energy Laboratory (SHEL) on RMIT University's Bundoora East campus. The cabinet is designed for hydrogen-based experiments and equipped with an exhaust fan and safety sensors. Figure 80 shows the experimental set up in the SHEL used for the PB experiments.

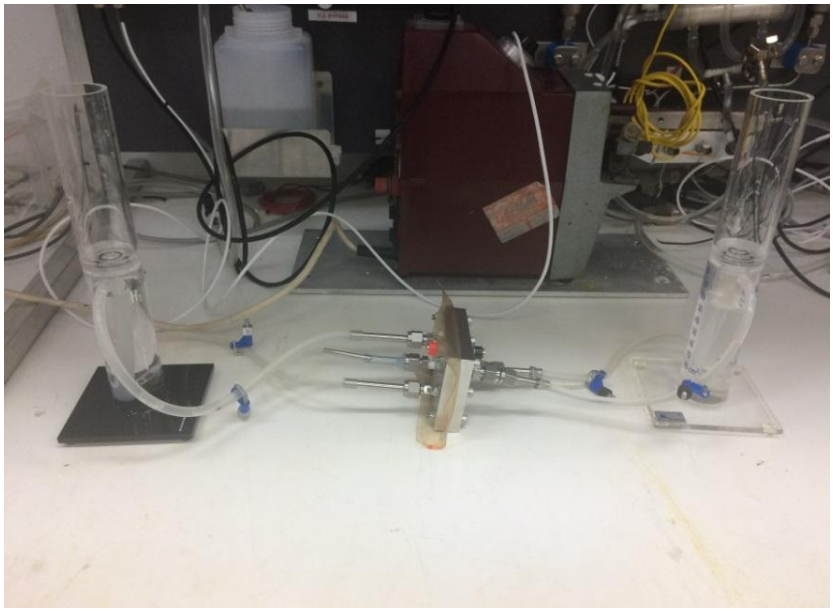

Figure 80: PB experiment set up in SHEL

Two graduated measuring cylinders as shown in Figure 80 were used in electrolyser mode to collect the oxygen and hydrogen gases produced. The PB was connected to a VERSASTAT 3 electrochemical workstation machine in charging mode to apply the power and in discharge mode to apply the load.

7.4 Experimental procedure during charging and discharging

The electric circuit in charging mode is shown in Figure 81. In this mode a DC voltage was supplied to the cell to produce the charging current. Distilled water was supplied to the oxygen side electrode and water is split into oxygen and protons (H^+) on the catalyst. Oxygen was collected from the other exit tube and protons pass through the nafion membrane to reach the carbon electrode where they are neutralised by electrons and stored by some form of C-H bonding.

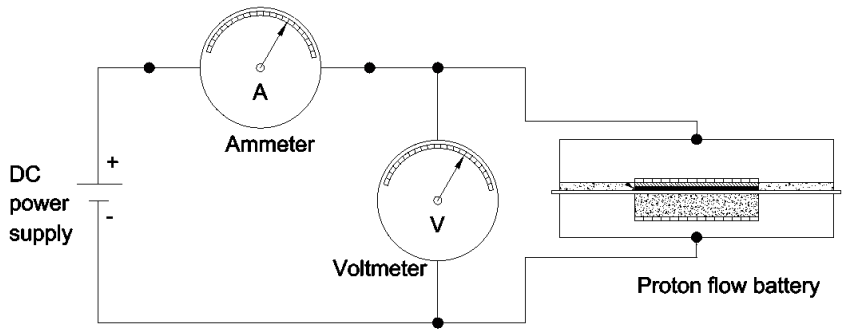

Figure 81: Electric circuit in E-mode operation of the PB

In discharge mode, the hydrogen collection cylinder was disconnected to make sure all the hydrogen used in the fuel cell was supplied from the carbon electrode. The oxygen-side electrode was also purged to remove the water supplied from the electrode. Oxygen gas was then blown from the oxygen storage cylinder as a stream of bubbles onto the electrode as the cell was run in discharge mode. The electric circuit in discharge mode is shown in Figure 82.

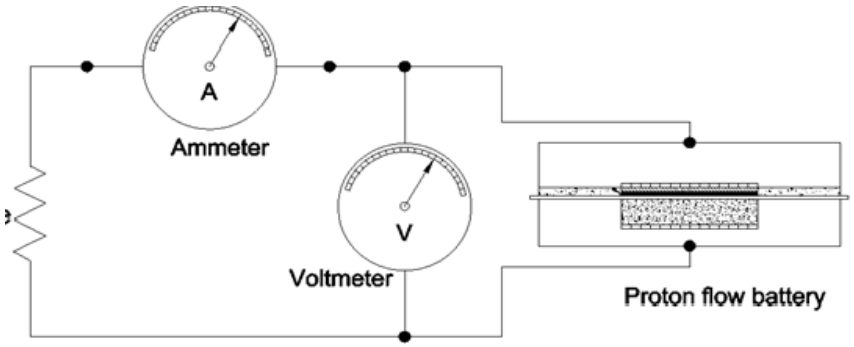

Figure 82: Electric circuit in FC mode of the PB

7.5 Experimental results and discussion

7.5.1 Charging mode

7.5.1.1 Results

The cell was charged in E-mode and then discharged in FC-mode using the two different electrodes. The first electrode was made from Phenolic resin KOH activation 1:7 mixed with 30 percent PTFE as binder. The second electrode was made from the same material but

mixed with 10 percent PTFE as binder. In both cases the cell was charged at a constant current of 80 mA while the voltage was gradually increased to keep the charging current constant. In E-mode water was split continuously into hydrogen and oxygen on the oxygen-side electrode. Some of the hydrogen generated entered the carbon storage electrode on the hydrogen side after passing through the nafion membrane in the form of hydronium. Oxygen was collected as a gas in the graduated cylinder from the oxygen-side electrode.

The V-I curve in E-mode for the PB with the integrated carbon-based electrode was first measured from zero to 2 V (Figure 83).

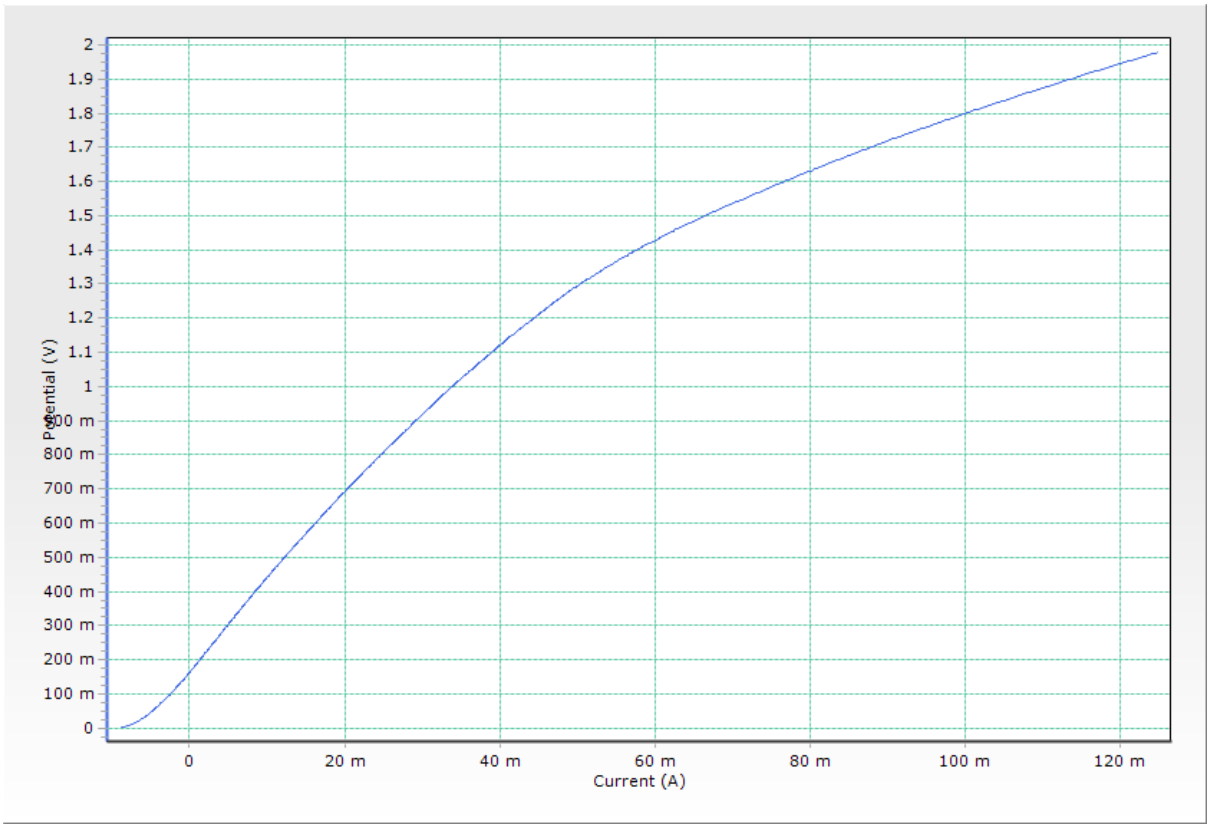

Figure 83: V-I curve for E-mode operation of the PB

The PB was then charged at a constant current of 80 mA for a period of 6744 seconds (112 mins). Figures 84 and 85 show the voltage – time curves for the PB in E mode using electrodes with 30 wt% and 10 wt% PTFE binder respectively in the first charge. As can be seen in both figures, the voltage was increased to keep the current constant until the voltage peaked at around 1.85 V. This was the first point hydrogen gas production observed. The rest

of the charging graph shows fluctuation around a certain voltage. 1.84 V for the sample with 30% PTFE and 1.83 for the sample with 10% PTFE.

From about 1800 seconds time in Figure 84, and 2000 seconds in Figure 85, the rate of H_2 production was much less than twice that of O_2. The rate of hydrogen gas production rose slowly and steadily from these times, until by around 6700 seconds time, the rates of H_2 production rose to almost double that of oxygen, indicating that all the hydrogen produced from water splitting was being released as gas and virtually none was storing.

In both graphs after around 1 hour of charging, the voltage started fluctuating around a certain voltage by +/- 0.02 V. The ups were observed when the hydrogen gas bubbles were produced and covered the carbon electrode, and the downs were observed as the bubbles of hydrogen gas left the electrode surface and rose to be collected in the gas collection cylinder.

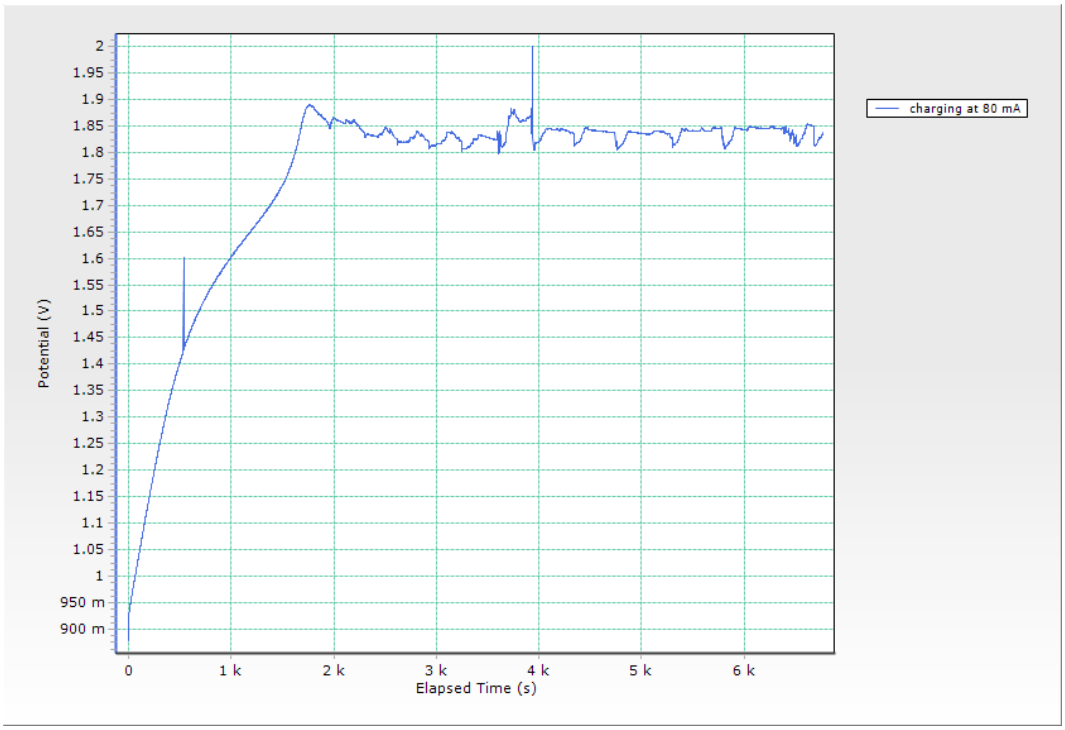

Figure 84: V-t graph fpr charging PB at 80 mA constant current for the aC KOH 1:7 and 30% PTFE

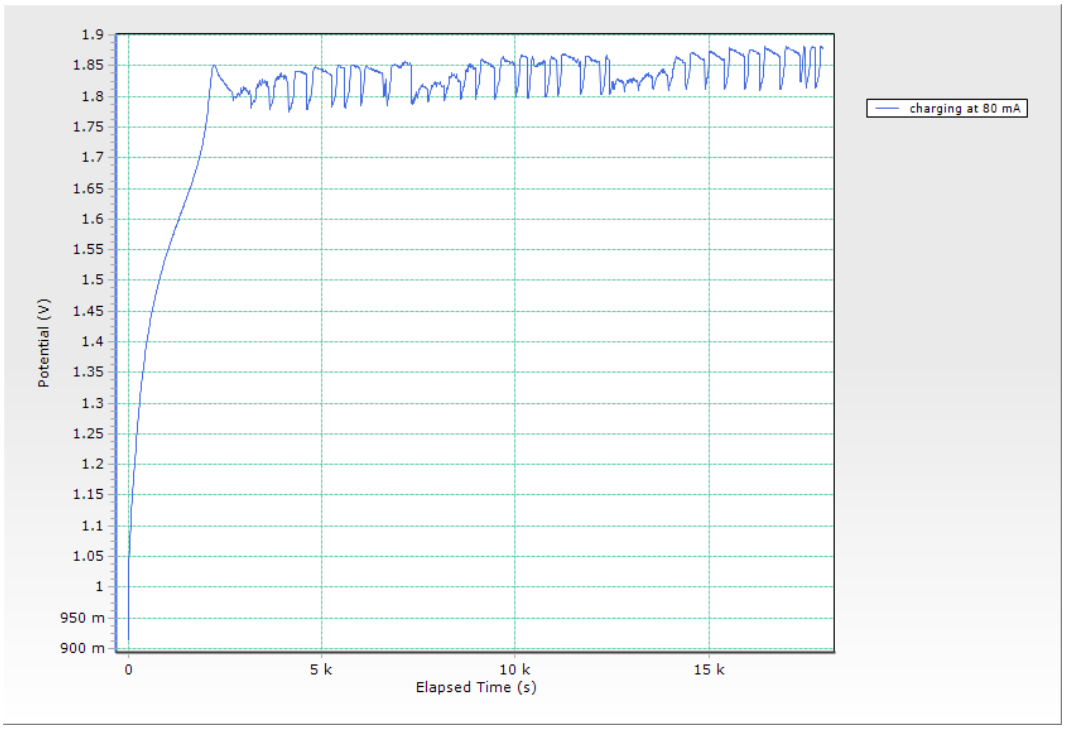

Figure 85: V-t graph of charging PB at 80 mA constant current for the aC KOH 1:7 and 10% PTFE

To avoid this fluctuation a very small pump would be required to circulate the flow in the hydrogen side electrode and prevent covering the surface of carbon electrode with hydrogen gas.

To calculate the amount of oxygen gas production and hydrogen storage in carbon-base electrode Faraday's law was applied:

Hydrogen gas production volume: $$V_H = \frac{I \times t}{2F \times 1000} \text{ x } \frac{\text{R .T}}{\text{P}} \quad (42)$$

Oxygen gas production volume: $$V_O = \frac{I \times t}{4F \times 1000} \text{ x } \frac{\text{R .T}}{\text{P}} \quad (43)$$

where:

V→ volume in L

I → current in amperes.

t → time in seconds.

F → faraday's constant = 96 485 J per volt gram equivalent.

R → gas constant = 8.314 J/mol.K

T → ambient temperature in Kelvin

P → atmospheric pressure in kPa.

Both oxygen and hydrogen gas generation during the charging period of the PBwas collected and measured. The total mass of hydrogen production was calculated from the Faraday's law. The mass of hydrogen gas generated was subtracted from this total mass of hydrogen generation to estimate the amount of hydrogen entering the storage medium. The mass of hydrogen that entered the storage was then divided by the mass of carbon powder in the electrode to get the stored wt % of hydrogen in the carbon-based electrode.

Table 23 summarises the results in E-mode for the selected electrodes.

Table 23: Performance of the PB with an integrated carbon-based electrode (activated carbon 1:7 KOH) in E-mode

Sample	Cycle	Current (mA)	Time (s)	Volume of collected hydrogen (cm^3)	Volume of collected oxygen (cm^3)	Total mass of entered hydrogen (g)	Mass of carbon electrode (g)	Wt% stored hydrogen
aC KOH 1:7 with 30% PTFE	1	80	6744	46	34	0.00191	0.35	0.545±0.005
	2	80	8464	65	41	0.00176	0.35	0.502±0.005
aC KOH 1:7 with 10% PTFE	1	80	17881	142	96	0.00326	0.33	0.988±0.01
	2	80	16041	125	85	0.00319	0.33	0.967±0.01

The results in terms of hydrogen storage for the two electrodes made from phenolic resin KOH 1:7 with the two portions of PTFE as binders were tested in the PB device in E-mode are shown in Table 23. Two charge-discharge cycles were run and the experiments were conducted in for each sample. It is interesting to note that in both electrodes slightly more hydrogen was stored in the first cycle than in the second cycle.

7.5.1.2 Discussion

In the first cycle the wt% of hydrogen stored in the electrode made with 30% PTFE was 0.545, and in the electrode with 10% PTFE it was muc higher at 0.988. A possible explanation of this difference is that the more PTFE is used, the less active area inside the

carbon electrode for hydrogen storage is present. Hence the amount of hydrogen stored decreases.

The volume of the oxygen gas produced calculated from the total charge flow using Faraday's law was fully in agreement with the volume of oxygen gas collected in the measurement cylinder. This equality confirms the nature of the reaction in E-mode: water split into oxygen and hydrogen). Hence the anomaly in oxygen gas collected in the previous work at RMIT on a PB with an integrated carbon-based electrode (see section 3.3.5.3) was avoided.

7.5.2 Discharge mode

7.5.2.1 Results

After charging the cell in E-mode the cell was allowed to rest for 30 minutes before being tested in discharge mode. It is very important and critical to choose an appropriate discharge current. Such a discharge current is one that the cell can hold the potential constant for some time almost in a range, however, as time passed the cell potential drops. A too high current would lead the cell to discharge very fast, and at a very small discharge current it may take days to fully discharge the carbon electrode. In the present work, all samples were first discharged at 10 mA until the voltage reached to zero. Then the cell was left to relax for one hour until the cell potential rose again to 200 mV. Next the cell was discharged at 5 mA.

After letting the cell rest for about 30 minutes, the same procedure was repeated in turn at 2 mA and 1 mA discharge currents, until the cell was fully discharged and no more current could be extracted from it.

Figures 86 and 87 show the performance of the PB in FC mode for the two electrodes in the first cycle. The successive steps in the discharge procedure at progressively lower currents can be seen in the multiple V-t curves plotted for each electrode. After the discharge run, the cell potential partially recovered so that the cell could be run in discharge mode again but with a lower current.

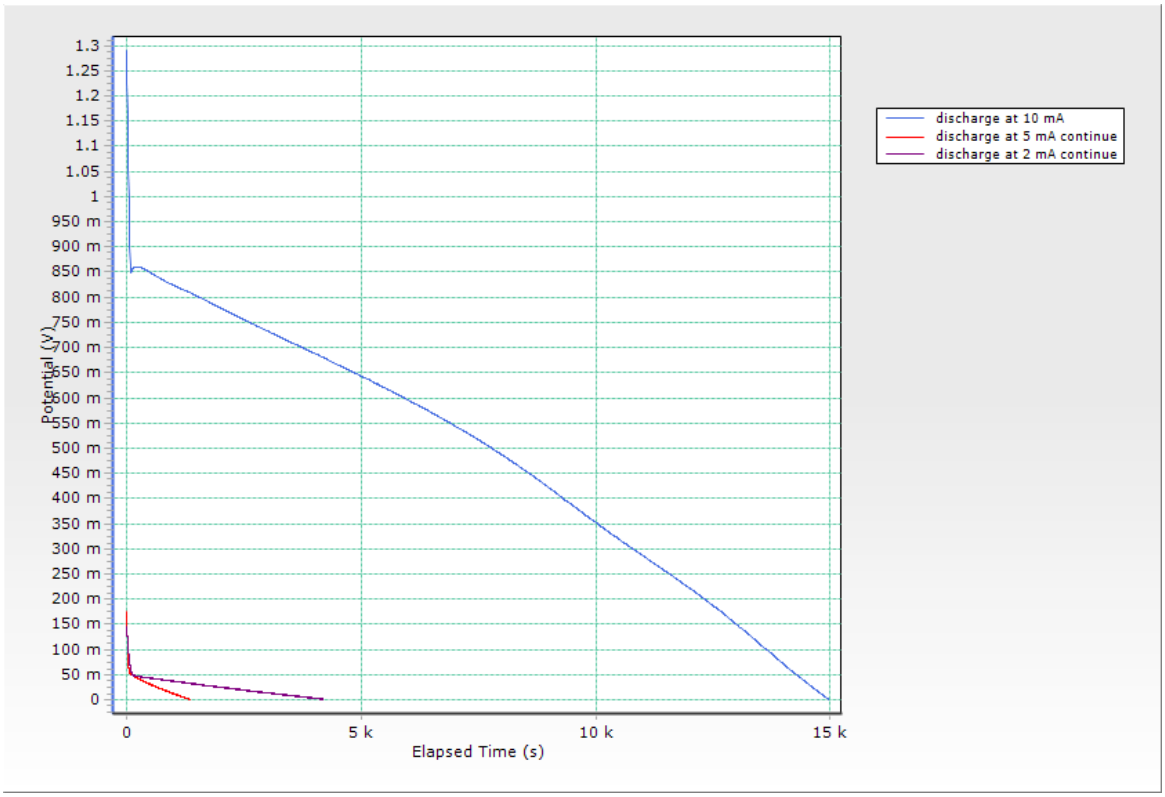

Figure 86: discharging PB at 10 then 5 and then 2 mA for the aC KOH 1:7 and 30% PTFE

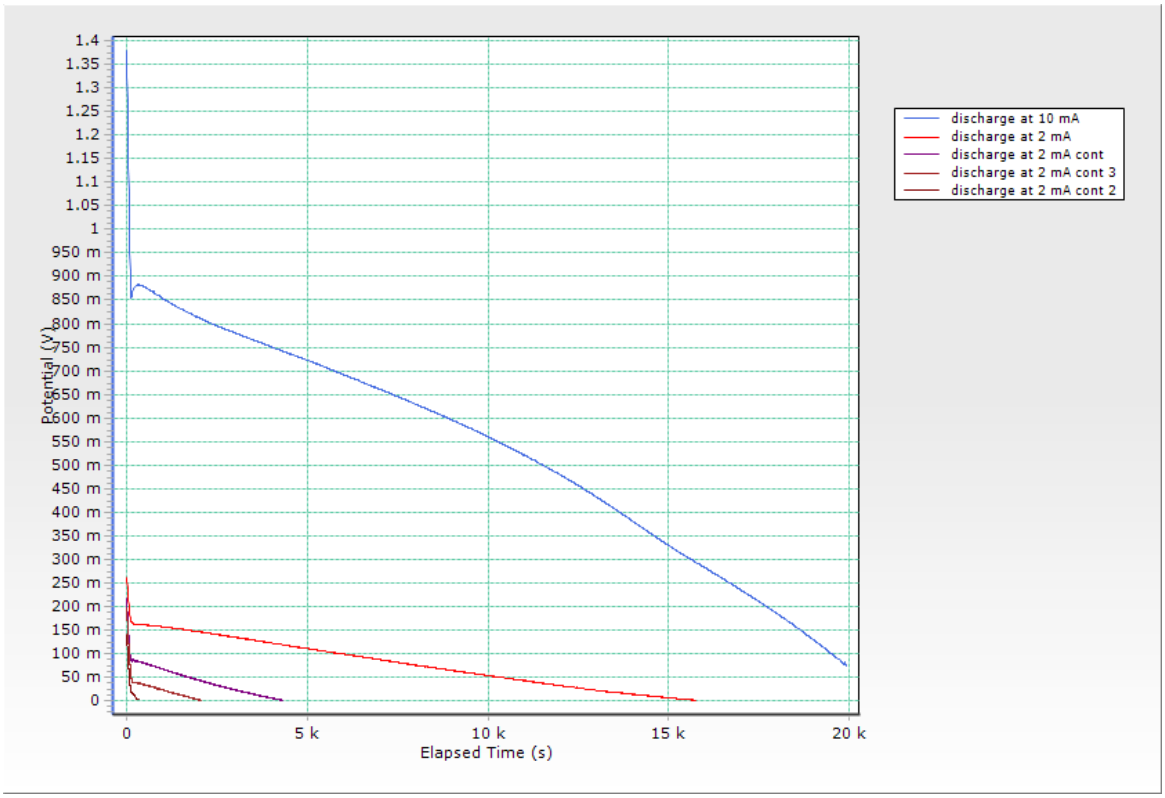

Figure 87: discharging PB at 10 then 2 mA for the aC KOH 1:7 and 10% PTFE

Table 24 shows the wt% hydrogen released from the carbon electrode in discharge (that is, fuel cell) mode for the two electrodes over the two discharge cycles.

Table 24: Wt% hydrogen released from the carbon electrode in the PB in discharge (that is, fuel cell) mode for the two electrodes tested

sample	cycle	Discharge current (mA)	Discharge time (s)	Wt% released in FC mode (total)
aC KOH 1:7 with 30% PTFE	1	10 5 2	14510 4100 804	0.524±0.005
	2	10 5 2	13203 2850 4326	0.486±0.004
aC KOH 1:7 with 10% PTFE	1	10 2	19950 26100	0.789±0.008
	2	10 5 2	22760 5840 4600	0.835±0.008

The aC electrode made with 10% PTFE had the higher value of discharge wt% in both cycles than the sample with 30% PTFE.

Table 25 summarises the results of charge and discharge in terms of wt% hydrogen stored/released for PBs employing in turn the two electrodes (aC with 10% PTFE and aC with 30% PTFE).

Table 25: Summary of the Wt% H charged and discharged by the two electrodes in a PB

sample	cycle	Total hydrogen wt% stored	Total hydrogen wt% released
aC KOH 1:7 with 30 wt% PTFE	1	0.545±0.005	0.524±0.005
	2	0.502±0.005	0.486±0.004
aC KOH 1:7 with 10 wt% PTFE	1	0.988±0.01	0.789±0.008
	2	0.967±0.01	0.835±0.08

7.5.2.2 Discussion

The highest amount of hydrogen discharged (0.835 wt%)was observed in the second cycle for the sample with 10% PTFE of. This value is slightly more than the amount of hydrogen released in the first cycle for this sample (0.789 wt%). A possible explanation for this increase from the first cycle to the second cycle may be related to the activation of the electrode storage sites with repeated cycling.

For the electrode made with 30% PTFE the discharge wt% in both cycles were very close to the wt% stored in charging mode. A comparison between Tables 23 and 24 shows that in the first cycle for the electrode with 30% PTFE 0.54 wt% hydrogen was stored and 0.52 wt% was released in FC mode, while in the second cycle 0.502 wt% hydrogen stored while 0.48 wt% hydrogen was release. The closeness of the amounts of hydrogen stored and released for the sample made with 30% PTFE suggests that with this electrode the PB performed almost reversibly.

In the first cycle of charging for the sample with 10% PTFE the amount of hydrogen storage was measured at 0.988 wt%, while the amount of hydrogen released in the same cycle in discharge test was just 0.789 wt%. These amounts were significantly higher than those for the electrode made with 30% PTFE, But with the 10% PTFE electrode there was slightly more irreversibility compared with the 30% PTFE electrode. It would appear that some of the hydrogen stored in the 10% PTFE electrode in charging mode is still staying in the electrode after discharging. Again, in the second cycle the discharge amount for the 10% PTFE electrode was larger than in the first. It seems that some of the active sites for hydrogen storage in the electrode had been activated during the first charge-discharge cycle: 0.835 compared to 0.789 wt%.

7.5.3 Shorter charge discharge cycle

7.5.3.1 Results

Figures 88 and 89 show the voltage – time curves for the PB in E mode and FC mode respectively using electrodes with 10 wt% PTFE binder respectively in the shorter charge discharge cycle.

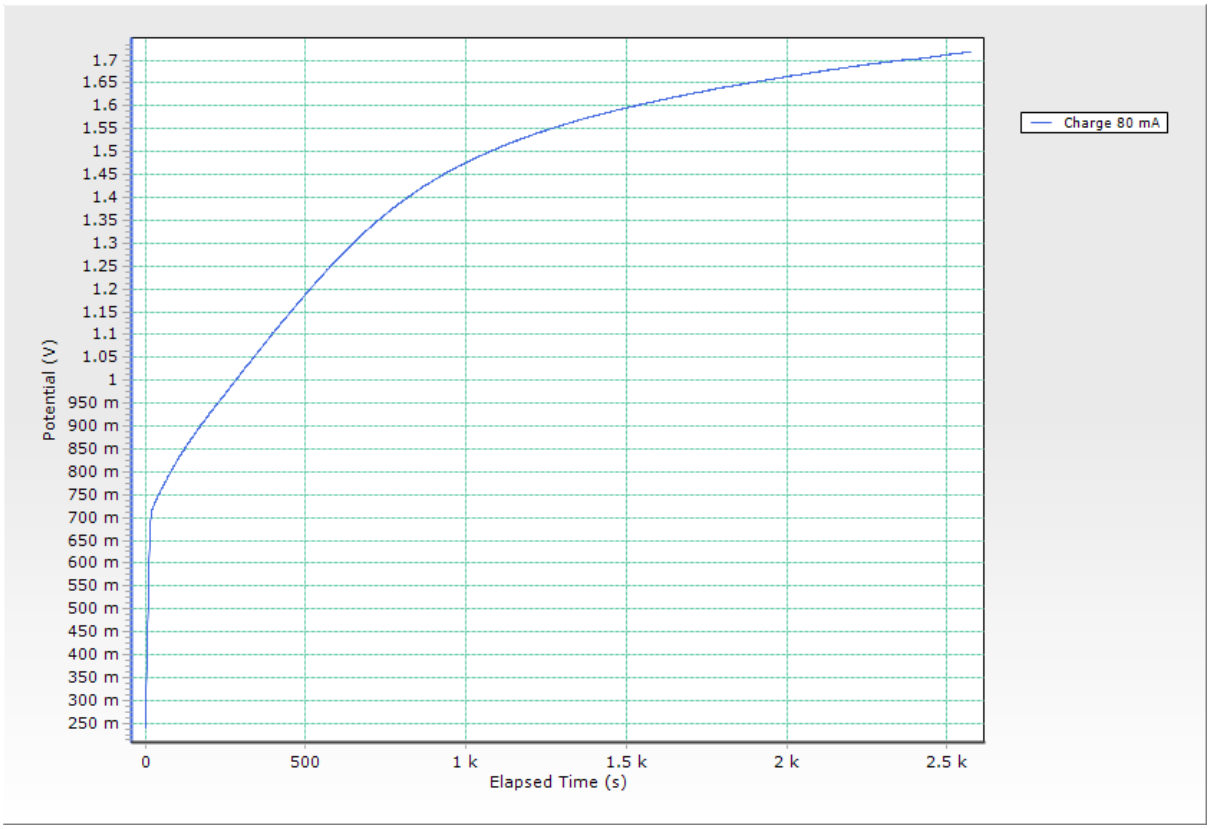

Figure 88: V-t graph of charging PB at 80 mA constant current for the aC KOH 1:7 and 10% PTFE

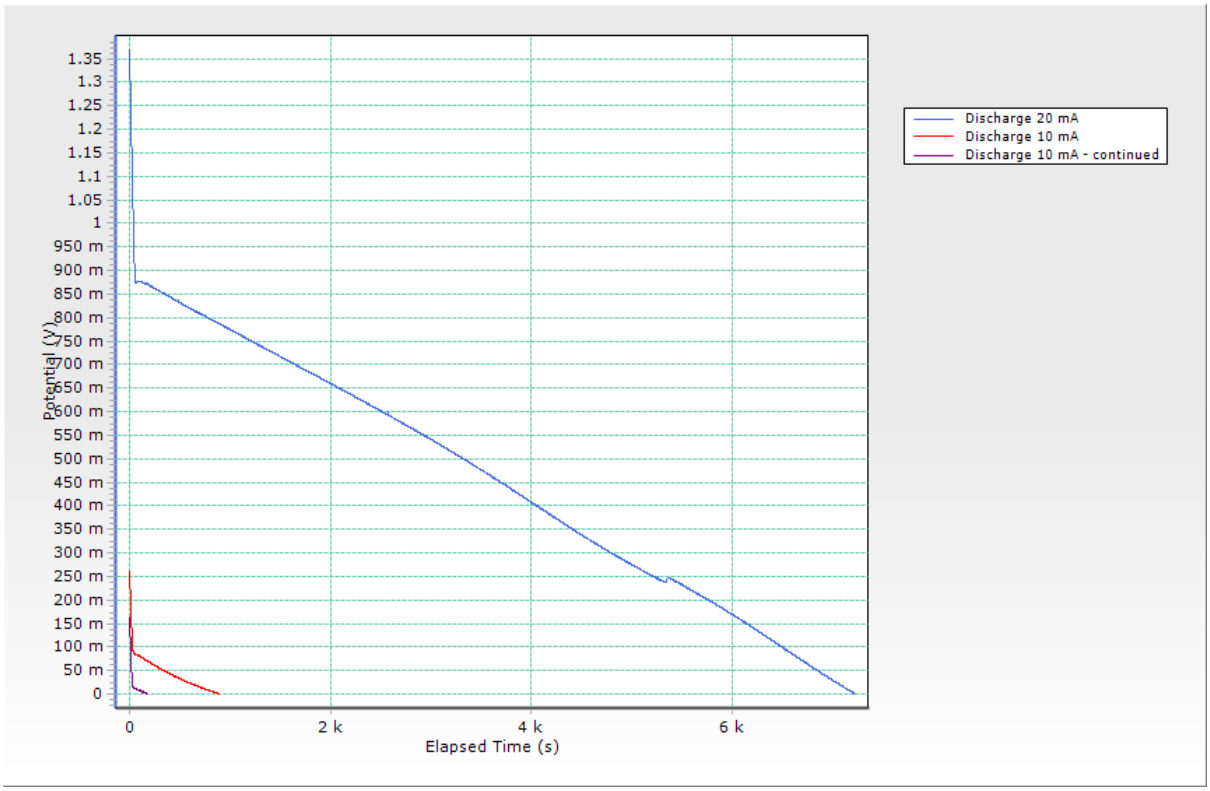

Figure 89: discharging PB at 20 then 10 mA for the aC KOH 1:7 and 10% PTFE

Table 26 shows the results for a much shorter charge time the sample made with 10% PTFE. This sample with 10% PTFE was charged up to 0.501 wt% hydrogen storage and then discharged with a total release of up to 0.486 wt%.

Table 26: Performance of the PB in short term charge and discharge

sample	Charging current (mA)	Charging time (s)	Discharge current (mA)	Discharge time (s)	Wt% hydrogen stored	Total Wt% hydrogen released
aC KOH 1:7 with 10% PTFE	80	2570	20 10	7212 1072	0.501±0.005	0.486±0.005

7.5.3.2 Discussion

When this PB cell was run for a long time, it can store more hydrogen up to around 1 wt% but can only discharge up to around 0.8 wt%. A possible explanation for this difference is that as more hydrogen is stored in the carbon-based electrode, some hydrogen penetrates into the very centre layers of the electrode. Then in discharge mode, the discharge potential is not strong enough to break the C-H bonds and attract H out of electrode and into the membrane for transfer to the oxygen side electrode.

7.6 Conclusion

In this chapter the results for charging and discharging of a proton battery with an integrated carbon-base electrode have been reported. The sample activated carbon 1:7 KOH was used to fabricate the solid hydrogen-storage electrode with PTFE binder. Dilute sulphuric acid of 1 mol concentration was used to act as the proton/hydronium conductor from the membrane into the electrode while operating the PB in E-mode, and as the proton conductor when the reverse process took place in FC mode.

The initial results for the non-optimised PB and carbon-based electrode made from phenolic resin showed the maximum amount of hydrogen storage was 0.989 wt %, while in discharge mode 0.834 wt% of it could be released. These are promising initial results and are comparable with the 1 wt% storage of many commercial metal hydride alloys.

The electrode made from aC from phenolic resin with 10% PTFE binder was found to store more hydrogen than the electrode with 30% PTFE binder. The likely explanation is the more PTFE is used, the less active area inside the carbon electrode for hydrogen storage is present.

Another significant finding was comparing long and short term charge and discharge for the sample with 10% PTFE. The results show that in short term charge almost all the hydrogen stored in carbon-base electrode can be released from the electrode in discharge mode (0.502 wt% in and 0.498 out). However, in long term charge some of the hydrogen getting into the central layers of the electrode may remain there under standard discharge conditions.

Most importantly, these experiments have shown for the first time that a PB with an integrated porous carbon-based electrode is technically feasible. With the particular electrode

material used here – aC made from phenolic resin with 1:7 KOH activation, and 10 wt% PTFE binder – a promising near 1 wt% H was able to be stored and releaed again from the electrode. Future work on the proton battery will need to focus on increasing this wt% and improving the reaction kinetics, as well investigating how temperature control may assist the overall performance

8 CONCLUSIONS AND RECOMMENDATIONS

8.1 Overview

This chapter presents the answers to the research questions set for this thesis based on the theoretical approach developed and the experimental data obtained (section 8.2). Additional conclusions from the research are then presented (section 8.3), followed by recommendations for future research and development in this area (section 8.4).

8.2 Responses to the research questions

8.2.1 To what extent can the theoretical model developed represent the hydrogen storage process in the selected carbon-based materials?

In the literature survey, it was clearly found that this area of knowledge is suffering from the lack of a theoretical model and explanation which can describe the process of hydrogen movement and storage into the storage material. So a comprehensive study was conducted to develop a better understanding of the process of hydrogen storage into the carbon-based material.

In the theoretical model, a Butler-Volmer type equation which relates the rate of hydrogen adsorption to the potential difference between the carbon surface and the electrolyte was used. This equation was then modified in the hydrogen side electrode where the carbon hydrogen reaction is taking place and with applying the boundary condition for the electrochemical cell set up, a second order type differential equation was developed. This model for the hydrogen storage electrode was then incorporated into a more general computer model based on MATLAB software of the entire electrochemical cell including the oxygen electrode.

A parametric study on the influence of key input parameters was then conducted and finally a theoretical VI curve for each sample was introduced.

It is interesting to point out that by fitting the theoretical V-I curve obtained from the theory into the experimental V-I curve for each electrode sample, at a constant current, a unique

variable values on the hydrogen side electrode was obtained. These variable values on hydrogen side can help us to understand better the process of hydrogen movement and storage into the storage material. It was clearly shown that the barrier potential shows the cut off on the V-I curve and the exchange current density introduces the rate of the storage reaction, while the charge transfer coefficient indicates how reversible the process of the storage can be.

8.2.2 What are the key structural and electrochemical characteristics and properties of composite carbon hydrogen storage materials that are dual proton and electron conductors and suitable for use in a proton battery?

The first experimental component of the thesis involved measuring the hydrogen storage capacities of carbon-based electrodes with a liquid acidic electrolyte. Four different forms of carbon were used to make sample electrodes: a commercial activated charcoal (Norit); an activated carbon made by treating phenolic resin with KOH at high temperature; spherical graphite, as used in lithium ion batteries; and 'graphene platelets' comprising around 20 stacked layers of graphene. Solid electrodes from these carbons were fabricated using a PTFE binder. Their bulk electron and proton conductivities, double layer capacitance, and reversible electrochemical hydrogen storage capacity when soaked in a dilute sulphuric acid electrolyte (as 'internal' proton conductor) were then measured. The electron conductivity of the samples was found to be in the range 4 to 12 S/cm, which compares to 16 S/cm for pure graphite. Their proton conductivities, due to the acid filling the pores, was found in the range 0.001 – 0.016 S/cm, compared, for example, to that of 1 M dilute sulphuric acid and fully hydrated nafion of ~0.1 S/cm. The double layer capacitance of the carbon electrodes was found to be in the range of 6–15 F/g, which compares to 200 F/g for supercapacitor materials. The total reversible electrochemical hydrogen storage capacities of the carbon electrodes immersed in 1 M dilute sulphuric acid were in the range of 0.01– 0.6 mass%.

It is interesting to point out that in terms of the structure of the storage material, porous activated carbon compare to the graphitic carbon-base materials showed better performance in storing hydrogen. Specifically porous activated carbon made from phenolic resin activated by KOH 1:7 with high BET surface area at around 3800 m^2/g revealed highest amount of hydrogen storage by 0.6 wt% compared to spherical graphite at 0.2 wt%.

A possible explanation for storing more hydrogen in porous activated carbon than the graphite is as the liquid electrolyte (1 Mol sulphuric acid) can penetrate into the meso and microporos channels of the activated carbon, the protons are transported to the active storage site and hence the storage wt% is higher than the graphite samples which the proton could not penetrate between the gaps of the graphite layers.

8.2.3 To what extent the best performing material can be used in the proton battery device?

The second experimental component of the thesis involved measuring the reversible hydrogen storage performance of the best performing carbon material identified from the earlier experiments in a proton battery. The aC KOH 1:7 sample was selected since it yielded the highest wt% hydrogen stored based upon the electrochemical hydrogen storage capacity experiment. This activated carbon had substantial micropore and mesopore volumes, a combination suitable for storing hydrogen.

It was therefore shown successfully that hydrogen can be stored electrochemically in the activated carbon electrode soaked in dilute sulphuric acid in a proton battery. Two samples from phenolic resin with 10 wt% and 30 wt% PTFE as binder were tested and the results showed that the more PTFE used, the less the hydrogen storage wt% obtained. The results for the non-optimised proton battery and carbon-based electrode showed the maximum amount of hydrogen storage was very nearly 1 wt%, while in discharge mode 0.83 wt% was released.

Overall this experiment has shown for the first time that a proton battery with an integrated solid carbon-based hydrogen storage electrode is technically feasible.

8.3 Conclusions

This thesis has contributed to a better understanding of the process of hydrogen movement and storage in carbon-based material by developing a theoretical analysis and introducing the effect of input variables into the shape of the theoretical V-I curve obtained for different structural carbon-based electrodes.

A one-dimensional theoretical analysis normal to the active surface of the electrodes in a reversible electrochemical cell has been developed. A Butler-Volmer type equation related the rate of adsorption of hydrogen to the potential difference between the activated carbon surface and the electrolyte in the porous hydrogen storage electrode. A second-order differential equation has been derived that relates the potential between the proton conducting medium and the hydrogen-storage medium.

A MATLAB program has been developed to solve the equation numerically. It was shown that changing the charge transfer coefficient on both sides changed the slope of both overpotential and V-I curves, while changing the exchange current density shifted these V-I curves up and down. Increasing the exchange current density decreased the overpotential in charging mode to obtain a given current. The reversible potential affected the cut-in value of voltage at which current starts to increase on the V-I curve.

The VI curves generated using the theoretical model and Matlab solution in electrolyser mode for a reversible electrochemical cell were found to be able to fit the corresponding experimental curves accurately.

In addition to the answers of the research questions, further key conclusions of this research are the following:

1. It has been shown that a working proton battery with an integrated carbon-based electrode is technically feasible. With the particular electrode material used here – aC made from phenolic resin with 1:7 KOH activation, and 10 wt% PTFE binder – a promising near 1 wt% H was able to be stored and released again from the electrode.

2. This hydrogen storage capacity is comparable with commercially-available MH hydrogen storage alloys.

3. In the galvanostatic charge and discharge experiments, it was found that the combined electrochemical cell –Hoffmann apparatus (Chapter 6, section 6.6.2.4) was the most suitable and sufficiently accurate in measuring the volumes of oxygen and hydrogen

gas evolved on the two electrodes, and hence the wt% of hydrogen storage in charge mode, and the wt% of the hydrogen discharged.

4. It has been shown that the spherical graphite material used in Li-ion batteries may not be useful in a proton battery. The most likely explanation is that, in charging mode as hydronium approaches the edge planes of the graphite, a relatively high negative potential is required to attract the ion in between the graphene layers. But this higher voltage also has the adverse effect of increasing production of hydrogen gas, which is not desired in a proton battery system. Interestingly, a similar voltage increase in Li-ion batteries in charging mode does not have the same adverse impact since lithium does not form a gas under these conditions.

5. A comparison between the small selection of carbon-based materials investigated for hydrogen storage in the present thesis showed a form of porous activated carbon was the best option for a proton battery. But the sample used in this study was small, and much further examination of a wide range of carbon materials in this application is still required.

6. One test of a long (280 mins) charge and discharge cycle, and a short (45 mins) charge-discharge cycle in a proton battery, showed that the shorter cycle had a much higher reversibility than the longer-term cycle. A possible explanation is that in the longer cycle some of the hydrogen that enters the electrode may penetrate further into the interior of the carbon particles, and hence required a higher reverse potential to get it out again, However, a lot of additional work is required to establish the degree of reversibility of the proton battery charge-discharge process under a wide range of different conditions.

8.4 Recommendations

The following recommendations are made based on this thesis:

- Further detailed study should be conducted to evaluate and investigate the performance in a proton battery of other forms of carbon-based materials such as

carbon hydrogels and carbon nanotubes, which can be designed and fabricated with the desired properties to improve and optimise the performance of this promising new battery technology.

- It is suggested that the theoretical analysis and associated MATLAB model is investigated also for its validity and accuracy in representing the discharge mode of hydrogen from a carbon-based electrode, to complement what was done in charging mode in this thesis. A VI curve in the discharge mode would be needed and the input parameters from the best-fit curve matching theory to experiment should be obtained.

- For a more precise analysis of hydrogen storage process into carbon-based material, a complete three-dimensional model of the hydrogen-side electrode should be constructed and applied, with comparison of the theoretical outputs with experiments wherever possible.

- The lower side of the electrochemical cell in this thesis where the two electrodes are located should be modified by reducing the gap between the oxygen and hydrogen side electrodes to minimise the internal resistance and allow the cell to work properly in discharge mode as well.

- It is recommended to modify the fabrication of electrode especially for the graphitic sample since their structure is very sensitive to the location of their particles. For activated carbon, the way of making the electrode from the cubic mould is acceptable as its structure is porous and is very random, but for the graphite samples a more controllable electrode-fabrication method is required.

- More research is needed to investigate the effect of parameters such as temperature in the hydrogen-side electrode and pressure on the oxygen-side electrode in a proton battery. It would be preferable to perform the discharge cycles at various temperatures, and also different pressures on the oxygen side, in order to achieve a more complete discharge.

REFERENCES

ACHAW, O.-W. 2012. A Study of the Porosity of Activated Carbons Using the Scanning Electron Microscope.

ANDREWS, J. & SHABANI, B. 2012. Re-envisioning the role of hydrogen in a sustainable energy economy. *International Journal of Hydrogen Energy,* 37**,** 1184-1203.

ANDREWS, J. & SEIF MOHAMMADI, S. 2014. Towards a 'proton flow battery': Investigation of a reversible PEM fuel cell with integrated metal-hydride hydrogen storage. *International Journal of Hydrogen Energy,* 39**,** 1740-1751.

BABEL, K., JANASIAK, D. & JUREWICZ, K. 2012. Electrochemical hydrogen storage in activated carbons with different pore structures derived from certain lignocellulose materials. *Carbon,* 50**,** 5017-5026.

BABEŁ, K. & JUREWICZ, K. 2008. KOH activated lignin based nanostructured carbon exhibiting high hydrogen electrosorption. *Carbon,* 46**,** 1948-1956.

BÉGUIN, F., KIERZEK, K., FRIEBE, M., JANKOWSKA, A., MACHNIKOWSKI, J., JUREWICZ, K. & FRACKOWIAK, E. 2006. Effect of various porous nanotextures on the reversible electrochemical sorption of hydrogen in activated carbons. *Electrochimica acta,* 51**,** 2161-2167.

BONE JS, GILMAN S, NIEDRACH LW, READ MD. Ion-exchange regenerative fuel cells. In: Proceedings of the 15th annual powersourceconf. N.J.: Ft.Monmouth;May9e11, 1961. p. 47e9.

BOUCHET, R. & SIEBERT, E. 1999. Proton conduction in acid doped polybenzimidazole. *Solid State Ionics,* 118**,** 287-299.

C. VIX-GUTERL, E. FRACKOWIAK, K. JUREWICZ, M. FRIEBE, J. PARMENTIER, AND F. BEGUIN (2005), 'Electrochemical energy storage in ordered porous carbon materials', *Carbon*, vol. 43, pp. 1293-1302.

CHEN, G., ZHANG, H., CHENG, J., MA, Y. & ZHONG, H. 2008. A novel membrane electrode assembly for improving the efficiency of the unitized regenerative fuel cell. *Electrochemistry communications,* 10**,** 1373-1376.

CANDELARIA, S. L., SHAO, Y., ZHOU, W., LI, X., XIAO, J., ZHANG, J.-G., WANG, Y., LIU, J., LI, J. & CAO, G. 2012. Nanostructured carbon for energy storage and conversion. *Nano Energy,* 1**,** 195-220.

CHANG, C.-F., CHANG, C.-Y. & TSAI, W.-T. 2000. Effects of Burn-off and Activation Temperature on Preparation of Activated Carbon from Corn Cob Agrowaste by CO< sub> 2</sub> and Steam. *Journal of Colloid and Interface Science,* 232**,** 45-49.

CHEN, H. & HASHISHO, Z. 2012. Fast preparation of activated carbon from oil sands coke using microwave-assisted activation. *Fuel,* 95**,** 178-182.

CHOI, P., JALANI, N. H. & DATTA, R. 2005. Thermodynamics and proton transport in Nafion II. Proton diffusion mechanisms and conductivity. *Journal of the electrochemical society,* 152**,** E123-E130.

DODDATHIMMAIAH, A. K. 2008. *Unitised regenerative fuel cells in solar–hydrogen systems for remote area power supply.* PhD thesis, RMIT University.

DE LA CASA-LILLO, M. A.; LAMARI-DARKRIM, F.; CAZORLA-AMORO´S, D.; LINARES-SOLANO, A. *J. Phys. Chem. B* 2002, *106,* 10930.

FANG, B., ZHOU, H. & HONMA, I. 2006. Ordered porous carbon with tailored pore size for electrochemical hydrogen storage application. *The Journal of Physical Chemistry B,* 110**,** 4875-4880.

FRACKOWIAK, E. 2010. Guest–host interaction in energy storage systems. *Journal of Physics and Chemistry of Solids,* 71**,** 692-695.

GAMBY, J., TABERNA, P., SIMON, P., FAUVARQUE, J. & CHESNEAU, M. 2001. Studies and characterisations of various activated carbons used for carbon/carbon supercapacitors. *Journal of Power Sources,* 101**,** 109-116.

GRUBB, W. T. 1959. Fuel cell. Google Patents.

GRIGORIEV, S., MILLET, P., DZHUS, K., MIDDLETON, H., SAETRE, T. & FATEEV, V. 2010. Design and characterization of bi-functional electrocatalytic layers for application in PEM unitized regenerative fuel cells. *International Journal of Hydrogen Energy,* 35**,** 5070-5076.

HARRIS, P. J., LIU, Z. & SUENAGA, K. 2008. Imaging the atomic structure of activated carbon. *Journal of physics: Condensed matter,* 20**,** 362201.

HE, R., LI, Q., XIAO, G. & BJERRUM, N. J. 2003. Proton conductivity of phosphoric acid doped polybenzimidazole and its composites with inorganic proton conductors. *Journal of Membrane Science,* 226**,** 169-184.

HOFMANN, D. W., KULESHOVA, L. & D'AGUANNO, B. 2007. A new reactive potential for the molecular dynamics simulation of liquid water. *Chemical Physics Letters,* 448**,** 138-143.

HOFMANN, D., KULESHOVA, L. & D'AGUANNO, B. 2010. Theoretical simulations of proton conductivity: Basic principles for improving the proton conductor. *Journal of Power Sources,* 195**,** 7743-7750.

IJERI A,, CAPPELLETTOA L, BIANCOB S, TORTELLOC M,SPINELLI A P, TRESSOA E. 2010. Nafion and carbon nanotube nanocomposites for mixed proton and electron conduction. *Journal of membrane science.* 363 . 265–270.

IOROI, T., KITAZAWA, N., YASUDA, K., YAMAMOTO, Y. & TAKENAKA, H. 2001. IrO2-deposited Pt electrocatalysts for unitized regenerative polymer electrolyte fuel cells. *Journal of applied electrochemistry,* 31**,** 1179-1183.

JAZAERI, 2013, M Eng by research thesis, 'the feasibility of a unitised regenerative fuel cell with a reversible carbon-based hydrogen storage electrode'

JUREWICZ, K., FRACKOWIAK, E. & BÉGUIN, F. 2001. Enhancement of reversible hydrogen capacity into activated carbon through water electrolysis. *Electrochemical and Solid-State Letters,* 4**,** A27-A29.

JUREWICZ, K., FRACKOWIAK, E. & BÉGUIN, F. 2001. Enhancement of reversible hydrogen capacity into activated carbon through water electrolysis. *Electrochemical and Solid-State Letters,* 4**,** A27-A29.

JUREWICZ, K., FRACKOWIAK, E. & BÉGUIN, F. 2002. Electrochemical storage of hydrogen in activated carbons. *Fuel processing technology,* 77**,** 415-421.

JUREWICZ, K., FRACKOWIAK, E. & BÉGUIN, F. 2009. Nanoporous H-sorbed carbon as anode of secondary cell. *Journal of Power Sources,* 188**,** 617-620.

JACOBSON, M. Z. & DELUCCHI, M. A. 2011. Providing all global energy with wind, water, and solar power, Part I: Technologies, energy resources, quantities and areas of infrastructure, and materials. *Energy Policy,* 39**,** 1154-1169.

JORDA´-BENEYTO, M.; SUA´REZ-GARCI´A, F.; LOZANO-CASTELLO´, D.; CAZORLA- AMORO´S, D.; LINARES-SOLANO, A. *Carbon* 2007, *45*, 293.

KAWAHARA, M., MORITA, J., RIKUKAWA, M., SANUI, K. & OGATA, N. 2000. Synthesis and proton conductivity of thermally stable polymer electrolyte: poly (benzimidazole) complexes with strong acid molecules. *Electrochimica acta,* 45**,** 1395-1398.

LUA, A. C. & YANG, T. 2004. Effect of activation temperature on the textural and chemical properties of potassium hydroxide activated carbon prepared from pistachio-nut shell. *Journal of colloid and interface science,* 274**,** 594-601.

LOTA, G., FIC, K., JUREWICZ, K. & FRACKOWIAK, E. 2011. Correlation of hydrogen capacity in carbon material with the parameters of electrosorption. *Central European Journal of Chemistry,* 9**,** 20-24.

LINARES SOLANO, Á., LILLO RÓDENAS, M. Á., MARCO LOZAR, J. P., KUNOWSKY, M. & ROMERO ANAYA, A. J. 2012. NaOH and KOH for preparing activated carbons used in energy and environmental applications.

MARSH, H. & REINOSO, F. R. 2006. *Activated carbon*, Elsevier.

MOLINA-SABIO, M. & RODRıGUEZ-REINOSO, F. 2004. Role of chemical activation in the development of carbon porosity. *Colloids and Surfaces A: Physicochemical and Engineering Aspects,* 241**,** 15-25.

MITLITSKY, F., MYERS, B., WEISBERG, A. H., MOLTER, T. M. & SMITH, W. F. 1999. Reversible (unitised) PEM fuel cell devices. *Fuel Cells Bulletin,* 2**,** 6-11.

MOPOUNG, S. 2008. Surface image of charcoal and activated charcoal from banana peel. *Journal of Microscopy Society of Thailand pp,* 22**,** 15-19.

NedStack fuel cell technology, 2007, *NedStack Projects Pending and concluded,* http://www.nedstack.com/content/NedStackProjects_100407.pdf viewed 8 October 2007.

OBEROI, A & ANDREWS**, J &** CHAFFEE, A & CIDDOR L. 2016. hydrogen storage capacity of selected activated carbon electrodes made from brown coal. *International journal of hydrogen energy,* 41, 23099–23108

OBEROI, 2015, PhD thesis, 'reversible electrochemical storage of hydrogen in activated carbons from victorian brown coal and other precursors'

PISANI, L., VALENTINI, M., HOFMANN, D., KULESHOVA, L. & D'AGUANNO, B. 2008. An analytical model for the conductivity of polymeric sulfonated membranes. *Solid State Ionics,* 179**,** 465-476.

POZZO, M. & ALFE, D. 2009. Hydrogen dissociation and diffusion on transition metal (= Ti, Zr, V, Fe, Ru, Co, Rh, Ni, Pd, Cu, Ag)-doped Mg (0001) surfaces. *International journal of hydrogen energy,* 34**,** 1922-1930.

ŞAHIN, Ö. & SAKA, C. 2013. Preparation and characterization of activated carbon from acorn shell by physical activation with H< sub> 2</sub> O–CO< sub> 2</sub> in two-step pretreatment. *Bioresource technology,* 136**,** 163-168.

SAKINTUNA, B., LAMARI-DARKRIM, F. & HIRSCHER, M. 2007. Metal hydride materials for solid hydrogen storage: a review. *International Journal of Hydrogen Energy,* 32**,** 1121-1140.

S. BULLER, M. THELE, RWAA DE DONCKER, AND E. KARDEN (2005), 'Impedance-based simulation models of supercapacitors and Li-ion batteries for power electronic applications', *IEEE Transactions on Industry Applications*, vol. 41, pp. 742-747.

SU, H., LIAO, S. & XU, L. 2009. Design, Fabrication and Preliminary Study of a Mini Power Source with a Planar Six-cell PEM Unitised Regenerative Fuel Cell Stack. *Fuel Cells,* 9**,** 522-527.

TREMBLAY, J., NGUYEN, N. L. & ROCHEFORT, D. 2013. Hydrogen absorption by a palladium electrode from a protic ionic liquid at temperatures exceeding 100° C. *Electrochemistry Communications,* 34**,** 102-104.

VIX-GUTERL, C., FRACKOWIAK, E., JUREWICZ, K., FRIEBE, M., PARMENTIER, J. & BÉGUIN, F. 2005. Electrochemical energy storage in ordered porous carbon materials. *Carbon,* 43**,** 1293-1302.

VARGAS, J., GIRALDO, L. & MORENO-PIRAJÁN, J. 2010. Enthalpic characterization of activated carbons obtained from Mucuna Mutisiana with different burn-offs. *Journal of thermal analysis and calorimetry,* 102**,** 1105-1109.

WITTSTADT, U., WAGNER, E. & JUNGMANN, T. 2005. Membrane electrode assemblies for unitised regenerative polymer electrolyte fuel cells. *Journal of power sources,* 145**,** 555-562.

WANG, J. & KASKEL, S. 2012. KOH activation of carbon-based materials for energy storage. *Journal of Materials Chemistry,* 22**,** 23710-23725.

WANG, H., GAO, Q. & HU, J. 2009. High hydrogen storage capacity of porous carbons prepared by using activated carbon. *Journal of the American Chemical Society,* 131**,** 7016-7022.

WU, S., LADANI, R. B., ZHANG, J., BAFEKRPOUR, E., GHORBANI, K., MOURITZ, A. P., KINLOCH, A. J. AND WANG, C. H., . "Aligning Multilayer Graphene Flakes with an External Electric Field to Improve Multifunctional Properties Of Epoxy Nanocomposites". *Carbon* 94 (2015): 607-618.

YIM, S.-D., PARK, G.-G., SOHN, Y.-J., LEE, W.-Y., YOON, Y.-G., YANG, T.-H., UM, S., YU, S.-P. & KIM, C.-S. 2005. Optimization of PtIr electrocatalyst for PEM URFC. *International Journal of Hydrogen Energy,* 30**,** 1345-1350.

YANG, S. J., JUNG, H., KIM, T. & PARK, C. R. 2012. Recent advances in hydrogen storage technologies based on nanoporous carbon materials. *Progress in Natural Science: Materials International,* 22**,** 631-638.

YAGMUR, E., OZMAK, M. & AKTAS, Z. 2008. A novel method for production of activated carbon from waste tea by chemical activation with microwave energy. *Fuel,* 87**,** 3278-3285.

Y. LENG (2008), Materials characterization: introduction to microscopic and spectroscopic methods, *John Wiley and Sons (Asia), Singapore.*

ZHAO, S., XIANG, J., WANG, C.-Y. & CHEN, M.-M. 2013. Characterization and electrochemical performance of activated carbon spheres prepared from potato starch by CO2 activation. *Journal of Porous Materials,* 20**,** 15-20.

ZAINI, M. A. A., AMANO, Y. & MACHIDA, M. 2010. Adsorption of heavy metals onto activated carbons derived from polyacrylonitrile fiber. *Journal of hazardous materials,* 180**,** 552-560.

ZHOU, L. 2005. Progress and problems in hydrogen storage methods. *Renewable and Sustainable Energy Reviews,* 9**,** 395-408.

ZÜTTEL, A., BORGSCHULTE, A. & SCHLAPBACH, L. 2011. *Hydrogen as a future energy carrier*, John Wiley & Sons.

PUBLICATIONS

Conference papers

- Heidari, S., Andrews, J., and Oberoi, A. S. "The proton flow battery for storing renewable energy: A theoretical model of electrochemical hydrogen storage in an activated carbon electrode", ICSREE 2015 : XIII International Conference on Sustainable and Renewable Energy Engineering, Montreal, Canada
- Heidari, S., Andrews, J. "Theoretical modelling of the proton flow battery with an activated-carbon hydrogen storage electrode", 6th world hydrogen technology convention, Sydney Australia

Journal papers (planned)

- Heidari, S., Andrews, J. "A theoretical model of hydrogen storage in a carbon-based electrode compared to experimental results" (drafted, nearly ready to submit to *International Journal of Hydrogen Energy*)
- Heidari, S., Andrews, J., Seif Mohammadi, S. "A proton battery with selected carbon-based electrodes: An experimental investigation", to be prepared

RMIT Invention Disclosure Form (internal, confidential)

- Heidari, S., Seif Mohammadi, S., and Andrews, J., 2017, "A proton battery with carbon electrode and liquid H+ conductor", submitted July 2017.